PROSTHETIC GROUP ORGANISATION AND INTERACTION IN THE 'ESCHERICHIA COLI' OXYGEN REDUCTASE; CYTOCHROME O

Mark Bacon

A Thesis Submitted for the Degree of PhD
at the
University of St Andrews

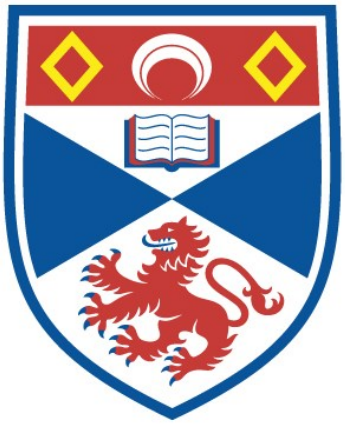

1993

Prosthetic group organisation and interaction in the *Escherichia coli* oxygen reductase; cytochrome *o*

Mark Bacon

1992

University of St. Andrews,
Department of Biochemistry and Microbiology,
North Street,
St. Andrews,
FIFE.

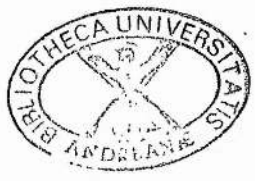

ProQuest LLC.
789 East Eisenhower Parkway
P.O. Box 1346
Ann Arbor, MI 48106 – 1346

Declaration

I, Mark Bacon, hereby certify that this thesis has been composed by myself, that it is a record of my own work, and that it has not been accepted in partial or complete fulfilment of any other degree of professional qualification.

Signed ..... Date 1/10/92

I was admitted to the Faculty of Science of the University of St. Andrews under Ordinance General No. 12 in October 1987, and as a candidate for the degree of Ph.D. in September 1988.

Signed ..... Date 1/10/92

CERTIFICATE

I, Dr W. J. Ingledew, hereby certify that the candidate has fulfilled the conditions of the Resolution and Regulations appropriate to the Degree of Ph.D.

Signature of Supervisor .....- Date 14/10/92..

Copyright Declaration

In submitting this thesis to the University of St. Andrews I understand that I am giving permission for it to be made available for use in accordance with the regulations of the University Library for the time being in force, subject to any copyright vested in the work not being affected thereby. I also understand that the title and abstract will be published, and that a copy of the work may be made and supplied to any *bona fide* library or research worker.

Acknowledgements

I would like to thank my supervisor W. John Ingledew for his help, guidance and understanding throughout my period of study in St. Andrews. Thanks are also due to Alan Moodie, John C. Salerno and Peter R. Rich for many helpful discussions and encouragement. I would also like to thank Alex Houston for his technical assistance. Finally, I would especially like to thank Jo and Kieran for bearing with me!

Abstract

The prosthetic groups of cytochrome *o*, the terminal ubiquinol:dioxygen oxido-reductase of *Escherichia coli*, were investigated in the purified and *in situ* enzyme. The interactions between the redox-active centres, of which there are three, were characterised using optical, magnetic resonance and X-ray absorption spectroscopy techniques.

The copper complement of this enzyme was investigated and the available data suggested a single copper centre associated with the ligand binding haem centre (haem *o*) forming a binuclear oxygen binding and reduction site. Two redox-active copper atoms are known to exist in the mammalian cytochrome *c* oxidase complex and the consequences of the different copper stoicheiometries, in these enzymes, are discussed.

Spatial and organisational investigations are described and a model for the binuclear reaction site presented. The location of the haem centres was determined using low-temperature EPR spectroscopy by observing the effects on the relaxation behaviour of these centres in the presence of an extrinsic paramagnetic probe.

CONTENTS

List of Figures and Tables

Chapter 1

Chapter 3

Chapter Four

Chapter Five

Abbreviations

ATP - adenosine 5'triphosphate

BES - N,N-bis[2-Hydroxyethyl]-2-aminoethanesulphonic acid

Dys-EDTA - Dysprosium(III)-EDTA

EDTA - ethylenediaminetetraacetic acid

E_h - redox potential (mV)

$E_{m,(x)}$ - mid-point potential (mV); at pH x

EPR - electron paramagnetic resonance

ETP - electron transport particles (membrane preparations)

EXAFS - extended X-ray absorption fine structure

FTIR - Fourier transform infra-red (spectroscopy)

HOQNO - 2-n-heptyl-4-hydroxyquinoline N-oxide

MES - 2-[N-morpholino]ethanesulphonic acid

MQ - menaquinone

NADH - nicotinamide adenosine dinucleotide, reduced form

NMR - nuclear magnetic resonance

P.M.F. - proton motive force

SDS-PAGE - sodium dodecyl (lauryl) sulphate polyacrylamide gel electrophoresis

TAPS - N-Tris[hydroxymethyl]methyl-3-aminopropane sulphonic acid

TES - (N-tris[Hydroxymethyl]methyl-2-aminomethanesulphonic acid

TMPD - tetramethyl-p-phenalenediamine

UQ,Q - ubiquinone, quinone

XAS - X-ray absorption spectroscopy

$\Delta\mu H^+$ - proton electrochemical gradient

CHAPTER ONE

Introduction

1.1 *Scope of review*

This introduction will concentrate on expanding on the recent extensive reviews by Poole, (1983), Anraku & Gennis, (1987), Ingledew & Poole, (1984), Poole & Ingledew, (1987) and Anraku, (1988). Unless specific points are felt to benefit clarification from these sources, retracing the work on cytochrome *o* by these authors will be kept to a minimum. A review of the alternative aerobic terminal oxidase, cytochrome *bd*, is not thought to warrant separate consideration, however, reference will be made to cytochrome *bd* when a comparison between the two aerobic oxidases proves interesting.

The nature of cytochrome *o* and its similarity to cytochrome *c* oxidase necessitates a consideration of this enzyme. However, in view of the overwhelming body of information which has been generated by so many laboratories over the last half century or so, a review of this nature cannot provide a comprehensive treatise of this topic, indeed it would be futile. Only areas which have direct bearing on cytochrome *o*, or are likely to prove

---

Individual haem centres will be refered to as haem. Haem *b* will denote the low-spin centre, whilst haem *o* will denote the five coordinate, high-spin centre at the bi-metallic site. In the literature, the holoenzyme is alternatively named either cytochrome *o* or cytochrome *bo*. As both haem centres appear to be incorporated into a single polypeptide, the latter would seem more appropriate. However, at the time of writing, there is debate as to whether the *o*-type oxidase of *E. coli* indeed possesses true *b*-type haems. For this reason alone the *o*-type oxidase, described herein, will be refered to as cytochrome *o* (*o* simply for oxidase). With regards to the description of the haem centres of cytochrome *c* oxidase a similar nomenclature will be used, however, both cytochrome *c* oxidase and cytochrome aa_3 will be used to represent the same enzyme.

interesting to those studying cytochrome *o* in the future, will be reported.

1.2 *General Introduction*

Central to efficient energy transduction by any organism, whether it be the higher animals or plants down to the simplest microbes, are the redox active cytochromes of the respiratory chain. The cytochromes, along with other components such as quinones and flavins, are spatially and thermodynamically organised in such a way as to collectively catalyse the transfer of electrons from substrate to oxidant. This results in the production of a trans-membrane proton electrochemical potential ($\Delta\mu H^+$), or proton-motive force (PMF), across the respiring membrane. The $\Delta\mu H^+$ is then available to do useful work such as the active transport of ions across membranes, reversed electron transfer as well as ATP synthesis.

Respiratory chains vary enormously in length and composition, responding to the constraints imposed by the local enviroment on the microorganism or respiring system. The mitochondrial respiratory chain is relatively long and complicated, yet well defined (for review see, Wikstrom *et al.*, 1981a). This apparent paradox is because of the consistency of supply of substrates which is afforded by the eukaryotic system in which the mitochondrion exists. This is not the case for most microorganisms where nutrient supply cannot be consistent at all times. This situation has led to

these organisms developing respiratory systems which are capable of diversification in response to prevailing conditions. For this reason the respiratory chains found in these simpler organisms are often branched, or are capable of branching, in an effort to maximally utilise and control the substrates and oxidants presented to them.

Escherichia coli is a Gram-negative bacterium found in the gut and exemplifies an organism capable of extracting energy from a wide range of reduced substrates under both aerobic or anaerobic conditions[1]. Such is the extent of regulation that manipulation of the growth conditions can lead to phenotypic differences in the chain, a method by which many of the pathways available to *E. coli* have been deconvoluted. Complementary to this is the ease with which this organism can be genetically manipulated, making it widely used by researchers in their efforts to distil the fundamental mechanisms of energy transduction. The advantages of using bacterial systems are therefore obvious in the context of studying respiratory chains.

---

[1]*E. coli* can also utilise fermentable carbon sources in substrate phosphorylation reactions, thus a functional respiratory chain is not necessarily required for growth.

1.3 *A comparative overview of cytochrome o and cytochrome aa_3*

Cytochrome *o*, an *E. coli* terminal oxidase, is of interest because there is a considerable body of evidence pointing to a similarity between this enzyme and the mammalian cytochrome *c* oxidase, a cytochrome aa_3-type oxidase. Recently, this area of study has taken on increased importance because of the realization of sequence similarity and biophysical similarity between the two enzymes. There have been many investigations into the mechanism of action of the mammalian cytochrome aa_3, both from a proton pumping aspect and regarding the dioxygen reduction mechanism, as well as structure (see Capaldi, 1990; Orii, 1988; Azzi & Muller, 1990; Capaldi *et al.*, 1987; Malmstrom, 1990; Chan & Li, 1990, for most recent reviews). However, these investigations are hampered by the complexity and availability of the mammalian enzyme. The cytochrome *o* enzyme is available in over-expressing strains of *E. coli* and there are very good reasons for increasing our efforts in studying it. These include an improved purification procedure for the enzyme (see Chapter 2) and the complete DNA sequence of the operon (Au & Gennis, 1987; Chepuri *et al.*, 1990a). In addition, the enzyme closely resembles the cytochrome aa_3-type oxidases in biophysical properties and predicted amino acid sequence (see below). Furthermore, cytochrome *o* is expressed in a bacterial system and is, thus, genetically and phenotypically maleable. This will allow site-directed mutagenesis and subunit deletion

techniques to be exploited in the future.

The cytochrome *o* enzyme is similar to the mammalian enzyme in terms of sequence identity (Section 1.4.1), and metal centre interaction (Chapter 3). Some of these properties are summarised in Table 1.1.

1.4 *Cytochrome o*

In bacteria, several oxidases may be expressed simultaneously, each competing for the available reducing equivalents and oxidants. Of the four or five major classes of oxidases utilised by bacteria, cytochrome *o*-type oxidases are the most widespread (reviewed by Poole, 1983).

Although the aerobic respiratory chain of *E. coli* does not posses a cytochrome aa_3-type oxidase, two major membrane bound protohaem IX (haem *b*) containing oxidases are produced which branch at the quinol level (for reviews see Poole, 1983; Anraku & Gennis, 1987). They are the ubiquinol-8 oxidases, cytochrome *bd* and cytochrome *o*, which reduce molecular oxygen to water (Minghetti & Gennis, 1988) and are differentially expressed in response, at least in part (see Section 1.4.1), to the oxygen tension experienced during growth (Rice & Hempfling, 1978; Kranz & Gennis, 1983). Cytochrome *bd* is preferentially expressed in culture conditions of limiting oxygen, whereas cytochrome *o* predominates under conditions of high oxygen tensions. The differences in enzymatic properties between cytochromes *bd* and *o* are illustrated in Table 1.2. Thus, cytochrome *bd* can be thought of as terminating the high affinity branch of the

Table 1.1

Biophysical Comparison between terminal oxidases

	Cyt *o*	**Cyt aa_3**	note
Haem	B type	A type	[1]
Copper	√	√	[2]
Proton pump	√	√	[3]
Haem/Haem interaction	√	√	[4]
Copper/Haem interaction	√	√	[5]
Subunits	4	~ 13	
Substrate	ubiquinol ($2e^-$)	cyt *c* ($1e^-$)	
O_2 Reaction (K_m)	0.1-6.5μM	4-7μM	

Notes

[1] see section 1.4.3 for discussion of haem identity.

[2] see section 1.4.1

[3] see section 1.9

[4] discussed in Chapter 4 and 5

[5] discussed Chapter 3; for copper/haem distance see Chapter 5

Table 1.2a
Enzymatic parameters of cytochromes o, bd and aa_3

			cyt *o*		cyt *bd*		cyt aa_3	
Reference	prep.	substrate	Km(μM)	Vmax[a]	Km(μM)	Vmax	Km	Vmax
[1]	memb.	O_2	1.4[b]	--	0.23[b]	--		
[2]	pure	O_2	2.9	--	0.38	--		
[3]	pure	O_2	10	--	--	--		
[1]	memb.	UQ-1	50	15.5	--	--		
[1,2]	pure	UQ-1	48	15	230	7.5		
[4]		O_2					4-7[c]	
[4]		O_2					0.3-3[d]	

[1] Kita *et al.*, 1984(a)
[2] Kita *et al.*, 1984(b)
[3] Matsushita *et al.*, 1984
[4] Poole, 1983
[a] Micromoles of O_2/min/nmol(cytochrome *o*); [b] values determined in membrane preparations from early exponetial phase (cytochrome *o*) and stationary phase (cytochrome *bd*); [c]prokaryote [d]mammalian

Table 1.2b
Effect of Inhibitors

		cyt *o*		cyt *bd*	
Reference	Inhibitor	K_i(μM)	I_{50}	K_i	I_{50}
Kita et al, 1984(b)[a]					
	KCN	--	10μM	--	2mM
	NaN_3	--	15mM	--	400mM
	HOQNO	--	2μM	--	7μM
	Piericidin A	--	2μM	--	15μM
	H_2O_2	--	300mM	--	120mM
	$ZnSO_4$	--	1μM	--	60μM
Matsushita et al,1984[b]					
	KCN	200[c]	--	--	--
	HOQNO	3.3[c]	--	--	--
Pudek & Bragg, 1974					
	KCN	1.4[d]	--	7.8[d]	--
Georgiou *et al.*, 1988[a]					
	KCN	--	10μM	--	--

[a] purified preparations; [b]proteoliposomes containing cytochrome *o* (lipid ratio 1:10(w/w)); [c]ubiquinol oxidase activity measured spectrophotometrically; [d]Millimolar

respiratory chain, whereas cytochrome *o* terminates the low affinity branch. Figure 1.1 presents a schematic representation of the respiratory chain of *E. coli*. The potentials are meant only as a rough guideline.

1.4.1 *The enzyme*

The cytochrome *o* complex is encoded by the *cyo* gene locus mapping at minute 10.2 on the genetic linkage map of *E. coli* (Au *et al.*, 1985) which corresponds to the positions 458 - 464 kbp (Calhoun *et al.*, 1991) on the physical map (Kohara *et al.*, 1987). The *cyo* operon contains five genes, *cyo*A, B, C, D and E (Chepuri *et al.*, 1990a). Introduction of the wild-type *cyo* allele into a *cyo*$^-$*cyd*$^-$ strain (lacking both aerobic oxidases) restores the ability of the double mutant to grow aerobically on non-fermentable carbon sources (Au *et al.*, 1985). Subsequently, the *cyo* operon has been subcloned into a multicopy plasmid (pBR322) and introduced into a *cyo*$^-$*cyd*$^-$ strain of *E. coli* resulting in a four to fivefold overexpression of ubiquinol-1 oxidase activity (Au & Gennis, 1987). A contruct of this plasmid was incorporated into the *E. coli* strain (RG145) used throughout this study.

The regulation of gene expression of *cyo*ABCDE (cytochrome *o*) and *cyd*AB (cytochrome *bd*) was examined in response to oxygen concentration using *lac*Z protein fusions in wild-type (MC4100) and *fnr* (SM1) deletion strains of *E. coli* (Cotter *et al.*, 1990; Georgiou *et al.*, 1988b).

Figure 1.1

An Overview of E. coli respiratory chain

The major dehydrogenases, such as α-glycerophosphate dehydrogenase, NADH dehydrogenase, succinate/lactate & formate dehydrogenases, are grouped together for the purposes of this diagram. Quinone, as ubiquinone (Q) and menaquinone (MQ), link these primary dehydrogenase complexes to the respiratory oxidases. In the transition from anaerobic, or low oxygen tension growth conditions, MQ is replaced by ubiquinol as the major quinol species. The total amount of quinol increases going from anaerobic to aerobic growth. Ubiquinol-8, the predominant ubiquinone species in *E. coli* membranes during aerobic growth, acts as a two electron, two proton, donor to the aerobic oxidases (Wallace & Young, 1977). It is a lipid soluble proton carrier composed of a quinol ring containing 8 isoprenoid units and able to move rapidly between the larger dehydrogenases and terminal oxidases (Hackenbrock *et al.*, 1986).

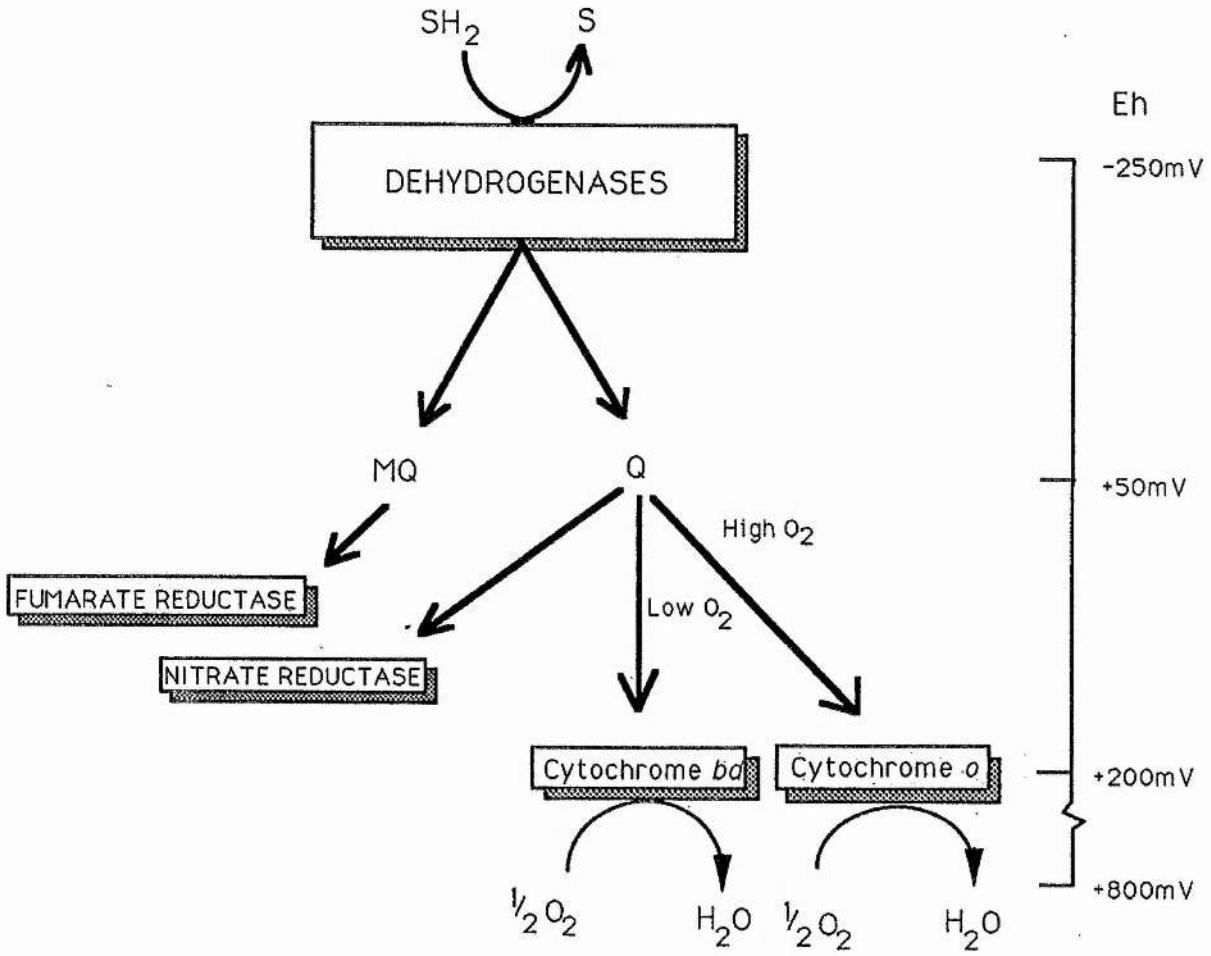
SH2
S
DEHYDROGENASES
MQ
Q
FUMARATE REDUCTASE
NITRATE REDUCTASE
High O2
Low O2
Cytochrome ba
Cytochrome o
1/2 O2
H2O
1/2 O2
H2O
Eh
-250mV
+50mV
+200mV
+800mV

Anaerobiosis saw a 140-fold repression of *cyo*A'-'*lac*Z expression relative to aerobic expression in the wild-type strain. Conversely, there was a threefold increase in *cyd*A'-'*lac*Z expression under similar conditions. A regulatory role for the *fnr* gene product was established in a *fnr* deleted strain, where the anaerobic expression of *cyo*A'-'*lac*Z was derepressed 30-fold i.e. a fourfold increase in expression over wild-type. Replacement of the *fnr* gene product led to a return of wild-type repression.

However, transcriptional control is not wholly attribuable to *fnr* since a fourfold repression is still observed in Δ*fnr* strains. The remaining regulation of *cyo*ABCDE expression is likely to be due to the *arc*A gene product (Iuchi & Lin, 1988). Interestingly, the expression of *cyd*A'-'*lac*Z (cytochrome *bd*) was also derepressed in the Δ*fnr* strain (*c.f.* Frey *et al.*, 1989). This strongly suggests the action of a second regulatory factor acting to activate *cyd*AB expression in anaerobic conditions, or alternatively, repressing *cyd*AB expression in conditions of high oxygen tension.

Using a similar fusion technique, direct transcriptional regulation was also demonstrated by Minagawa *et al.*, (1990). Their results suggested catabolite involvement in the regulation of the promoter region responsible for the *cyo* operon, possibly through protein-DNA interaction sites (CAP sites), as well as regulation in response to dissolved oxygen concentration and pH. The regulatory region was identified within the *cyo*A gene and

its 5'-flanking region. Significantly, homologous nucleotide sequences to the possible CAP-site identified in the *cyo* operon were found in regions of other enzymes known to be regulated by oxygen concentration, including *cyd*, the operon encoding the cytochrome *bd* complex.

Note that two other gene loci, *cyd*C and *cyd*D, have been shown to be required for the expression of a functional cytochrome *bd* in *E. coli*, (Georgiou *et al.*, 1987; Poole *et al.*, 1989).

Sequence analysis of the *cyo* operon reveals evidence for strong structural similarity between cytochrome *o* from *E. coli* and the cytochrome aa_3 of *Paracoccus denitrificans* (Saraste *et al.*, 1988). Three subunits, COI, COII and COIII, have been identified in the *Paracoccus* cytochrome aa_3 enzyme. These show a high degree of sequence identity with the three mitochondrial encoded subunits of cytochrome *c* oxidase, which might suggest a common origin. What is important is that COI, COII and COIII show close identity with deduced amino acid sequences encoded by the *cyo*B, A and C genes, respectively. The fourth *E. coli* gene, *cyo*E^2, has extensive homology with a putative polypeptide encoded by an open reading frame (ORF-1) found between the COII and COIII genes (Raitio *et al.*, 1987) of the *Paracoccus* enzyme. No gene product has, as yet, been identified for ORF-1 in *Paracoccus*.

A comparison between *cyo*B (subunit I) and COI shows the most extensive homology (37% identical residues) (Saraste *et*

al., 1988). Sequence alignments between subunit I (*cyo*B) of cytochrome *o* and those from other known sequences are shown in Figure 1.2. In particular, six histidines are totally conserved in all sequences examined, whilst a seventh, His at position 411, is conserved in all except that from *Bradyrhizobium japonicum* (glutamine) (Lemieux *et al.*, 1991). Replacement of this residue, with glycine, results in a functional oxidase, His411 is, therefore, not thought to be involved in ligand binding to the metal centres of cytochrome *o* (Chepuri *et al.*, 1990a; Lemieux *et al.*, 1991).

*cyo*A (Subunit II) lacks a putative copper binding site present in COII (two cysteines and a histidine) (Chepuri *et al.*, 1990a). COI codes for the major subunit of the *Paracoccus* aa_3 enzyme and, like subunit I of the mammalian cytochrome aa_3, is thought to contain both haems and Cu_B (Holm *et al.*, 1987; Chan & Li, 1990).

1.4.2 *Subunit topology*

The deduced amino acid sequences and hydropathy profiles of the five ORF's of the *cyo* operon suggest that each contains multiple membrane-spanning helices (Saraste *et al.*, 1988; Chepuri *et al.*, 1990a; Chepuri *et al.*, 1990b).

---

[2]Subsequent work performed by Chepuri *et al.*, (1990a) identified a fifth ORF sandwiched between *cyo*C and *cyo*D of *E. coli* (as originally assigned by Saraste *et al.*, (1988)). In all subsequent work the *cyo*D of Saraste and co-workers is reassigned *cyo*E.

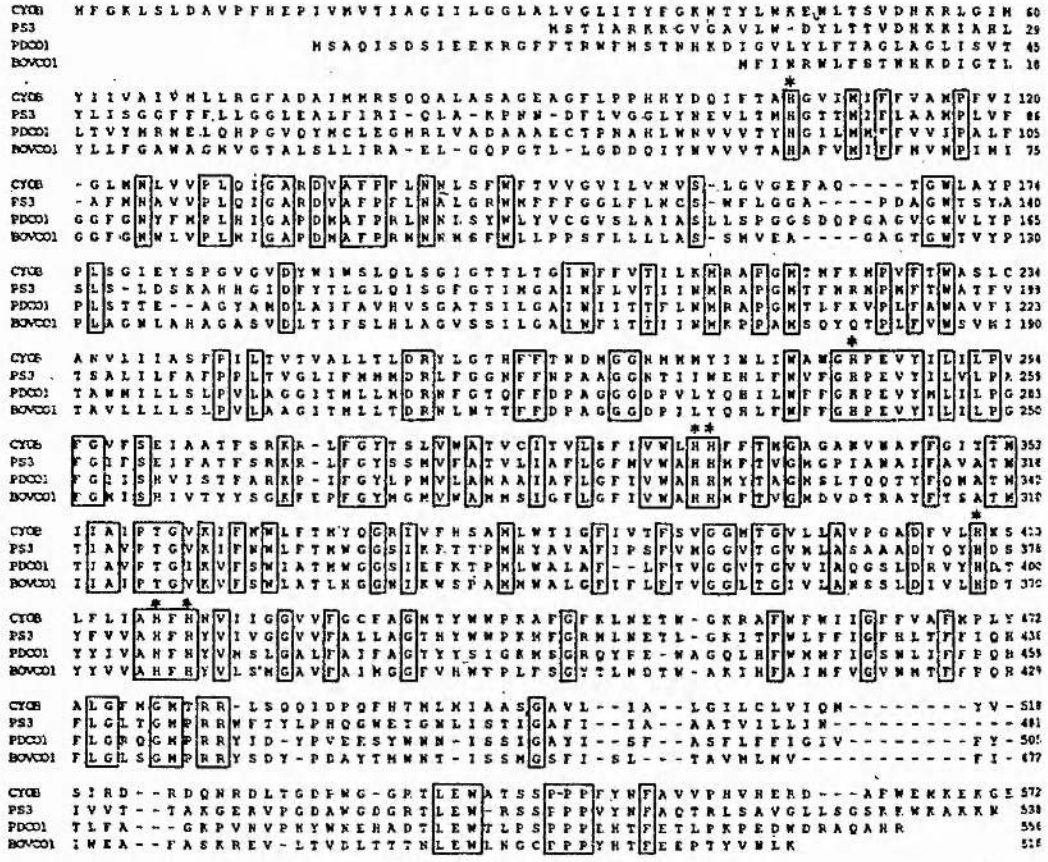

Figure 1.2

Comparisons between amino acid sequence alignments from subunit I

Shown are alignments of the deduced amino acid sequences from *E. coli* cytochrome *o* subunit I (*cyo*B), cytochrome *c* oxidase, subunit I from *PS3* (PS3), *Paraccocus denitrificans* cytochrome *c* oxidase subunit I (PDCOI) and bovine mitochondrial cytochrome c oxidase subunit I (BOVCOI) (Chepuri *et al.*, 1990a). The boxed amino acids are conserved in all four sequences. 37% sequence identity exists between subunit I from the *E. coli* and *P. denitrificans* enzyme (extending over a region of more than 550 residues). Totally conserved histidine residues are marked by an asterisk.

Experimental evidence, based on gene fusions, supports this obvious contention (Chepuri & Gennis, 1990). *Cyo*B, subunit I of cytochrome *o*, models with 15 transmembrane regions. A proposed model, based on Kyte-Doolittle hydropathy profiles, is shown in Figure 1.3 (Chepuri *et al.*, 1990a). Helix II contains the conserved His106; helix VI, His284; helix VII, His333 and His334; helix X, His421 and His419. The seventh partially conserved histidine residue, His411, resides in a loop section between helices IX and X (Lemieux *et al.*, 1991). This subunit is likely to contain both *b*-type haems and the copper involved in the binuclear reaction site, however, isolated expression of *cyo*B suggests that expression of the remaining gene products is also required for stable incorporation of copper and haem *b* (Nakamura *et al.*, 1990). Each of the conserved histidine residues have been changed by site-directed mutagenesis in an attempt to identify the ligands to the redox centres of cytochrome *o* (Lemieux *et al.*, 1991). There is optical and EPR evidence to suggest that His106 and His421 are the ligands to the low-spin haem *b* centre,. However, the other ligands could not be unequivocably assigned to haem *o*. Calhoun *et al.*, (1992) have similarly substituted His333 and His334 and established these to be ligands to the copper. A possible model for ligand coordination is given in Figure 1.4.

*cyo*A (subunit II) contains the least hydrophobic sequences and models with two membrane-spanning regions. The models for *cyo*C, D and E reveal 5, 3 and 7 putative membrane-spanning regions, respectively (N.B. either *cyo*D or

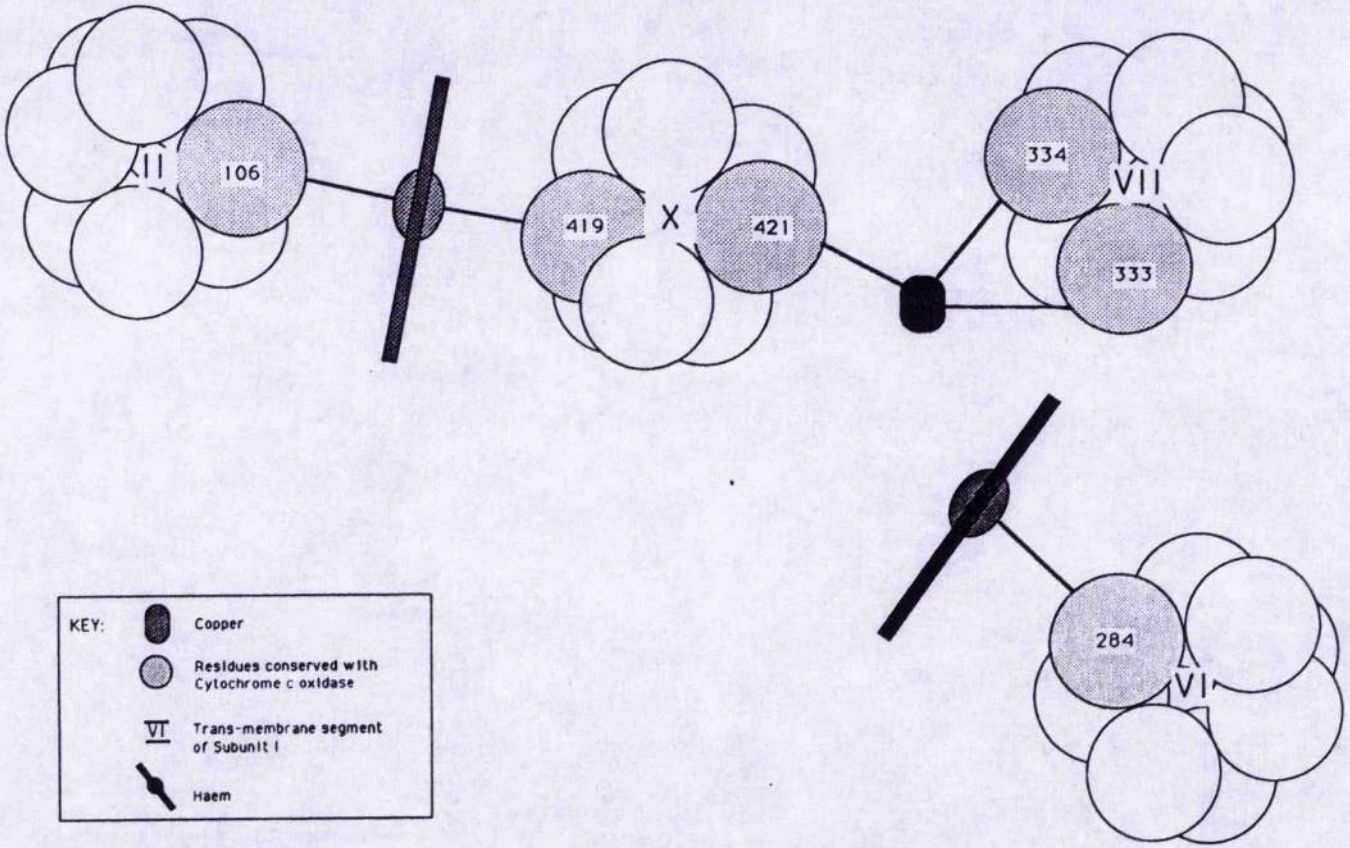
XII
106
419
X
421
334
VII
333
284
VI
KEY:
Copper
Residues conserved with Cytochrome c oxidase
VI
Trans-membrane segment of Subunit I
Haem

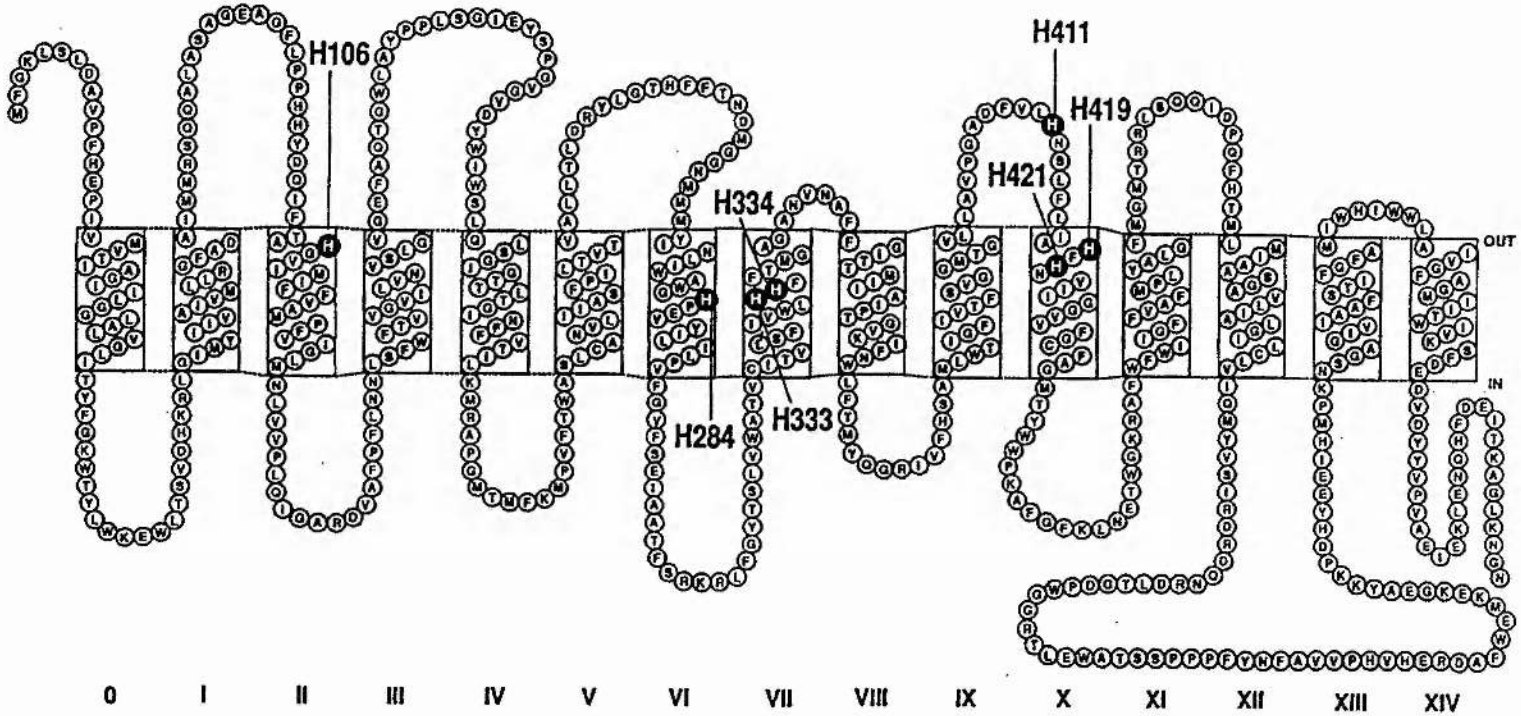
H106
H411
H419
H421
H334
H284
H333
OUT
IN
0
I
II
III
IV
V
VI
VII
VIII
IX
X
XI
XII
XIII
XIV

Figure 1.3

A proposed topological model of subunit I (cyoB) from E. coli cytochrome o.

The model is proposed based on evidence from Kyte-Doolittle hydropathy profiles and gene fusion experiments (Chepuri *et al.*, 1990a; Chepuri & Gennis, 1990). Totally conserved histidine amino acid residues are indicated. The 15 transmembrane α-helices are numbered O-XIV.

Figure 1.4

A possible coordination model for ligands to the metal centres of E. coli cytochrome o

A diagram of the possible ligand arrangement to both high- and low-spin haems and copper, is presented. The shaded amino acids correspond to known conserved histidine residues in Subunit I (*cyo*B) from *E. coli* and other sources (see text and Figure 1.3). The model is based on available published data discussed in text. The diagram is viewed normal to the membrane plane.

E are not part of the native enzyme).

The enzyme has recently been purified by a number of groups and was shown to contain 4 (Matsushita *et al.*, 1983; Matsushita *et al.*, 1984; Georgiou *et al.*, 1988a) or 2 subunits (Kita *et al.*, 1984a) by SDS-PAGE analysis. A small amount of ubiquinol (0.18mol per mol haem *b*) and less menaquinol (0.08mol per mol haem *b*) has been identified in one of the preparations (Carter & Gennis, 1985). At this time there is no physical evidence to support the existence of a fifth ORF polypeptide product which could corresponding to either *cyo*D or *cyo*E.

Deduced amino acid sequences for the five ORF's give apparent molecular weights of 35,000, 75,000, 23,000, 12,000 and 32,000, respectively for *cyo*A through *cyo*E (Chepuri *et al.*, 1990a). Subclones of *cyo*A and B (Nakamura *et al.*, 1990) produce polypeptides with apparent molecular weights of 33,000 and 66,000, which react with antibodies formed against subunit II and I, respectively. This positively identifies them with the two larger subunits obtained in the purified preparations above. In a recent examination of the radiation-induced inactivation of ubiquinol-1 oxidase activity in a cytochrome *bd* deficient mutant of *E. coli*, Williams *et al.*, (1991) determined the functional size, *in situ*, of cytochrome *o* to be 38.3 ± 2.65 kDa. This value is perhaps somewhat unexpected when we consider that subunit I (*cyo*B) contains the redox active centres for the enzyme complex and, from the deduced amino acid sequence, could be as much as 75 kDa. In any case, PAGE-analysis would seem to

confirm an apparent molecular weight for subunit I of approximately 66 kDa (Nakamara *et al.*, 1990). In trying to explain this discrepancy, these authors point out that one possible candidate might be subunit II (*cyoA*; 35 kDa, by sequence analysis) which may posses the ubiquinol binding site. However, this postulate, as these authors concede, requires access to an oxygen binding/reduction site. This would indeed be the case if the minimum functional size was truly 38 kDa. However, in the study by Williams and colleagues, the functional size of cytochrome *o* was determined from ubiquinol-1 oxidation alone. In this case the functional size of ubiquinol binding and auto-oxidation may well be 38 kDa, but this is not to say the functional size for cytochrome *o* catalysis, i.e. the oxidation of quinol coupled to the reduction of molecular oxygen, is 38 kDa.

Where atomic absorption analysis has been applied to the study of the purified preparations of cytochrome *o*, two moles of copper have been determined per complex (Kita *et al.*, 1884a). This data is at variance with the most recent EPR and optical data, which will be discussed in Chapters 3 and 4 (although, see Hata *et al.*, 1985), as well as the sequence data already discussed above (Chepuri *et al.*, 1990a).

1.4.3 *The haem prosthetic groups of cytochrome o*

A resonance Raman study of cytochrome *o* in various oxidation states indicates the presence of both high- and

low-spin components in the reduced state, low-spin ferrihaem and a weaker high-spin ferrihaem component in the air oxidised state and, in the presence of carbon monoxide, two Raman bands assignable to CO-Fe stretching frequencies (Uno *et al.*, 1985). Only one of these CO-Fe bands (the major one) was found to be photodissociable. Some spectral characteristics of cytochrome *o* are presented in Table 1.3.

New evidence (Puustinen *et al.*, 1991; Puustinen & Wikstrom, 1991), based on molecular weight analysis and uncharacteristic pyridine haemochromagen spectra (a 3-4nm blue shift from the expected protohaem derivatised spectra; Berry & Trumpower, 1987), has led Wikstrom and collaborators to suggest that the haems of cytochrome *o* are not protohaems but have modified porphyrin ring structure, possibly with a hydroxylalkyl side chain at position C2 of the porphyrin ring. This makes the haems of cytochrome *o* more akin to haem A (c.f. cytochrome aa_3) in this respect.

It is interesting to note that, at about the same time, Salerno & Ingledew (1991) made a tentative suggestion that the differences observed in the orientation of the x and y axes of the haem g-tensor seen between cytochrome aa_3 and cytochrome *o* (see below) could be accounted for by differences in side chain groups, although at the time this was thought unlikely.

Partially dehydrated oriented multilayers have been used to determine the orientation of several redox centres

Table 1.3

Spectroscopic characteristics of cytochrome o

Species	Absorbance maxima(nm)	Notes
Matsushita et al, 1984		
Reduced	427.5(427[a]), 530, 555-563	
oxidised	408.5(410[a])	
red + CO	419-426(427[a]), 531, 563	dithionite reduced
Poole et al, 1979		
CO difference spectra	415-416, 432(trough), 531, 567	(red+CO) - reduced
oxygen compound[b] "Compound A"	~430	

[a]Kita *et al.*, 1984(a)
[b]spectra obtained by repetitive difference scans after photolysis of CO-inhibited cytochrome o at low temperature in the presence of O_2.

in mitochondrial and bacterial respiratory components (e.g. Salerno & Ingledew, 1991; Blum *et al.*, 1978a & b; Erecinska *et al.*, 1978; Salerno *et al.*, 1979a & b). This technique has one major advantage over alternative orientational revealing techniques, which is the ability to look at centres *in situ*. The overall organisation of the individual subunits of cytochrome *o* has been the subject of discussion above. However, further characterisation of the haem plane orientation has been established recently in a report by Salerno & Ingledew (1991); the haems were found to be oriented with their haem planes parallel to the membrane normal. This data is consistent with data from cytochrome *c* oxidase (Blum *et al.*, 1978a) and suggests that the haems are held between membrane bound α-helical regions of the polypeptide in both enzymes. Further orientational characterisation of the haem centres will be reported in Chapter 5.

1.5 *Cytochrome aa_3*

1.5.1 *Cytochrome aa_3 in appropriate detail*

The respiratory chain of mitochondria, in common with those from many bacteria, is terminated by cytochrome *c* oxidase (ferrocytochrome *c* :O_2 oxidoreductase, EC 1.9.3.1), alternatively known as cytochrome aa_3 because of the two haem species found in this enzyme complex; haem *a* and haem a_3. Cytochrome *c* oxidase has been the subject of extensive study since the 1920's when Warburg described an

'*Atmungsferment*' and first implicated the involvement of an iron containing moiety in the reduction of molecular oxygen to water. Since that time much progress has been made towards an understanding of its structure and function. For more on this topic the reader is directed towards an extensive (but dated) review by Wikstrom *et al.* (1981a). Despite intense scrutiny, many questions remain unanswered, in particular the precise role of the terminal oxidase in the production of a $\Delta\mu H^+$ and the actual mechanism of dioxygen reduction (see Malmstrom, 1979, Wikstrom *et al.*, 1981b; Wikstrom & Krab, 1979 and Azzi, 1980 for reviews).

Mitochondrial cytochrome *c* oxidase consists of at least 13 subunits (Wikstrom *et al.*, 1981a) and is thought to be functional *in situ* as a dimer, although the "basic functional unit" is the monomer containing four redox centres (Azzi, 1980). Electrons are sequentially supplied to cytochrome *c* oxidase by the peripheral protein cytochrome *c*, although artificial electron donors, such as TMPD with ascorbate as reductant, can also transfer electrons to the enzyme. Cytochrome *c* oxidase contains four redox centres; two haem groups, haems *a* and a_3 and (at least) two copper atoms capable of undergoing Cu^+/Cu^{2+} oxidation-reductions. The copper centres are often assigned the labels Cu_A and Cu_B and are distinguishable by characteristic electron paramagnetic resonance spectra: Cu_A is "EPR-detectable" (in the g=2 region) whereas Cu_B is "EPR-invisible". Cu_A is more closely associated with the six coordinate low-spin haem *a*, whilst haem a_3 and Cu_B form a binuclear reaction centre

capable of binding, and in the case of molecular oxygen, reducing ligands. Haem a_3 binds molecular oxygen, carbon monoxide and nitric oxide (NO), via the sixth (axial) coordinate position of the haem iron when reduced and fluoride (F^-), formate, cyanide (CN^-) and peroxide when oxidised.

The sequence of electron transfer through the various metal centres of cytochrome *c* oxidase has traditionally been accepted as follows. Haem *a* accepts electrons from cytochrome *c*, which in turn donates them to Cu_A. Finally, the electrons are transfered to the binuclear centre. This sequence has been favoured on the basis of measured mid-point potentials. However, the situation is less clear cut in light of findings that (i) the mid-point potential of haem a is decreased (from approx. +350mV to 280mV) when the enzyme has turned over (Thornstrom *et al.*, 1988), (ii) there is rapid electron equilibration between haem *a* and Cu_A (Morgan *et al.*, 1989) and (iii) the position of Cu_A is closest (within the surface 10% of the dielectric barrier) to the cytoplasmic aspect of the inner mitochondrial membrane (Rich *et al.*, 1988). In addition, the proposed Cu_A binding site is situated near a concentration of negatively charged amino acid residues which may act as a cytochrome *c* binding site (Holm *et al.*, 1987). Indeed, Hill has proposed, on the basis of results from rapid transient absorption spectroscopy, that it is the cytochrome *c*-Cu_A couple, mediated by the haem *a* centre, which transfers electrons to the binuclear site (Hill, 1991). That Cu_A is required for

function is seen by a loss in activity in Cu_A depleted cytochrome *c* oxidase, although, there appears to be a residual 20% activity not affected by this treatment (Gelles & Chan, 1985; Li *et al.*, 1987; Yewey & Caughey, 1988).

In addition to the redox active metal centres described above, cytochrome *c* oxidase contains a zinc atom and a magnesium atom (Yewey & Caughey, 1988). The function of magnesium is not well understood at this time but the zinc atom (as Zn^{2+}) may have a structural role (Naqui *et al.*, 1988). Recently, there have been reports that cytochrome *c* oxidase contains a third, non-redox-active copper atom (Cu_X) (Einarsdottir and Caughey, 1984, 1985; Steffens *et al.*, 1987; Yewey & Caughey, 1988; Li *et al.*, 1989). Accurate atomic emission analysis has subsequently confirmed a stoicheiometry of 5Cu/4Fe/2Zn/2Mg per dimer (Pan *et al.*, 1991). On the basis of this investigation, Pan and colleagues suggest Cu_X plays a structural role in enzyme dimerization, and is possibly associated with subunit III.

1.5.2 *Conformations of cytochrome c oxidase*

There is substantial evidence that cytochrome *c* oxidase can exist in at least two conformational states (Brunori *et al.*, 1979; van Buuren *et al.*, 1972a & b; Malmstrom, 1990). The rate-limiting electron transfer events are those to the bi-metallic reaction centre (haem a_3 / Cu_B) (Gibson *et al.*, 1965) and have been estimated for the "resting" (k_1= 5 sec^{-1}) and "pulsed" (k_2 = 30 sec^{-1}) states for the reaction below (Wilson *et al.*, 1981);

$$R_r + 2\ \text{Cyt}\ c_r \xrightarrow{\quad k_1 \quad} R^* + 2\ \text{Cyt}\ c_o \qquad \ldots 1.1$$

$$P_r + 2\ \text{Cyt}\ c_r \xrightarrow{\quad k_2 \quad} P^* + 2\ \text{Cyt}\ c_o \qquad \ldots 1.2$$

(after Wilson *et al.*, 1981)

Here, R and P denote the resting and pulsed enzyme, subscript r and o denote the half reduced (haem *a* and Cu_A reduced) enzyme or reduced and oxidised cytochrome *c*. The asterisk (*) denotes the fully (4 electron) reduced enzyme and k_1 and k_2, the rate constants for the Reactions 1.1 and 1.2, respectively. Whether these differences are due to structural reorganisations or ligand binding (see Chapter 5) states is unresolved. Establishing whether or not cytochrome *o* has similar states may well provide the key as to whether such conformational states have any functional role. Chapter 3 will discuss the possibility of multiple states in cytochrome *o*.

1.6 *The chemistry of Oxygen reduction*

The chemistry of dioxygen reduction is important because it is likely to control the electron transfer events which ultimately mediate the proton pumping activity associated with proteins such as cytochrome *c* oxidase and cytochrome *o*. Although many of the intermediates proposed in the stepwise reduction of dioxygen have been observed, they have only been detected under extreme conditions (for review, see Hill *et al.*, 1986; Chan *et al.*, 1988 and Orii, 1988). The current understanding of dioxygen reduction by

Figure 1.5

A mechanism for di-oxygen reduction

A model of di-oxygen reduction is shown. Only the metal centres of the bimetallic reduction site are presented. Step 1: Starting with the fully reduced reaction site molecular oxygen forms an adduct with the haem (a_3) centre, Compound A. Step 2: the bridged oxygen species is formed. Step 3: an electron is fed to the reaction centre forming a ferryl intermediate. Step 4: a further electron enters the reaction centre, the di-oxygen molecule is now half reduced. Two protons are consumed in Steps 3 and 4, presumably coming from the matrix (in) side. Step 5: a further two protons are consumed to form two molecules of water. This brings to a total four protons consumed from the matrix side in the oxidase reaction. It should be noted that the consumption of these protons contributes to the electrogenic nature of the oxidase reaction, as well as the redox linked proton pumping activity (not represented) and the charge transfer of electrons (from cytochrome *c* via Cu_A and Fe_a) from the outside (cytosol) to the reaction centre somewhere within the membrane. Step 6: the fully reduced reaction centre is produced by two more electrons, completing the catalytic cycle.

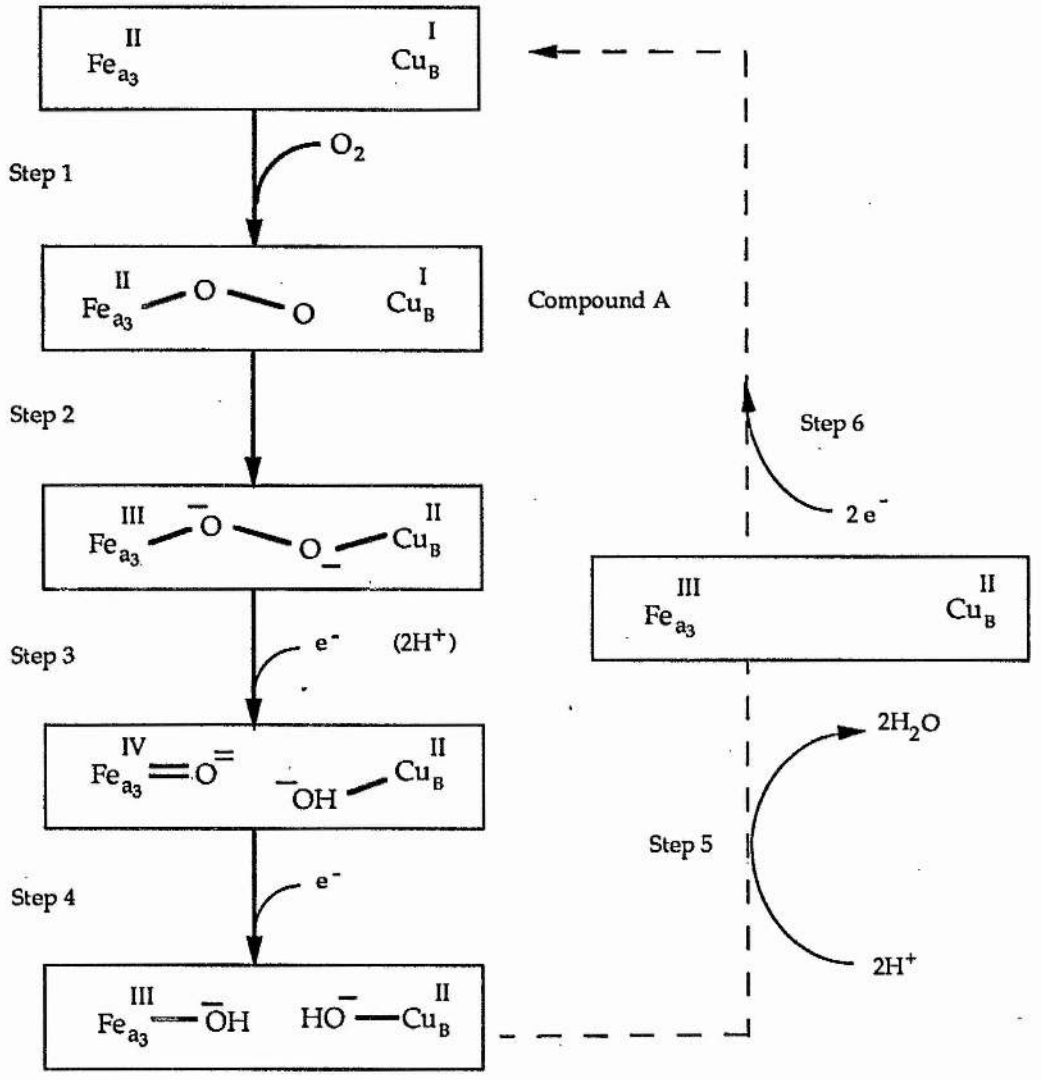
II
Fe a3
I
Cu B
O2
Step 1
II
Fe a3
O
O
I
Cu B
Compound A
Step 2
III
Fe a3
O
O
II
Cu B
Step 6
2 e-
III
Fe a3
II
Cu B
Step 3
e-
(2H+)
IV
Fe a3
O
OH
II
Cu B
2H2O
Step 5
Step 4
e-
III
Fe a3
OH
HO
II
Cu B
2H+

cytochrome *c* oxidase is summarised in Figure 1.5. The addition of oxygen to the reduced enzyme is followed by the formation of a dioxygen adduct to ferrohaem a_3 (step 1), the so called Compound A (Chance *et al.*, 1975). Electron redistribution (step 2) results in the formation of a μ-peroxy (bridged O_2) compound, Compound C (Chan & Li, 1990). Likewise, a controlled stoicheiometric addition of hydrogen peroxide results in the formation of a stable Compound C (Chan *et al.*, 1988). The transfer of another electron to the binuclear site results in the cleavage of the O—O bond product yielding an oxyferryl intermediate, Compound B (step 3), probably via a transient cupric hydroperoxide complex (Chan & Li, 1990; Chan *et al.*, 1988). The reaction between cytochrome *c* oxidase and excess hydrogen peroxide also produces a species identified as compound B (Chan *et al.*, 1988). The final single electron reduction step (4) generates the pulsed enzyme comprising a ferric hydroxy and cupric hydroxy intermediate. Both Compound B and Compound C have been produced in a highly oxidising enviroment by the one electron and two electron oxidation products of water, respectively i.e. reversed electron flow through the enzyme (Wikstrom, 1988, 1981). It has been proposed (Wikstrom, 1989) that electron transfer from the low potential centres, haem *a* and Cu_A, to the binuclear centre in the "peroxy" state (Compound C) and "oxyferryl" state (Compound B) (i.e. the electron reduction steps involved in steps 3 and 4) provides the driving force for proton pumping. This is consistent with an observed

increase in the mid-point potential of the binuclear centre when in either of these intermediate states (approx. +800mV and +940mV, respectively) (Wikstrom, 1988). Electron transfer to the binuclear centre in steps 3 and 4 are, for this reason, energetically most favourable with respect to coupling the transfer of protons across the membrane against a proton electrochemical gradient. Steps 5 and 6 complete the reduction of oxygen to water and form the fully reduced oxidase, respectively.

Rather less is known about the intermediates involved in the reaction between cytochrome *o* and molecular oxygen. However, ligand exchange experiments (tripple-trapping) have identified an early oxygenated intermediate (b^{2+}-O_2) (Poole *et al.*, 1979a & b) similar to the Compound A of cytochrome aa_3 (Chance *et al.*, 1975). The consequences of the different electron donor systems in cytochrome *o* and cytochrome aa_3 (two and one electron transfers, respectively) are discussed in relation to an oxygen reduction mechanism in Chapter 3.

1.7 *Chemiosmotic considerations and proton pumping*

In their simplest form, oxidases primarily catalyse electron transfer to an oxidant, producing a reduced product. In addition to this catalytic function, however, there are a number of oxidases which promote the direct redox linked translocation of protons across the respiratory membrane, a phenomenon known as vectorial proton transfer, or "proton pumping". The actual mechanism is unclear, and the debate continues, but the important dogma is that

internal electron transfer events are intimately, although not necessarily spatially, coupled in an all or nothing fashion to the extrusion of protons, i.e. one cannot occur without the other, a phenomenon often referred to as "electron gating" (Blair *et al.*, 1986b).

Cytochrome *c* oxidase (ferrocytochrome *c*:O_2 oxidoreductase) catalyses the 4 electron reduction of molecular oxygen to 2 moles of water (Reaction 1.3).

$$4 \text{ cyt } c^{2+} + 4H^+ + O_2 \text{ -----> } 4 \text{ cyt } c^{3+} + 2H_2O \quad .....1.3$$

$$4H^+_m \text{ -------> } 4H^+_c \quad .....1.4$$

The enzyme also uses the redox free energy available from Reaction 1.3 to catalyse Reaction 1.4, the translocation of four protons from the matrix (m) side of the membrane to the cytosolic (c) side, that is redox-linked proton translocation, producing a $\Delta\mu H^+$ (Wikstrom, 1977).

For the purposes of function, the mitochondrial respiratory chain can be visualised as a modular system. In such a scheme the redox active centres are arranged into distinct enzyme complexes. Complexes I and II, the dehydrogenases, feed electrons to complex III, the bc_1 complex. This in turn donates electrons to cytochrome *c* oxidase, complex IV, which catalyses the reduction of molecular oxygen. In this description the role of quinol has been omitted for clarity, but suffice it to say quinols serve to mediate between the dehydrogenases and the bc_1

complex and function in a proton motive Q cycle (reviewed in Trumpower, 1990). *E. coli* does not have a complex III and the terminal oxidase complex encompasses the function of both complex III and IV of the mitochondrial system, oxidising quinol and reducing molecular oxygen (see Figure 1.6). It is clear that the arrangement found in *E. coli* has a major energetic consideration, that of losing a potential energy coupling site. The redox potential difference between the quinol pool and the O_2/H_2O couple at pH 7.0 is approximately 800mV. A potential drop of this magnitude can theoretically translocate 3 mol H^+ per mol electrons against a $\Delta\mu H^+$ of 230mV. Figure 1.6 schematically demonstrates the potential for cytochrome *c* oxidase to couple proton extrusion to electron transfer as compared to cytochrome *o*. Thus, the hybrid arrangement of cytochrome *o* may not be as energetically efficient as the mitochondrial one but a higher turnover number ($>500 sec^{-1}$) may be the trade off (Saraste *et al.*, 1988).

Purified cytochrome *o* has been shown to generate a proton electrochemical potential of approximately -145 mV (interior negative and alkaline) in reconstituted proteoliposomes (Kita *et al.*, 1984a; Matsushita *et al.*, 1983; Kita *et al.*, 1982). When reconstituted together with purified *lac* carrier protein, ubiquinol oxidation by cytochrome *o* promotes lactose accumulation against a concentration gradient (Matsushita *et al.*, 1983). A proton electrochemical gradient may arise from the scalar

Figure 1.6

Comparison between the quinol oxidising regions of the mitochondrial and E. coli (cytochrome o only) respiratory chains

Two schematics are presented to illustrate the differences in the quinol oxidising portions of the respiratory chains containing cytochrome *c* oxidase (CyOx) and cytochrome *o* (CyO). In mitochondria, quinol oxidation involves the function of the bc_1 complex (III), which contains iron sulphur (FeS) groups and contributes to the $\Delta\mu H^+$ by a Q cycle (see text). The mobile cytochrome *c* mediates between the bc_1 complex and cytochrome *c* oxidase, transfering a single electron between these two complexes. The relative proton to electron transfer stoicheiometries are shown below.

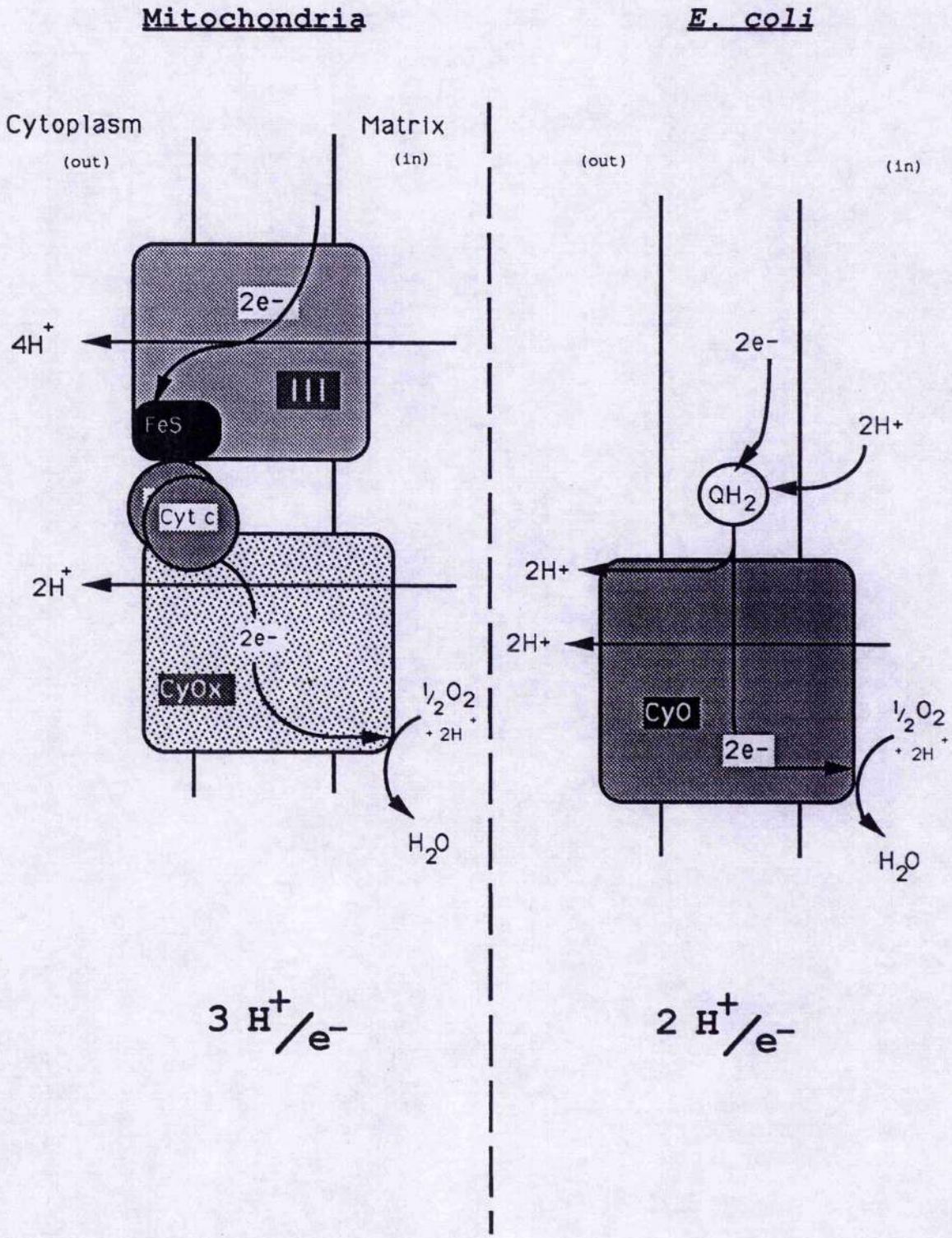
Mitochondria
E. coli
Cytoplasm
(out)
Matrix
(in)
2e-
4H+
III
FeS
Cyt c
2H+
2e-
CyOx
½O2
+ 2H+
H2O
3 H+/e-
(out)
(in)
2e-
2H+
QH2
2H+
2H+
CyO
2e-
½O2
+ 2H+
H2O
2 H+/e-

separation of protolytic reactions across the respiring membrane or through vectorial proton translocation, that is "proton pumping" by enzyme complexes. Cytochrome *o* from *E. coli*, and a cytochrome *o*-type oxidase from *Paracoccus denitrificans*, have been shown to contribute to the proton electrochemical gradient by such a proton pumping action (Puustinen *et al.*, 1989; however, see Matsushita *et al.*, 1984). This evidence has significant consequences for those proposing models for vectorial proton extrusion in cytochrome *c* oxidase, involving Cu_A (Chan, 1988; Gelles *et al.*, 1986), since cytochrome *o* lacks an analogous copper site, see Section 1.4.1 and below.

The oxidation and reduction of ubiquinone may also contribute to the electrochemical proton gradient by means of non-vectorial consumption and/or release of protons on different sides of the membrane in a so called "half loop" (see Figure 1.6).

By contrast, cytochrome *bd* is not thought to be a true proton pump (Puustinen *et al.*, 1991) and contributes to the $\Delta\mu H^+$ by the scalar distribution of redox reactions. With regard to proton-pumping activity, it remains to be seen whether it is significant that this enzyme does not contain copper (at the catalytic site) (Miller & Gennis, 1983).

1.8 *Cytochrome o in other organisms*

Oxidases of the o-type are found to be the most common of all oxidases in bacterial systems. They are often co-synthesised with other terminal oxidases, for example

cytochrome *bd* (*c.f. E. coli*) or cytochrome aa_3 (*c.f. P. denitrificans*). However, the subunit composition, electron donor systems and locale, within the bacterial cell, are often quite different. Webster and his co-workers identified a soluble cytochrome *o* from the gliding bacterium *Vitreoscilla*. This soluble oxidase contains two equivalent polypeptide chains, a bound quinone and two haem groups with quite disparate mid-point potentials and is thought to be an oxygen transport protein ($E_{m,7}$ = +118mV and -122mV), (Tyree & Webster, 1978a & b; Webster & Hackett, 1966). The oxidase of *Azotobacter vinnelandii*, on the other hand, is composed of a single polypeptide of 28 kDa molecular weight and possesses two identical *b*-type haems, $E_{m,7}$ = -6mV (Yang & Jurtshuk, 1978; Yang *et al.*, 1979). This enzyme is often co-purified with a *c*-type cytochrome (possibly c_4). Sone *et al.*, (1990) have recently described the purification and characterisation of a cytochrome *o*-type oxidase from the thermophilic bacterium PS3. The enzyme does not appear to contain copper and is composed of 3 subunits. It shows considerable cytochrome *c* oxidase activity and, although it generates a transmembrane potential, it does not appear to pump protons. Of those bacteria, besides *E. coli*, which have been tested, only cytochrome *o* from *Paracoccus denitrificans* has been shown to act as a proton pump (Puustinen *et al.*, 1989).

Ubiquinol oxidases of the *bo*-type (i.e. like that from *E. coli* described herein) have been purified from *Gluconobacter suboxydans* (Matsushita *et al.*, 1987) and

Vitreoscilla sp. (Georgiou *et al.*, 1988a). Like the enzyme isolated from *E. coli*, four subunits have been identified in the membrane bound protein from *G. suboxydans* (76K, 35K, 21K & 15K). The *G. suboxydans* enzyme also contains two b-type haems and exhibits λ_{max} at 558nm and 562nm. There is some evidence to suggest that both are separate cytochrome *o* components with differing carbon monoxide binding affinities and λ_{max} (see Daniel, 1970). The *Vitreoscilla* bo-type terminal oxidase also contained 4 subunits by SDS-PAGE analysis, copper and two *b*-type haems per complex. There is some cross-reactivity between polyclonal antibodies raised against subunit II of the *E. coli* enzyme and subunit II from the *Vitreoscilla* enzyme. However, the specificity would appear to be low, requiring a four hundred fold increase in protein concentration to elicit a comparable immunoresponse (Georgiou *et al.*, 1988a). Kranz & Gennis, (1985), have looked at the distribution of cytochromes immunologically related to the cytochrome *o* of *E. coli* in a number of bacteria but found poor cross-reactivity amongst those examined (although the effectiveness of the technique was questioned).

Acetobacter pasteurianus contains a nonsedimentable *o*-like pigment which resembles cytochrome *o* from *E. coli* in spectral, ligand-binding, and kinetic characteristics and, thus, can truly be described as an oxidase (Williams & Poole, 1988). Although other soluble haemoproteins resembling oxidases have been identified, they are considered to act as bacterial oxygen transport proteins. If

this enzyme is confirmed as a soluble oxidase it is potentially very interesting because energy cannot be conserved from the oxidase reactions and the electron donor is unlikely to be a lipid soluble quinol. It is intriguing to know what possible physiological advantage is gained from such an oxidase.

Cytochrome *o* preparations from a variety of bacteria have been summarised in Table 1.4

1.9 *Research objectives of this thesis*

The experimental aims of this project were:-

1. To characterise the potentiometric behaviour of the haem centres of cytochrome *o* in the purified enzyme by optical and EPR spectroscopy.
2. To establish the existence of multiple conformational/functional states of the enzyme (c.f. cytochrome *c* oxidase).
3. To characterise the ferrous nitrosyl haem adduct of cytochrome *o* for use in subsequent saturation experiments.
4. To determine the spatial organisation of the prosthetic groups of cytochrome *o* using the physical techniques of EPR and EXAFS.
5. To investigate the origin of the split γ absorption band in the visible light spectrum and characterise more fully the optical spectrum of purified cytochrome *o*.
6. To determine the copper complement of cytochrome *o*.

Notes to Table 1.4

(1) oxidases of the *bo*-type refer to those which contain *b*-type haem only; *co*-type enzymes contain, or are closely associated with, *c*-type cytochrome.

(2) Georgiou, *et al.*, 1988a

(3) 2 CO binding sites, possibly two cytochrome *o* components (Matsushita *et al.*, 1987).

(4) UQ-2 proved to be the most efficient substrate for this enzyme.

(5) likely that higher oxidation rates will be achieved in situ using other physiological ubiquinol species (e.g. *E. coli*; Q-8).

(6) appears to be closely associated to a cytochrome *c* (E_m = +260mV), but unclear whether this species could function as the physiological reductant.

(7) Matsushita *et al.*, 1982

(8) Frond & Anthony, 1984

(9) Yang *et al.*, 1979; see also Yang, 1986

(10) Hudig & Drews, 1984

(11) Sone *et al.*, 1990

(12) copper reported to be associated with enzyme (Shagger *et al.*, 1985).

(13) confirmed as not being able to pump protons

(14) a soluble *o*-like pigment acting as a bacterial haemoglobin (Wakabayashi et al., 1986)

(15) closely associated with cytochrome c_{554} (Yang, 1982)

Table 1.4
Cytochrome o from other sources

Type (1)	Source	Subunits (MWt) x10^3	electron donor	E_m (mV)	λ_{max} (nm)	notes
bo	*E. coli*		quinol		555-558.5 & 562-564	(6)
	Vitreoscilla	4 (55,35,19,10)	quinol	+165	---	(2)(5)(12)
	Vitreoscilla	2(13.5,13.5)	quinol	+118,-122		(14)
	G. suboxydans	4 (76,35,21,15)	quinol	---	558,562	(3)(4)(5)
co	*A. vinelandii*		cytochrome c(6)	-18	558	(9),
	P. aeruginosa		cytochrome c	+25	561	(7)(15)
	M. methylotrophus		cytochrome c			(8)
	R. capsulata		cytochrome c			(10)
	PS3	2(60,30)	cytochrome c		558.5	(11)(13)

CHAPTER TWO

Materials & Methods

2.1 *The organism*

The *Escherichia coli* strain used in this study was RG145/pRG110 (F⁻ *rpsL thi gal nadA cydA2 lon100 cyo sr1300::Tn10 recA*). pRG110 contains a 5·7 kb SphI-SalI fragment of the *E. coli* genome carrying the *cyo* gene cloned into pBR322 (Au & Gennis, 1987). This strain was generously provided by Dr. R.B. Gennis (University of Illinois). The organism was maintained in 15% glycerol/75% Luria broth, pH 7.0 at -70°C and sub-cultured onto Nutrient Agar plates containing 100 $\mu g ml^{-1}$ ampicillin when required.

2.2 *Cell growth conditions and media*

Sub-cultured cells were inoculated by loop-transfer into 500 ml shaker flasks containing 150 ml of the desired growth medium supplemented with 100 $\mu g ml^{-1}$ ampicillin and grown aerobically for 18-20 hours at 37°C. Alternatively, an inoculum was taken from these flasks and used for inoculation of a fermentor with a working volume of 12 l. *E. coli* strain RG145 were aerobically grown in batches on a rich glucose medium which contained high levels of iron (III) chloride. To all media 0.1 ml of 0.5 M magnesium (II) chloride was added after autoclaving. The growth media used are described below. If larger volumes of cells were required batches were grown at the University of Dundee in a 500l fermentor. The 500l cell broth was harvested by tangential flow across a 0·22µm microporous Durapore filter cassette system. Approximately 4 litres of cell slurry was recovered and washed in the tangential flow system with 20l

40mM phosphate buffer, pH 7·5.

2.2.1 *Rich Glucose Medium*

This contained the following, l^{-1}: 5g, *di*-potassium hydrogen phosphate; 3g, potassium *di*-hydrogen phosphate; 5g, *d*-glucose; 2g, tryptone; 2g, yeast extract; 0·5g, acid hydrolysed casein; 1g, ammonium sulphate; 5mg, copper (II) sulphate; 2mg, iron (III) chloride; 1·0 ml of a solution containing 50 mM sodium selenite and 50 mM ammonium molybdate; 1·0 ml of trace elements (see section 2.2.6). The pH of this medium was adjusted to between 7·0 and 7·5 with potassium hydroxide, if required.

2.2.2 *CR-glycerol Medium*

This medium contained the following, l^{-1}: 5g, *di*-potassium hydrogen phosphate; 3g, potassium *di*-hydrogen phosphate; 2.25g, potassium hydroxide; 10 ml, glycerol; 0·5g, acid hydrolysed casien; ammonium sulphate; 1·0 ml of the selenite /molybdate solution (see section 2.2.1); 1·0 ml of the trace elements solution. The pH of this media was adjusted to between 7·0 and 7·5, if required.

2.2.3 *Luria broth*

This medium contained the following, l^{-1}: 10g tryptone; 5g yeast extract; 0.5g sodium chloride and adjusted to pH 7.0 with NaOH. A 15% (v/v) solution of glycerol in Luria broth was used for stock cultures.

2.2.4 *Nutrient Agar*

Nutrient broth, containing 1% (w/v) of bacterial agar (Grade 1), was autoclaved before being poured onto plates or used for slopes to maintain strains. The antibiotic, ampicillin, was added to 100 $\mu g ml^{-1}$ to ensure plasmid amplification.

2.2.5 *Trace elements solution*

This solution contained the following: 3mM iron (III) choride; 2 mM manganese (II) chloride; 1·2 mM cobalt (II) sulphate; 4·5 mM boric acid; 15 mM, zinc (II) chloride. In order to prevent contamination 1 ml of chloroform was added to each litre of solution and the pH was adjusted to 7·0.

2.2.6 *Copper Limited Growth*

For batches of RG145 that required controlled amounts of copper in the growth medium, CR-glycerol medium was used (which has no added copper, c.f. Rich Glucose Medium), as described before, with trace elements added, as described, except that the zinc concentration was $^1/_{10}$ that used for normal rich glucose medium. The zinc concentration was reduced to prevent substitution of this metal into the bi-metallic centre.

2.3 *Cell harvesting*

Cells were harvested using continuous flow on a continuous flow rotor running at 18 000 rpm in a MSE High Speed 18 centrifuge. Cells were washed twice in 50 mM

BES/KOH, pH 7·0 buffer (0-4°C) using a Sorvall RC-5B Superspeed centrifuge (Dupont) at 9 000 x g for 10 minutes. When whole cells were required the cells were resuspended in a minimum volume of 50 mM BES/KOH, pH 7·4 buffer and used immediately.

2.4 *Preparation of membrane particles (e.t.p.)*

Frozen cells were thawed and resuspended in 100mM TES/KOH, pH 7·5 containing 5 mM magnesium sulphate, 10mg of bovine spleen deoxyribonuclease II and 1mg PMSF (dissolved in ethanol) and stirred, on ice, for 15 minutes before 20mg of lysozyme and EDTA (di-sodium salt), to a final concentration of 10 mM, were added. Cells were broken by passing the slurry of cells through a French Pressure cell (Aminco) operating at 15 MPa. Cell debris and remaining whole cells were removed by centrifugation at 9 000 x g for 15 minutes (4°C). The supernatant was retained and the membrane fragments pelleted using a Prepspin 50 ultracentrifuge operating at 125 000 x g for 60 minutes (4°C). The membrane fragments were washed by resuspension of the pellet in 100 mM TES/KOH, pH 7·5 buffer containing 5 mM EDTA and recentrifugation at 125 000 x g for 60 minutes. Where stated a second wash was performed before the membrane fragments were resuspended, by homogenisation, in a minimal volume of the required buffer and frozen by dropping the slurry into liquid nitrogen by way of a pipette. The membrane fragments were finally stored under liquid nitrogen until required.

2.5 *Optical spectroscopy*

Optical difference spectra of *E. coli* were recorded using a split beam spectrophotometer constructed at the Department of Biochemistry and Microbiology at the University of St. Andrews. Both room- and low-temperature spectra could be recorded using this instrument. For other spectrophotometric assays a single beam spectrophotometer (version CE272, Cecil Intruments) was used.

Repetitive wavelength scanning and carbon monoxide difference spectra (flash photolysis) were recorded on a scanning dual-wavelength Aminco-Chance DW2 spectrophotometer (reference wavelength, 575nm) which had a digital memory facility to store and subtract scans. A suspension of cytochrome *o* (final concentration, approx. 7µl) was reduced by the addition of 1-2µl of a saturated solution of dithionite in a cuvette with internal lightpath of 3mm and incubated for 2 minutes. The suspension also contained 30% ethylene glycol to act as cryosolvent. To produce the carbon monoxide-inhibited enzyme complex, the suspension was bubbled with carbon monoxide gas via a pasteur pippete dipped in antifoam (Sigma) to prevent excessive bubbling. The cuvette was placed in tin-foil and equilibrated at 25°C in an ethanol/solid CO_2 bath. When required, the cuvette was transfered, protected from light, to the sample chamber of a dual-wavelength scanning spectrophotometer which could be thermostatically controlled to the desired operating temperature by a liquid

nitrogen transfer line and heater unit. The spectrum of the carbon monoxide-inhibited enzyme could be stored in the digital memory of the spectrophotometer. The reaction between carbon monoxide and cytochrome *o* was initiated by the photolysis of carbon monoxide from the ligand inhibited enzyme by a focused projector lamp.

2.5.1 *Spectrophotometric redox titrations*

Conventional redox titrations were carried out anaerobically under Argon gas in a buffer system containing potassium salts of EDTA (2mM) and phosphate (50mM), pH 7·2. For titrations at other pH values 50mM MES (pH 6.0) or 50mM TAPS (pH 8.0) replaced phosphate. Enzyme concentrations were approximately 10μM final and the redox mediators used were; anthraquinone-2-sulphonate, anthraquinone-2,6-disulphonate, methyl-viologen, benzyl-viologen, phenazine methosulphonate, phenazine ethosulphonate, 2-methyl-1,4-benzoquinone, 2,6-dimethyl-1,4-benzoquinone, trimethyl-1,4-benzoquinone, duroquinone, hexammineeruthenium chloride, diaminodurene, 5-hydroxy-1,4-napthoquinone, 2-hydroxy-1,4-naphthoquinone, 1,4-naphthoquinone-2-sulphonate and pyocyanine, all at between 20 and 100μM except pyocyanine (5μM). Catalase was also present at 90 units/ml. Potentials were varied with anaerobic additions of ferricyanide, dithionite or NADH. Scans were run 3mins from the time of additions to allow for full equilibration. Data was taken randomly in both the oxidative and reductive directions to compensate for any hysteresis in the system

(and as a check on any irreversibility) and the average potential of the system was taken during a scan. Ambient redox potentials were measured using a glassy carbon rod (Sigradur K, Sigri Ltd.) sealed into a PTFE sleeve (Goodfellows, Cambridge) with epoxy resin or vaseline. The reference electrode was a conventional silver chloride-coated silver wire immersed in 3M KCl connected to the test solution via a 3M KCl salt bridge. The electrode was calibrated against quinhydrone (296mV, pH7) before and after titrations. To optimise detection scans in the visible range (below 700nm) were made with a photomultiplier screened with a Schott glass GG495 filter, but detection in the near IR used a $1cm^2$ photodiode. Carbon monoxide gas replaced Argon in those titrations requiring the presence of carbon monoxide.

2.6 *EPR spectroscopy*

EPR spectra were obtained using a Bruker ER 200D electron paramagnetic resonance spectrometer (Bruker Analytische Messtechnik GmbH, Silberstreifen, D-7512 Rheinstetten 4, FRG) equipped with a variable temperature cryostat and liquid helium transfer line (Oxford Instruments, Osney Mead, Oxford, England). Helium flow rate and cryostat temperature were controlled using a DTC2 temperature controller (Oxford Instruments).

2.6.1 *EPR sample preparation*

Samples for epr spectroscopy were prepared in quartz

tubes with an internal diameter of 3 mm. Rapid freezing of the samples was effected by immersion of the tubes in a mixture of isopentane and methylcyclohexane (1:4, v/v) kept at approx. -80°C with a liquid nitrogen cold finger. The samples were stored under liquid nitrogen until required.

2.6.2 *Potentiometric redox titrations employed for EPR spectroscopy*

Redox titrations were performed as described by Dutton (1978) in 100mM BES/KOH, 2mM EDTA, pH 7.0 buffer at 30°C. The oxidation reduction mediators used at 50 - 100μM were: tetrahydroquinone, N,N,N',N'-tetramethylene-p-phenylene -diamine (TMPD), safranine, anthroquinone 2,6-disulphonate, resrufin, duroquinone, N,N-dimethyl-p-phenylene diamine, 1,4-naphthoquinone-2-sulphonate, tetrachlorohydroquinone, dibromophenolindophenol, phenazine methosulphate (PMS), 1,2-naphthoquinone and ascorbate. Additions of aliquots of saturated ferricyanide were used to oxidised the sample; saturated sodium dithionite was employed as the reductant. The ambient redox potentials (E_h) were measured using a combination platinum/reference (Pt/PtCl) redox cell with a platinum disc-face configuration (Russell pH-Ltd, Auchtermuchty, Scotland). The sample was kept anaerobic by flushing the redox vessel with oxygen-free nitrogen which had first been passed through a Nil-Ox oxygen scrubber (Jencons Scientific).

2.7 *Preparation of DyEDTA and LaEDTA solutions*

These solutions were prepared as 100 mM stock solutions by mixing 400 mM $DyCl_3$ (or $LaCl_3$) with 600 mM Na_2EDTA;

$$DyCl_3 + Na_2EDTA \text{ -----> } Dy_2(EDTA)_3 \quad \text{-------} \quad 2.1$$

2.8 *Preparation of sphaeroplasts for sidedness studies*

Sphaeroplasts where prepared in order to determine the effect of dysprosium on right-side-out enclosed *E. coli* membranes of RG145. Sodium EDTA (10mM) and lysozyme ($0.5mgml^{-1}$) were added to a cell suspension (approximately $30mgml^{-1}$ in a 200mM sucrose solution for osmotic support) and stirred gently for 30 secs. The lysozyme suspension was left for a further 20 mins at room temperature without stirring.

2.9 *Oriented multilayer preparation*

Oriented multilayers were prepared as previously described by Blum *et al.*, (1978a). Membrane preparations from RG145 were diluted to approximately 5mg protein ml^{-1} in 4mM TES, pH 7·5 buffer and were deposited onto nitrocellulose coated acetate sheets by centrifugation in a swing-out rotor for 90 minutes at 95 000 g using inserts machined from polycarbonate to give a flat internal bottom to the centrifuge tube. The multilayers were dried under controlled conditions in the presence of saturated ammonium sulphate solution over 48 hours. For reduced samples the multilayers were dried under a nitrogen gas atmosphere in a

desiccator under reduced pressure. After drying the acetate sheets were cut into thin (<3mm) strips and inserted into epr tubes. For increased signal-to-noise ratios two strips were inserted with the plane of the multilayers kept parallel. Reduction and formation of the nitrosyl ferrohaem *o* adduct (haem *o*-NO) was accomplished by immersing the inserted multilayers in 50% glycerol containing 20mM sodium nitrite and a few grains of sodium dithionite, before freezing and storage in liquid nitrogen after 7 minutes. The angle between the multilayer plane and the incident magnetic field was measured using a pointer and a protracter.

2.10 *Purification of cytochrome o ubiquinol oxidase from E. coli strain RG145*

Purified cytochrome *o* was obtained using a method provided by Dr R.B. Gennis (University of Illinois). Membranes obtained from RG145 strain were resuspended in 75ml of 50mM potassium phosphate, pH7·5, using a tissue homogeniser and mixed with an equal volume of 10M urea which was freshly prepared at room temperature. The urea-membrane solution was centrifuged at 150,000g for 1 hour in an MSE Prepspin 50. The washed pellet contained two distinct layers; the upper red translucent layer was removed and suspended in 70ml phosphate buffer, pH7·5. To this 30ml of 6M cholate (20% final, pH 7.8) was added and left stirring on ice for 30mins before being centrifuged at 150,000g for 1 hour. The cholate washed pellet was washed

by centrifugation in 75mls of ice cold 50mM phosphate buffer, pH7·5 and the pellet resuspended in 40mls of 50mM phosphate, 0·1% Triton X-100, 1·0% *n*-octyl-β-glucopyranoside, pH 7·5 and centrifuged at 150,000g for 90mins. The red supernatant, containing the solubilised cytochrome *o* complex, was retained ready for column chromatography.

2.10.1 *Column chromatography*

The red supernatant was retained and applied to a DEAE-Sepharose CL-6B column. The solubilized fraction contained approximately 1.25mgml^{-1} protein and was applied to a 40ml column (2.5 x 10cm). This corresponds to about 1.25mg of protein per ml of bed volume.

The column had been pre-equilibrated with 5mM tris-HCl, 0·1% Triton X-100 (PC grade, Sigma), pH 8.0, before application of the protein. After application of the sample, the column was washed with one bed volume of equilibrating buffer. Cytochrome *o* was then eluted with 400ml of 10mM Tris-HCl, 1% Triton x-100, pH 8.0, containing a linear gradient of 0-300mM sodium chloride at a flow rate of 15ml per hour.

The fraction containing cytochrome *o* eluted with 200-220 mM sodium chloride as a single peak. Fractions containing ubiquinol 1 oxidase activity were pooled and dialysed against 50mM potassium phosphate, 1% triton x-100, pH 7.5, overnight at 4°C. Cytochrome *o* was then frozen in liquid nitrogen and stored at -80°C. The protocol for

isolating cytochrome *o* for use in EXAFS experiments was changed in order to reduce the effect of contaminating chloride ions which cannot be distinguished from sulphur atoms by this method. All chloride containing solutions were replaced with the appropriate sulphate salt. Elution of the enzyme from the column usually required higher salt concentrations, typically the protein could be eluted with 250 - 280mM sulphate.

2.10.2 *Detergent Exchange*

The detergent can be exchanged from triton x-100 to sarkosyl by use of a hydroxyapatite column. A hydroxyapatite column (1.5 x 5cm) was equilibrated with 10mM potassium phosphate, 0.05% sarkosyl, pH 7.5. Cytochrome *o*, either directly from the DEAE-sepharose column or after dialysis, was applied to the hydroxyapatite column. The column was washed with a gradient of 25ml of 10mM potassium phosphate, 0.05% sarkosyl, pH 7.5, to 500mM potassium phosphate, 0.05% sarkosyl, pH 7.5. Cytochrome *o* was eluted as a single peak with 700mM potassium phosphate, 0.05% sarkosyl, pH 7.5. The red fractions were pooled, dialysed against 50mM potassium phosphate, 0.025% sarkosyl, pH 7.5, frozen in liquid nitrogen and stored at -80°C.

2.11 *EXAFS spectroscopy*

EXAFS spectra, at the Cu K-edge, were recorded at the SERC Synchrotron Radiation Source at the Daresbury Laboratories, Warrington, England, on the EXAFS station

8.1. Collimation was via a silicon monochrometer. All data was taken at low temperature (77K) using a liquid nitrogen transfer line. Data was taken as fluorescence excitation spectra and measured by 12 sodium iodide scintillation counters. The reported EXAFS spectra are the sums, after normalisation, of at least 5 scans, each scan requiring at least 80 minutes. Throughout the analysis k-squared weighting was applied, and distances and Debye-Waller factors were refined by iteration.

2.12 *Sample preparation for EXAFS*

Purified cytochrome *o* ubiquinol oxidase (see section 2.10) was concentrated in an Amicon ultrafiltration unit, packed with ice, using a PM10 filter, until the enzyme was to a concentration of around 0·5-1·0 mM. The concentrated enzyme was either reduced or oxidised, using a few crystals of sodium dithionite or ammonium persulphate, respectively, before being transfered to an aluminium EXAFS sample cell. The EXAFS cells had an internal volume of 175 µl and had been windowed with thin Mylar sheet. Reduced samples were allowed to go anaerobic before freezing in liquid nitrogen. Samples were stored under liquid nitrogen until EXAFS spectra were recorded.

2.13 *Synthesis of ubiquinone-1 (Q1)*

The synthesis of ubiquinone was performed using a procedure provided by Dr. Robert B. Gennis (University of Illinois) with a number of modifications. One gram of UQ-0

was dissolved in 15 ml of ethanol and mixed with 3 ml of 0·1 M potassium phosphate, pH 7·5, buffer. This was then reduced with sodium dithionite until the solution went light yellow/colourless, before being extracted three times with 50 ml ether. After extraction, and drying under nitrogen gas, a yellow residue is produced (light yellow) which was dissolved in 15 ml of dioxane and mixed with 3g of potassium bisulphite, under nitrogen gas. 10 ml of a solution containing 3-methyl-2-buten-1-ol and dioxane (1:1, v/v) was added dropwise to the benzoquinone mixture over 3 hours under nitrogen gas at 75-80°C. After cooling, the mixture was filtered and any solvents remaining in the filtrate were removed under a flow of nitrogen gas. The resulting residue was redissolved in 100 ml ether. To this 5g of silver (II) oxide and 2g of anhydrous magnesium sulphate were added and the mixture was stirred overnight and then filtered, the filtrate was concentrated in a rotary evaporator. The oil was dissolved in 100 ml of petroleum ether and extracted three times with 100 ml of water. The petroleum ether solution was dried over anhydrous sodium sulphate, filtered and concentrated yielding a red oil. The oil was dissolved in hexane and put on a column of magnesium silicate. This was washed with 200 ml of hexane and given a further wash with 2% ethanol in hexane. The eluant was dried under nitrogen gas and the resulting red oil dissolved in ethanol. Ubiquinone-1 was reduced using aliquots of sodium borohydride. The concentration of ubiquinone-1 was calculated using an

extinction coefficient of 5 $mM^{-1}cm^{-1}$ at 289 nm.

2.14 *General techniques*

2.14.1 *Oxidase Activity*

Substrate dependent oxidase activities were measured at 30°C using a Clark-type oxygen electrode (Rank Brothers) fitted to the base of a glass reaction vessel constructed by Mr C. Smith at the University of St. Andrews, St. Andrews. The reaction vessel had a working volume of 2·55 ml and had a ground glass stopper with a capillary hole through which additions could be made while limiting the back-diffusion of oxygen from the atmosphere. The buffers used were; pH 6.8-7.4, 50 mM TES; pH 7.5-8.0, 50mM BES; pH 5.0-6.0, 50mM KH_2PO_4; pH <5.0, 50 mM beta-alanine. The protein concentrations were approximately 0·25 mg (protein) ml^{-1}, reactions were initiated with the addition of 200µM (final) ubiquinol 1 (UQ_1H_2). Quinone was reduced with additions of borohydride. Basal oxidation rates were measured before addition of substrate and subtracted from substrate oxidation rates.

2.14.2 *Protein Determination*

Protein determinations were performed using the method of Lowry *et al.* (1951) with the inclusion of 1% (w/v) of sodium dodecyl (lauryl) sulphate to the reagent. The reagents and blanks were kept at 40°C throughout the assay. Bovine serum albumin (BSA) was used as a standard and a

standard curve was set up for each assay.

2.14.3 *SDS-Polyacrylamide gel electrophoresis analysis*

Discontinuous Tricine sodium dodecyl sulphate-polyacrylamide gel electrophoresis was used for the separation of cytochrome *o* subunits using a method by Schagger & Jagow (1987). The acrylamide/bisacrylamide mixture was made up as a 49.5% total acrylamide stock, with the crosslinker (bisacrylamide) constituting 1.5% of the total concentration. A 10% acrylamide resolving gel was used containing; 0.1% SDS; 13% glycerol (w/v); 0.375% poly(acrylamide); 0.05% ammonium persulphate for polymerisation, in 1M Tris-HCl, pH 8.45. A 4% acrylamide stacking gel (total acrylamide to crosslinker ratio as per resolving gel) without glycerol was used. The anode buffer was; 0.2M Tris-HCl, pH 8.9. The cathode buffer was; 0.1M Tris, 0.1M Tricine, 0.1% SDS. Protein samples were prepared by incubation at 40°C (30 minutes) in 4% SDS, 12% glycerol (w/v), 50mM Tris-HCl, pH 6.8. Coomassie blue G was used as a tracking dye.

2.15 *Chemicals*

Redox dye mediators were either obtained from the Aldrich Chemical Company or Koch-Light Laboratories. All gases were obtained from BOC. Yeast extract, tryptone and acid hydrolysed casein were obtained from labM. Dysprosium chloride and lanthanum chloride were obtained from

Koch-Light Laboratories. Bacteriological Agar was obtained from Oxoid.

All other chemicals were obtained from BDH or Sigma.

Succinate-cytochrome c oxidoreductase and cytochrome c oxidase were gifts from Drs Peter R. Rich and A. John Moody, Glynn Research Institute, Bodmin, Cornwall.

CHAPTER THREE

General characterisation of cytochrome o from purified and in situ preparations

3.1 Introduction

Chapter 1 (section 1.4) presented a review of the experimental data to date on cytochrome *o* from both purified and *in situ* preparations. The principal aim of this chapter will be to further characterise cytochrome *o* from both these source types, using EPR and optical spectroscopy.

The wealth of experimental evidence available shows the great similarity between both cytochrome *o* from *E. coli* and cytochrome aa_3, linking these enzymes both structurally and functionally (for review see Ingledew & Bacon, 1991). Gennis and colleagues have recently suggested these enzymes are members of a "superfamily" in which the importance of certain very similar structural motifs is becoming increasingly apparent (Chepuri *et al.*, 1990a; Lemieux *et al.*, 1991). Thus, when studying cytochrome *o*, two primary concerns must be addressed. Firstly, the biology of cytochrome *o* must be determined, and secondly, this biology must be related to cytochrome *c* oxidase in order that the degree to which these similarities extend, can be established. To this end the results from this study will be related to data from cytochrome *c* oxidase. It is also important to focus attention on the differences between these two very closely related enzymes, as it is these that may prove to be of greater importance in the long run.

As has been discussed in section 1.5 purified cytochrome *c* oxidase can exist in two states. The "resting" form has a number of features which are distinct from those

of the "pulsed" form. These include differences in ligand binding kinetics, internal electron transfer rates, optical spectra (reviewed in Antonini *et al.*, 1981) and dioxygen reaction site structure (Kumar *et al.*, 1988). Turnover (i.e. reduction followed by re-oxidation) results in "resting" cytochrome *c* oxidase being converted to the "pulsed" enzyme which slowly returns to the "resting" form with time. The rate of return of "pulsed" to "resting" state can be increased by lowering the pH and decreased if there is a source of electrons. However, under normal turnover and physiological conditions, the "resting" enzyme is unlikely to be formed. It might be argued, therefore, that studying preparations with significant amounts of "resting" or "slow" enzyme could be misleading; only recently have preparative protocols, in which homogeneous preparations of cytochrome *c* oxidase with high percentages of fast enzyme, been produced (Brandt *et al.*, 1989). Much of the biophysical evidence collected on cytochrome *c* oxidase before this time must be viewed in light of this. On the other hand, addition of formate to "pulsed", or "fast", cytochrome *c* oxidase preparations induces an enzyme with "resting", or "slow", characteristics. This chapter will deal with whether or not cytochrome *o* exists in more than one form when purified.

The use of nitroxide spin labels in the study of biological systems, coupled to low temperature EPR spectroscopy, has enhanced our understanding of these systems greatly (for more detailed discussion see Knowles *et al.*, 1976). Likewise, nitrosyl (NO) adducts of

metalloproteins have yielded information on many proteins. The ability of cytochrome *o* to reduce nitrite and bind nitric oxide has meant that this relatively sensitive tool can also be utilised to study this enzyme. The formation of the nitrosylferrohaem *o* complex by the addition of nitrite or hydroxylamine will be examined.

3.2 Results and Discussion

3.2.1 *Characterisation of cytochrome o*

A number of groups have isolated cytochrome *o* from *E. coli* where the subunit composition has been found to vary from 2 (Kita *et al.*, 1984a), in the earlier studies, to 4 (Kranz & Gennis, 1983; Matsushita *et al.*, 1983; Matsushita *et al.*, 1984; Georgiou *et al.*, 1988a) including one band in PAGE analysis being present as a duplex (Withers & Bragg, 1990). Figure 3.1 shows a SDS-PAGE analysis of cytochrome *o* as isolated by the method described in Chapter 2. Three bands are observed with apparent molecular weights of 44, 32 and 17 kDa. A fourth subunit is sometimes observed migrating with an apparent molecular weight of 20-25 kDa. There was no evidence for the expression of a fifth subunit implicated by the presence of an additional ORF (*cyo*E) in the *cyo* operon (Chepuri *et al.*, 1990a). It is possible that this gene product is involved in transcriptional processing and transport and is lost in the final inserted enzyme complex.

As an initial study on the purified preparation used in this research (see Section 2.10) the pH dependence of the quinol oxidase activity was examined. The enzyme turnover was measured polarographically in a Clarke-type oxygen electrode and the reaction was initiated by the addition of ubiquinol 1 (see Section 2.12 for protocol of UQ 1 synthesis). There was appreciable activity between pH 5 to pH 9.4 with maximum activity (turnover 430 sec^{-1}) at pH 7.8 (Figure 3.2). The temperature dependence was also determined

Figure 3.1

SDS-PAGE electrophoresis of purified cytochrome o from E. coli strain RG145

Gel electrophoresis of purified cytochrome *o* in the presence of sodium dodecyl sulphate in 10% polyacrylamide (see Materials & Methods). BDH molecular weight standards (76 - 16.3 kDa) were used. Three bands are observed with a fourth band sometimes present, although not seen here. This band is often missing from cytochrome o preparations and may be easily lost from the gel matrix during washing (J. Horrocks, personal communication). Lane I, molecular weight standards; Lane II, 5µl (1mg cytochrome *o* ml^{-1}) protein; Lane III, 10µl (1mg cytochrome *o* ml^{-1}) protein.

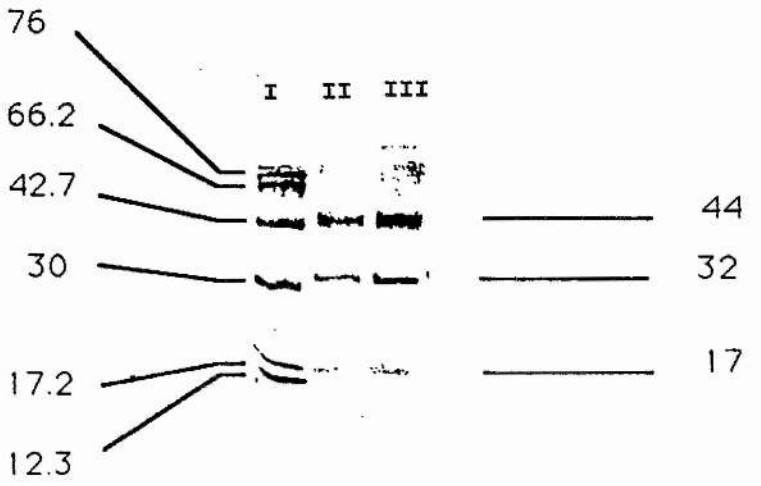
76
66.2
42.7
30
17.2
12.3
I
II
III
44
32
17

Figure 3.2

pH dependence of quinol oxidase activity

Data on the dependence of quinol (UQ_1H_2) oxidase activity of cytochrome *o* are shown. Initial oxidase activities were measured with an oxygen electrode, at 30°C, as described in Chapter 2. Activities are expressed in mol O_2·mol cytochrome o^{-1}·sec^{-1} and are plotted on pH of buffer system. A maximal activity was observed at pH 7.8 (50mM BES). The buffer systems used are given in Chapter 2.

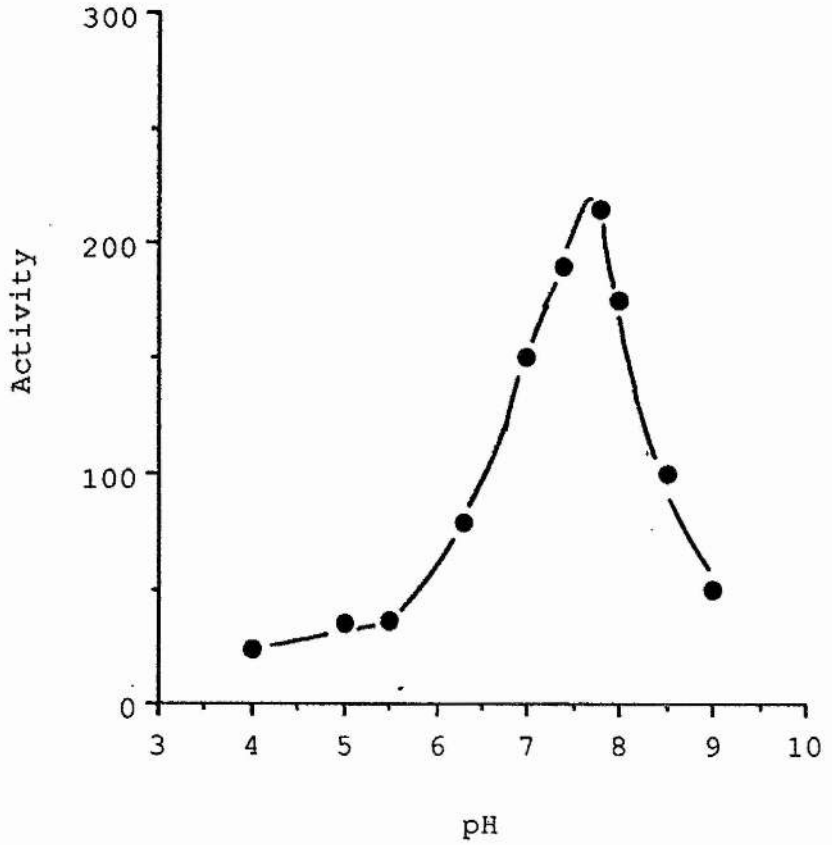
300
200
100
0
Activity
3
4
5
6
7
8
9
10
pH

and maximal activity was seen at 38°C (data not shown). The membrane bound enzyme exhibited similar temperature and pH dependencies to the purified enzyme. The purified enzyme did not show any cytochrome *c* oxidase activity, in agreement with published observations (Matsushita *et al.*, 1984), consistent with the quinol oxidase function of this enzyme (data not shown).

3.2.2 *Effect of copper limitation on growth of E. coli strain RG145*

Copper, an endogenous coordinated ligand of cytochrome *o*, plays an important role in the reduction of molecular oxygen at the bimetallic site. Salerno *et al.*, (1990) reported that membranes obtained from RG145, grown in the absence of added copper, incorporate an enzyme in which the high-spin (haem *o*) centre appears less spin-coupled i.e. acts as if magnetically isolated. It is reasonable to assume that copper is missing from the bimetallic reaction site. However, could the copper-deficient enzyme support growth? In order to answer this a series of batches of RG145 were grown on a non-fermentable carbon source (glycerol) to ensure aerobic respiratory growth (for media, see Methods & Materials). These were supplemented with controlled amounts of copper and the growth rates monitored by the increase in cell density measured spectrophotometrically at 600 nm. Where there was no copper supplement, growth was significantly reduced. A correlation between copper concentration and growth was also observed (Figure 3.3).

Figure 3.3

Effect of copper limitation on the growth of E. coli strain RG145

Data is presented to show the effect of supplemented copper concentration on growth curves. Growth was determined by optical density (600nm) and is plotted against time. Curves are; (open circles), no copper supplement; (closed triangles), 3μM final copper concentration; (open triangles), 30μM final copper concentration (further increases in concentration did not increase growth rate). Medium and growth conditions were as described in methods section.

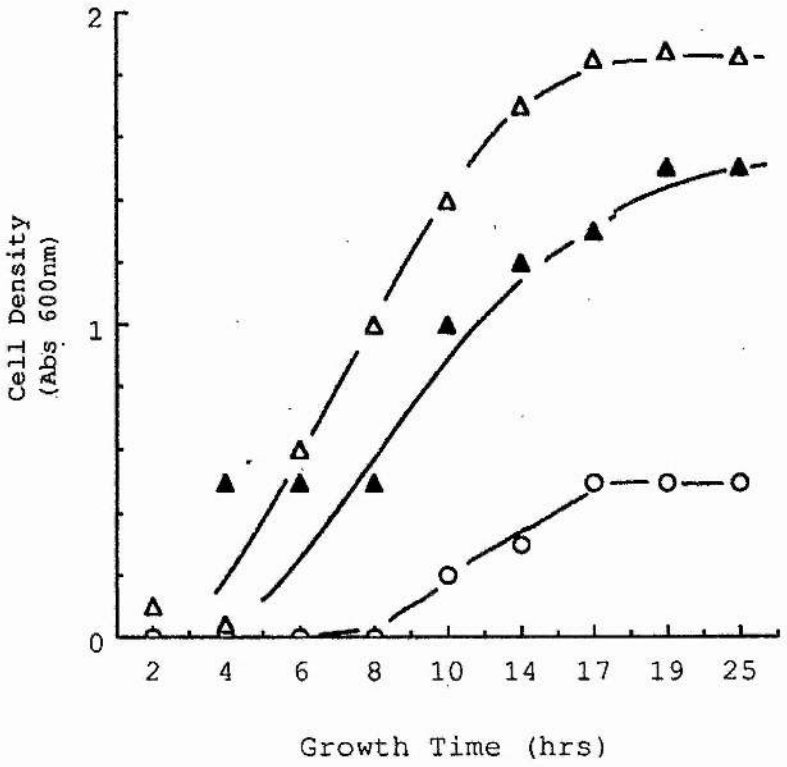
2
1
0
Cell Density
(Abs 600nm)
2
4
6
8
10
14
17
19
25
Growth Time (hrs)

From these findings it is concluded that copper is obviously required for a functional cytochrome *o* complex. However, in cultures where there was no copper-supplement, some slow growth was always observed. For the reason mentioned above, this can be attributed to growth through the respiratory chain and thus coupled through a functional cytochrome *o* (N.B. RG145 is a *cyd*$^-$ strain). It is proposed that the growth observed in the copper-unsupplemented media is the result of copper contamination from growth media products.

Before these findings can be confirmed, more controlled growth studies should be attempted in which copper is chemically extracted from all sources (Giorgio *et al.*, 1963) and very pure growth media used to ensure a total lack of copper contamination.

Studies are currently underway in which it is hoped copper can be substituted by zinc. Whether cytochrome *o*, incorporating zinc at the bimetallic site, can support catalytic activity and thus growth, is not clear. However, by utilising a strain in which there is an alternative terminal oxidase, such as cytochrome *bd*, it is hoped that cell viability can be maintained even if activity in the Zn-substituted cytochrome *o* is slow or non-existent. Use of a Zn-substituted enzyme will allow NMR spectroscopy to be used as a means of analysis in the future and provide further insight into the interactions between high-spin haem *o* and Cu_o.

3.2.3 *Oxidation-reduction potentials of purified cytochrome o*

The EPR spectrum of oxidised cytochrome *o* has a resonance at g=6 attributable to the five coordinated ligand binding haem centre at the bi-metallic centre, i.e., haem *o*. In addition to this, there are resonances at g=3, 2.25 and 1.46 which correspond to the principal g-values of the low-spin haem *b* centre (Salerno *et al.*, 1989 & 1990; Kita *et al.*, 1984a).

Figure 3.4 plots the EPR signal intensity of the low-spin signal measured at g=3 (a) and the high-spin signal measured at g=6 (b) *versus* the ambient potential prior to freezing. The titration was performed on purified cytochrome *o* at pH 7.5 under anaerobic conditions as described in Chapter 2. The high-spin signal follows a bell-shaped titration curve (Figure 3.4b) and increases as the potential is raised to approximately +290mV. The signal then diminishes as the potential is raised, giving rise to a bell-shaped titration curve. The low-spin signal (Figure 3.4a) also increases in intensity as the potential is raised but does not exhibit the loss in signal at higher potentials.

The low-spin data can be fitted with two n=1 components. The lower potential component, contributing approximately 60% of the total signal height, has a mid-point potential of +140mV, whilst the higher potential component has a potential of +240mV and accounts for the remaining 40%. The Nernst curve used to fit the titration

Figure 3.4

EPR redox titrations of haem b and haem o from purified cytochrome o

Plots are shown of the intensities of (a) the low-spin (g=3.01) and (b) high-spin (g=6) signals against the ambient redox potential (E_h) of the poised sample. Redox titrations were carried out at pH 7.0 as described in Chapter 2, with a final protein concentration of approx. 2μM. Titration data are plotted and the representative redox curves used to fit points are shown (solid lines), as discussed in text. The loss of signal intensity in (a) is due to a copper (Cu^{I}/Cu^{II}) transition and antiferromagnetic coupling to the high-spin haem *o* component.

a

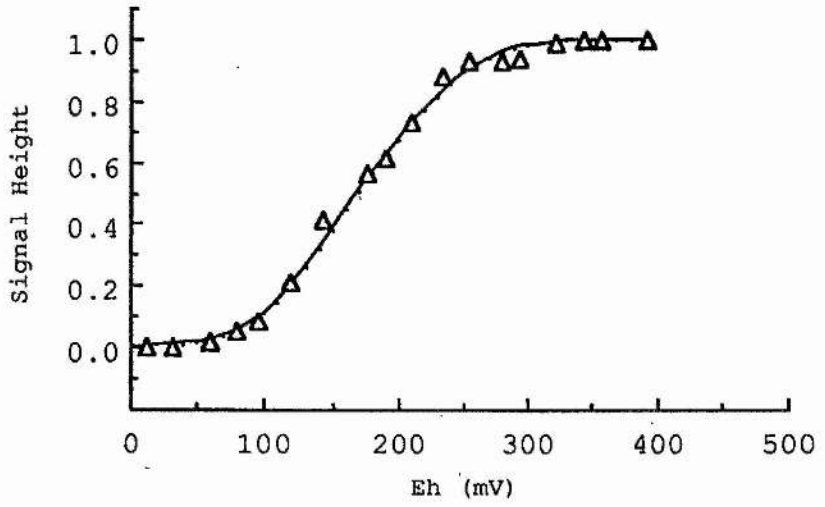
Signal Height
1.0
0.8
0.6
0.4
0.2
0.0
0
100
200
300
400
500
Eh (mV)

b

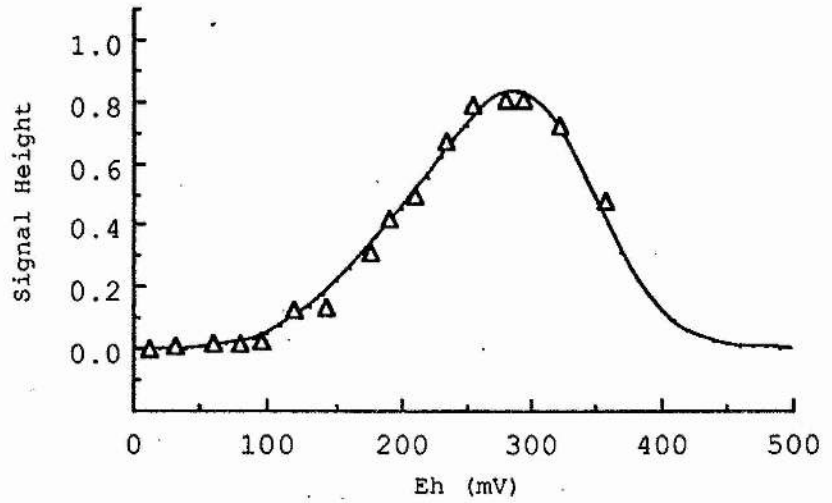
Signal Height
1.0
0.8
0.6
0.4
0.2
0.0
0
100
200
300
400
500
Eh (mV)

data is shown for comparison.

The low potential phase (<+290mV) of the high-spin titration data can similarly be fitted to two n=1 processes (Figure 3.4b). The lower potential component models with a mid-point potential of +150mV and the higher potential component of this phase can be modelled with mid-point potential of +250mV, each contributing to 40% and 60% of the predicted maximum signal height, respectively. The high potential phase, characterised by a loss in signal intensity, was fitted to a single theoretical n=1 transition with a mid-point potential of +350mV. The Nernst curves used to model the high-spin data are also shown.

These data are in excellent agreement with, and confirm, published results from membrane preparations of cytochrome *o* (Salerno *et al.*, 1990). The high-spin feature at g=6 (haem *o*) increases in amplitude as the potential rises, until a second centre, proposed by Salerno *et al.*, (1990) to be the copper at the bimetallic reaction site (hereafter Cu_o because of its association with haem *o*), begins to titrate to the Cu^{2+} state. This results in a tightly spin-coupled system with net even (EPR silent) spin.

Antiferromagnetic spin-coupling was originally suggested by van Gelder and Beinert, (1969) to explain the lack of EPR signals from haem a_3 and Cu_B in cytochrome *c* oxidase at highly oxidising potentials (summarised in Malmstrom, 1979). The potential of these components are so similar that often little high-spin signal is observed in cytochrome *c* oxidase preparations. This made assignment of

the EPR features from cytochrome *c* oxidase difficult in the past (*c.f.* Beinert *et al.*, 1976). Other metalloproteins, for example laccase (a trinuclear copper enzyme), and haemocyanin, also show spin-coupled systems in the oxidised state (see Brudvig *et al.*, 1980 for references).

The simpler potentiometric behaviour of the low-spin feature implies this centre is magnetically isolated from other centres within cytochrome *o*, suggesting separation by at least 10Å. The double wave seen in both high- and low-spin titration data is a function of site interactions and is discussed in relation to optical potentiometric data in Chapter 4. The question of spatial separation of redox centres within cytochrome *o* will be dealt with in more detail in Chapter 5.

3.2.4 *Studies with ligands*

3.2.4.1 *Carbon monoxide*

Purified cytochrome *o* exhibits a broad absorbance peak in the α band at room temperature which can be further resolved into a split band which is slightly assymetrical with λ_{max} at 558nm and 564nm, at 77K (Figure 3.5a). A reduced-*plus*-carbon monoxide *minus* reduced optical difference spectra obtained from purified cytochrome *o*, is shown in Figure 3.5b. This spectrum exhibits a peak at 415nm and trough at 432nm, respectively, in the Soret (γ band). The peak at 415nm is due to the absorbance spectra of the carbon monoxide ligated cytochrome *o*. These values are in

Figure 3.5

Optical spectra of purified cytochrome o

Shown are (a) the low temperature (77K) dithionite-reduced *minus* oxidised difference spectra and (b) the room temperature carbon monoxide difference spectra of purified cytochrome *o*. Enzyme concentrations used were; trace (a) approximately 1.5μM and (b) approximately 3μM. To obtain trace (b), two stoppered cuvettes were filled with protein solution and reduced with dithionite. To one, 30μl of carbon monoxide saturated buffer was added through a capillary hole to produce the carbon monoxide-inhibited oxidase. Spectra were recorded on a split-beam spectrophotometer. Peak positions are indicated above spectra (nm). Bars indicate absorbance (O.D.)

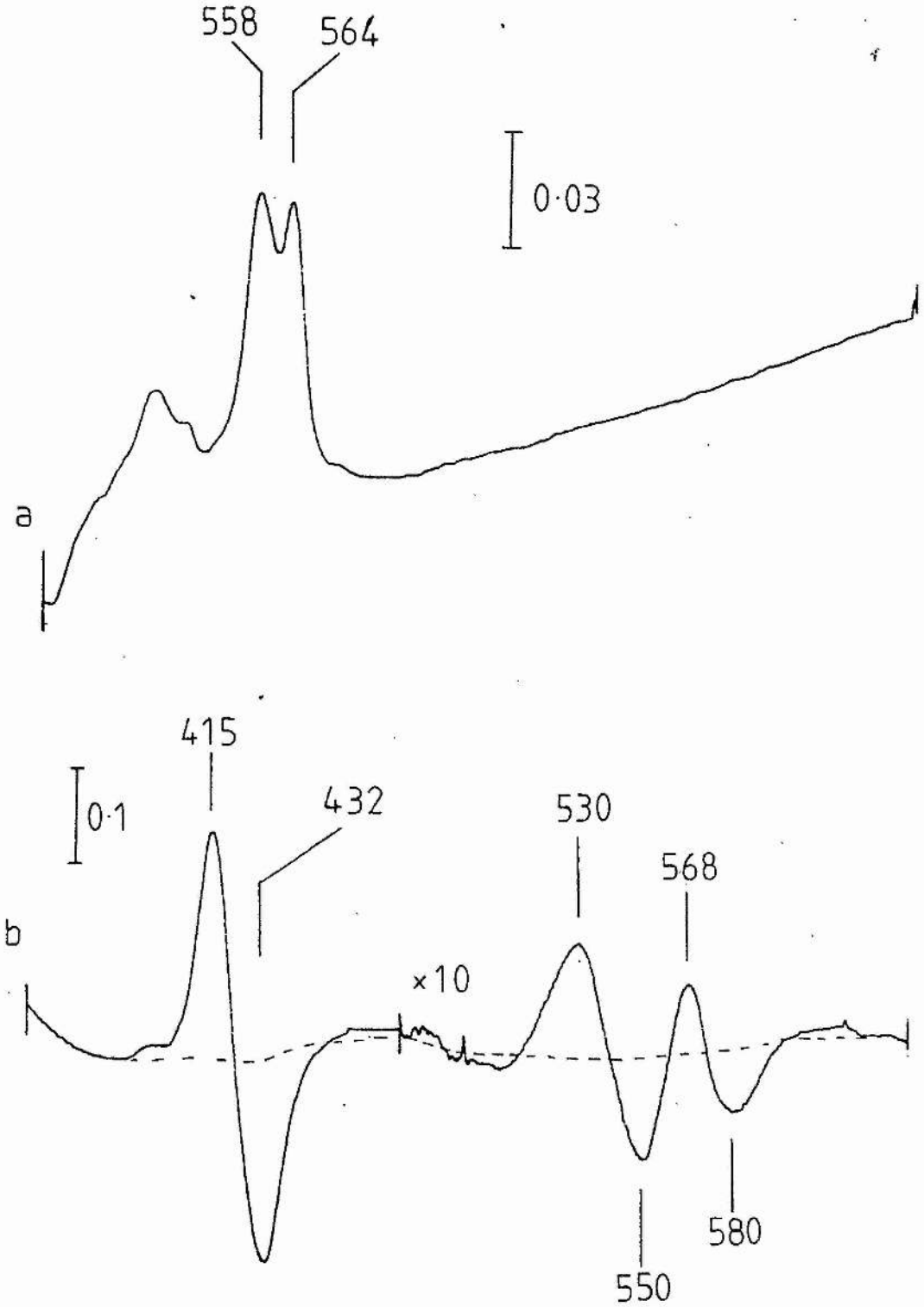
558
564
0·03
a
415
0·1
432
530
568
b
×10
550
580

agreement with previously reported values from membrane preparations obtained from an unamplified strain (Poole *et al.*, 1979b).

In anoxic (anaerobic) conditions, carbon monoxide-inhibited samples kept at low temperatures can be photolysed allowing the reaction of cytochrome *o* with carbon monoxide to be monitored (Caster & Chance, 1959; Chance, 1978; Poole *et al.*, 1979b). Figure 3.6 shows a series of repetitive scans in the Soret region following photolysis of the carbon monoxide-inhibited cytochrome *o* complex at -70°C. The spectra were generated using a scan of the pre-photolysed carbon monoxide-inhibited enzyme as a baseline i.e., the spectra are essentially reduced *minus* reduced-*plus*-carbon monoxide difference spectra, the inverse of Figure 3.5b. Loss of the trough-peak feature (415nm and 432nm, respectively) is due to reassociation of the "free" carbon monoxide onto the high-spin haem *o* after photolysis. Difference spectra, identical to the original immediate post-photolysis *minus* pre-photolysis (equivalent to reduced *minus* reduced-*plus*-carbon monoxide), are obtained upon reflashing the sample (not shown). Thus, the photolysis/reassociation cycle is fully reversible.

Shown in Figure 3.7 is the loss of the trough at 415nm, post photolysis, plotted as a function of time using 450nm as a reference wavelength. At -120°C (Figure 3.7a) there is little reassociation of the ligand, as evidenced by a lack of spectral change towards the baseline after photolysis. Figure 3.7b shows the reassociation of carbon monoxide at

Figure 3.6

Repetitive wavelength scanning of the reaction of carbon monoxide and reduced cytochrome o from E. coli

Purified cytochrome *o* was reduced with dithionite and the spectrum of the carbon monoxide-inhibited oxidase was formed and recorded using 575nm as reference wavelength, as described in Chapter 2. After photolysis, the subsequent difference spectra could be plotted by subtraction of the stored, carbon monoxide-inhibited, spectrum from post-photolysis scans. An initial scan was taken before photolysis to give the base-line, that is, the reduced ligand-bound *minus* reduced ligand-bound difference spectra (dashed line). Indicated is the first spectrum recorded post photolysis (~10 seconds). The second and eighth spectra were recorded 50 seconds and 200 seconds after photolysis, respectively.

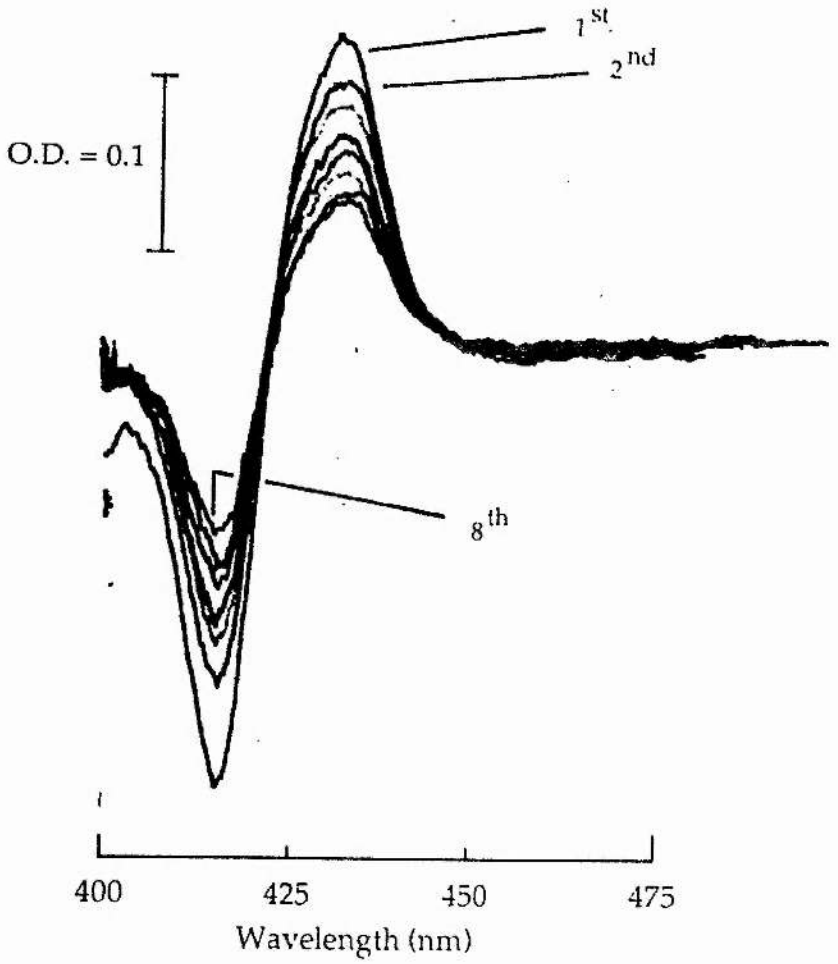
1st
2nd
O.D. = 0.1
8th
400
425
450
475
Wavelength (nm)

Figure 3.7

Reassociation kinetics of the reaction between carbon monoxide and reduced cytochrome o after flash photolysis at various temperatures

The reaction between purified dithionite reduced cytochrome *o* and carbon monoxide was monitored by the difference in absorbance between the carbon monoxide feature at 415nm and reference wavelength 450nm (see Figure 3.4). The reaction was initiated by a 30 second flash from a projector lamp onto the carbon monoxide-inhibited enzyme. The temperature of reaction was -120°C (a), -100°C (b) and -70°C (c). At -70°C the reaction appears bi-phasic as discussed in the text.

a

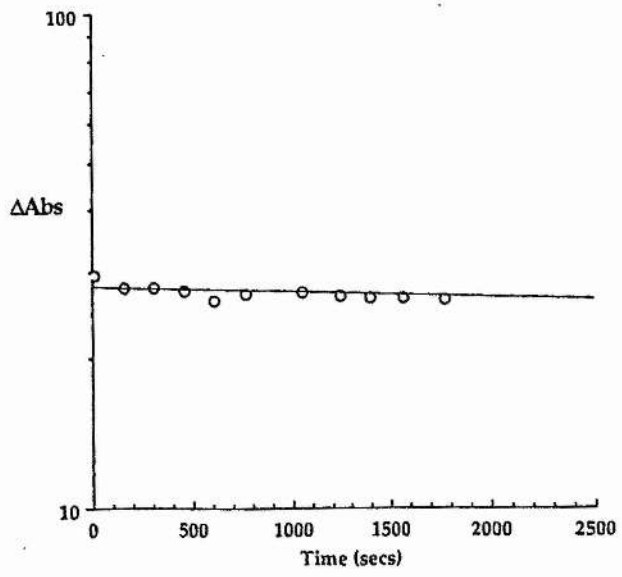
100
ΔAbs
10
0
500
1000
1500
2000
2500
Time (secs)

b

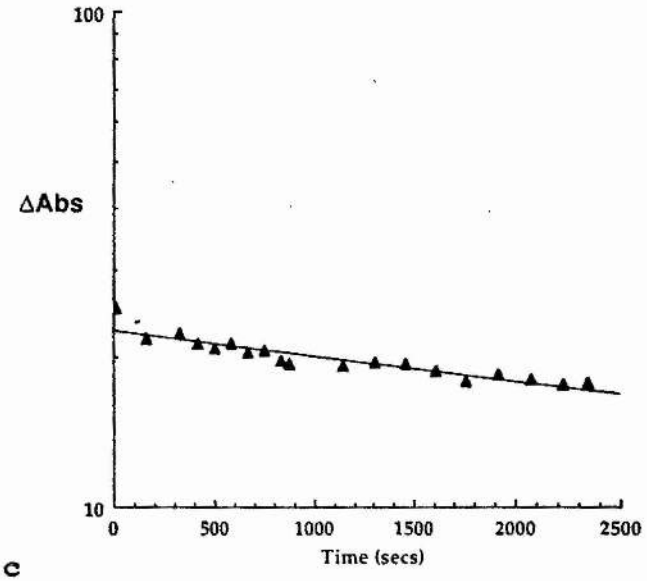
100
ΔAbs
10
0
500
1000
1500
2000
2500
Time (secs)

c

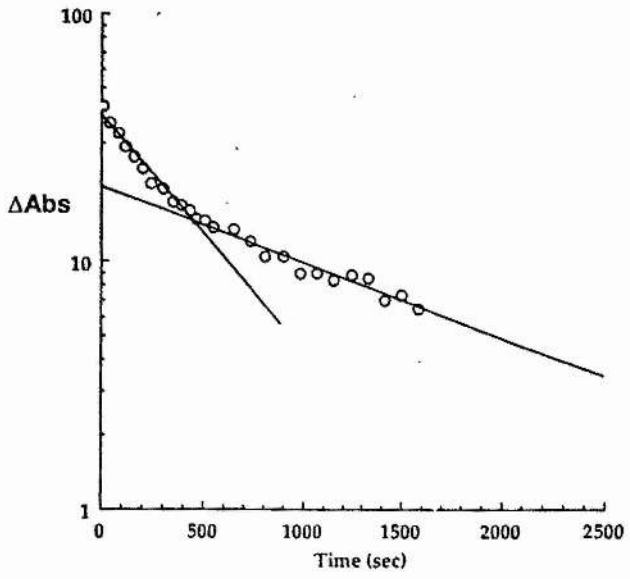
100
ΔAbs
10
1
0
500
1000
1500
2000
2500
Time (sec)

-100°C. At this temperature (and lower) carbon monoxide recombination is extremely slow and difficult to monitor; a half-time of 47 minutes at -105°C has been reported for membrane bound cytochrome *o* (Poole *et al.*, 1979b). On increasing the temperature an enhancement of carbon monoxide reassociation can be seen (Figure 3.7c). The data obtained at -70°C appears to exhibit biphasic binding kinetics with apparent first order rate constants of 7.9×10^{-4} sec^{-1} and ~ 3.0×10^{-5} sec^{-1} for the fast and slow processes of reassociation, respectively.

In cytochrome *o*, as in cytochrome aa_3 (Chance *et al.*, 1975), carbon monoxide binding is slower than in myoglobin, haemoglobin (Iizuka *et al.*, 1974) and cytochrome *bd* (Poole *et al.*, 1982; see also Poole, 1983). Ligand binding to copper, after the photolytic event, may account for the slower kinetics observed in cytochrome aa_3 and cytochrome *o*. Alben *et al.*, (1981) has provided evidence from low temperature FTIR spectroscopy, that carbon monoxide binds Cu_B after photolytic dissociation from haem a_3 in cytochrome *c* oxidase, although this has yet to be established in cytochrome *o*. Further confirmation of the involvement of copper in ligand binding comes from multicopper complexes such as laccase and ascorbate oxidase, where the former has dioxygen reduction catalytic function. Under certain conditions, Poole *et al.*, (1979b) also reported biphasic kinetics in the reaction between carbon monoxide and reduced cytochrome *o* in membrane preparations, although no reasons were put forward as to the source of this behaviour (see

also Poole, 1983). The nature of the biphasic reaction between carbon monoxide and cytochrome *o* is as yet undefined. While carbon monoxide binding to the Cu_o centre probably accounts for the slower rate of reassociation of the ligand (compared to haemoglobin etc.), the bi-phasicity is more difficult to explain. Binding of a second carbon monoxide molecule whilst the Cu_o centre remains occupied with the "photolysed" carbon monoxide may be allowed within the reaction site "pocket", steric hindrance may result and very much slower binding of a carbon monoxide, in such cases, might be observed. Alberding *et al.*, (1976), discussed the importance of perturbations in protein structure and solvent "barriers" on the dynamics of carbon monoxide binding to protohaem.

Establishing ligand binding by copper in oxygen reductases, such as cytochrome *o* and aa_3, is important in the context of proposing models for a dioxygen reduction mechanism (see later).

3.2.4.2 *Cyanide*

As with carbon monoxide, cyanide is a potent inhibitor of cytochrome *o* activity (K_i=23μM; Matsushita *et al.*, 1984). Purified cytochrome *o* (1.9μM, final), treated with 5mM KCN (50 mM phosphate buffer; 10 mM EDTA; pH 7.0) results in a shift in the Soret maximum for the oxidised enzyme at 410nm, to 413nm (Figure 3.8a). The resulting cyanide-inhibited *minus* oxidised difference spectrum of cytochrome *o* has a peak at 420nm and a trough at 402nm (Figure 3.8a, *dotted*

Figure 3.8a

Cyanide binding spectrum of purified cytochrome o in the Soret (γ) region

Repetitive wavelength scanning of cytochrome o absorption spectra after addition of cyanide, is presented. An isolated enzyme preparation was added to a cuvette containing 10mM phosphate buffer, pH 7.0, to give a final volume of approximately 0.6ml. The oxidase was oxidised with 2.5µl of ferricyanide solution (200mM stock) and scanned to give the first spectrum. The enzyme concentration used was 1.9µM (final). Sequential spectra were recorded following the addition of 20µM cyanide to initiate the ligand binding reaction. Also shown is the difference spectrum, oxidised *minus* oxidised-*plus*-cyanide (- - -). The kinetics of reaction are presented in Figure 3.8b.

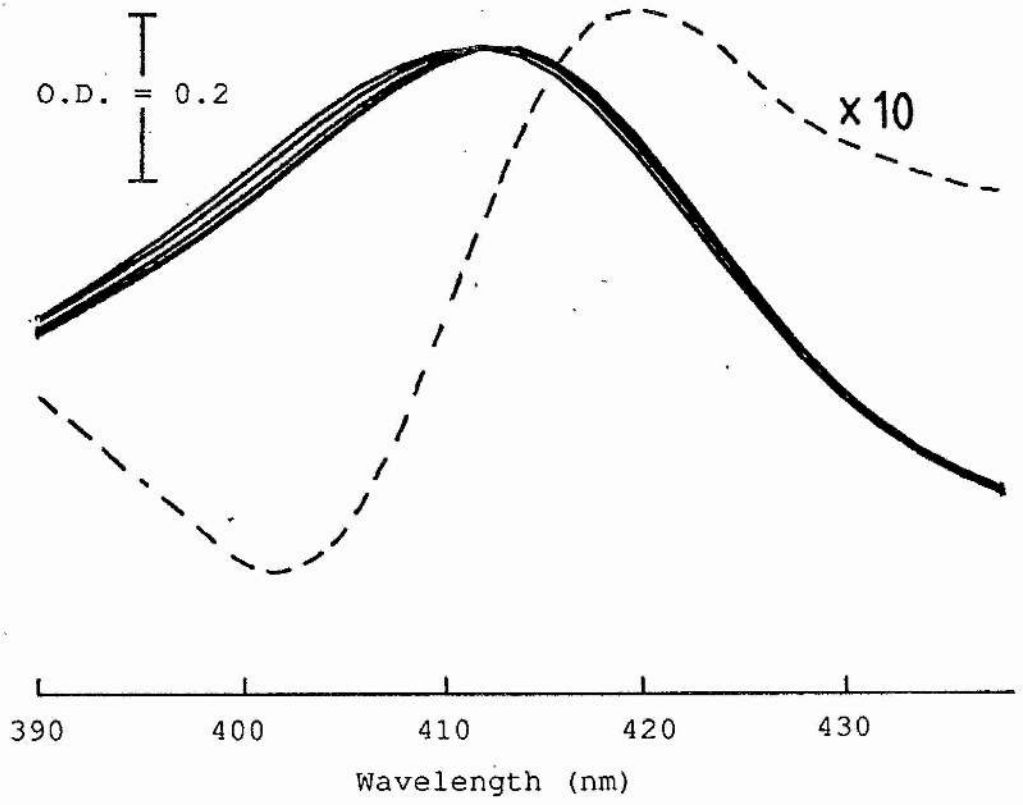
O.D. = 0.2
x 10
390
400
410
420
430
Wavelength (nm)

line). The kinetics of this reaction are not simple and can be fitted to two distinct phases. Figure 3.8b shows the reaction between cytochrome *o* and cyanide, followed by a three wavelength cycle of 402nm, 420nm, 402nm. The data could be fitted with two exponential components; 40% reacting in the fast phase (k_{app} = 0.035 sec^{-1}) and 60% reacting at a much slower rate (k_{app} = 0.0025 sec^{-1}). This can be interpreted in two way, (i) there are two subpopulations of cytochrome *o* (or binding sites) in the purified state with vastly differing reactivities to cyanide or, (ii) there is a single population (single site) reacting rapidly with cyanide but which undergoes a slower spectral change/relaxation (i.e. there are two conformations of the bound cyanide complex with different spectral properties).

The reaction between cytochrome *c* oxidase and cyanide has been characterised in detail by Baker *et al.*, (1987). They describe between one and three phases depending on the preparative procedure used. The slowest phase, on average ~ 0.001 sec^{-1}, is somewhat slower than the slow phase observed in cytochrome *o* (0.0025 sec^{-1}). The fast and intermediate phases in cytochrome *c* oxidase are characterised by binding rates of ~ 0.06 sec^{-1} and 0.016 sec^{-1}, respectively. The fast phase of cytochrome *o* is between these values. If cytochrome *c* oxidase, exhibiting significant amounts of slow and intermediate enzyme, is subjected to a cycle of reduction followed by oxidation, it can be made to convert to a form which possesses monophasic cyanide-binding kinetics characteristic of the fast enzyme component (Baker *et al.*,

Figure 3.8b

Kinetics of cyanide binding to cytochrome o

The kinetics of reaction are presented for the reaction between oxidised cytochrome *o* and cyanide. Changes in the absorbance difference spectrum, ΔAbs(420/402), of Figure 3.8a are plotted against time. The reaction conditions were as in Figure 3.8a. The reaction could be fit with two kinetic components, a faster phase, k_{app} 0.035 sec^{-1}, accounting for approximately 40% of the total absorbance change, and a slower phase, k_{app} 0.0025 sec^{-1} (60%). The arrow indicates point of cyanide addition.

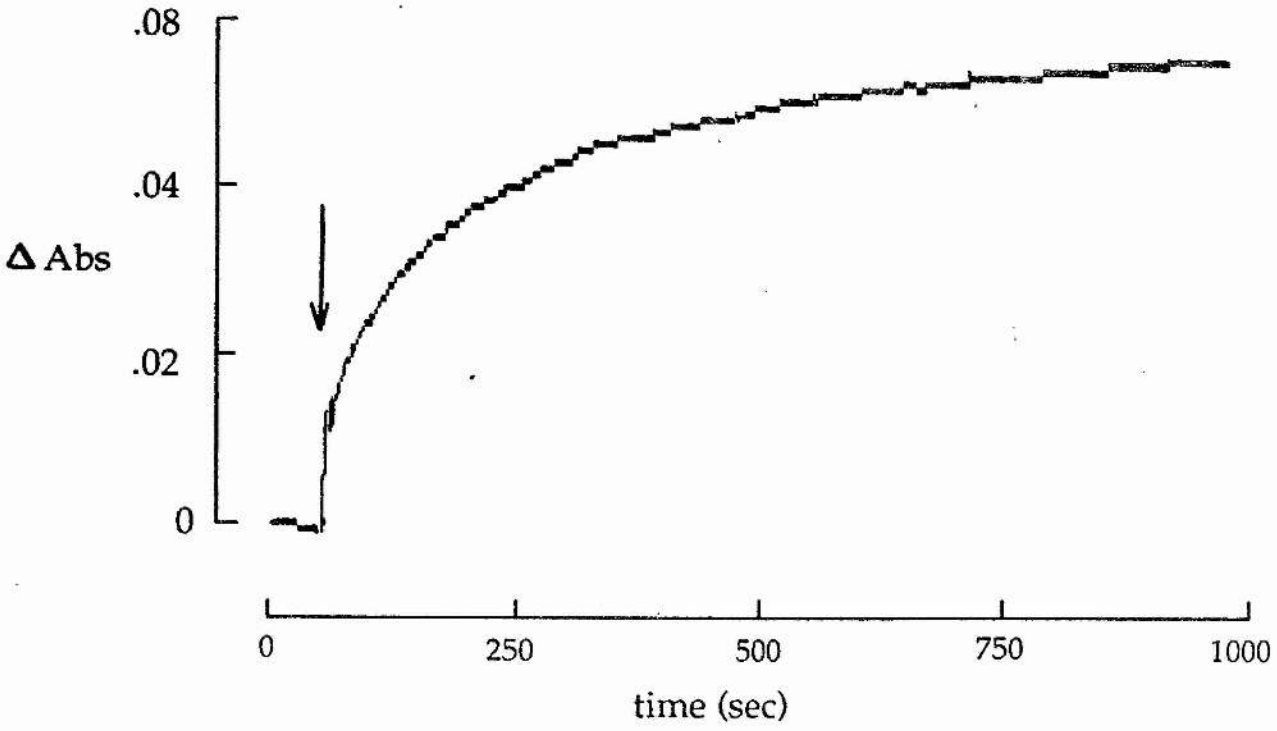
.08
.04
.02
0
Δ Abs
0
250
500
750
1000
time (sec)

1987). By contrast, if cytochrome *o* is redox cycled (i.e. reduced with dithionite followed by reoxidation) the rates and proportions of the two phases remain identical (not shown).

Figure 3.8(c) shows kinetic data obtained from an identical experiment to that described in Figure 3.8(b) above, except that cytochrome *o* was pretreated with 50mM formate prior to the addition of cyanide. The rate of cyanide binding was found to be significantly affected by such treatment. These data could, again, be fitted to two phases; a fast phase of binding with k_{app} = 0.038 sec^{-1} and a slow phase, k_{app} = 0.0023 sec^{-1}. Each phase contributed to approximately 20% and 80% of the total signal, respectively. In cytochrome *c* oxidase formate treatment induces a "slow" enzyme complex with concomitant changes in ligand (cyanide) binding kinetics i.e. formate treated cytochrome *c* oxidase shows slow monophasic cyanide binding (see Section 3.2.4.3, below) [A.J. Moody, Bodmin Research Institute, personal communication]. Comparing the effect seen in Figure 3.8c with that observed in cytochrome *c* oxidase after similar treatment reveals a difference between the two enzymes. From the data in Figure 3.8c, we can conclude that formate treatment of cytochrome *o* does produce a higher percentage of the enzyme population with slow ligand binding properties. However, there does appear to be some residual fast component.

Figure 3.8c

Kinetics of cyanide binding to cytochrome o: the effect of formate

The kinetics of reaction are presented for the reaction between cyanide and oxidised cytochrome o pretreated with formate. Changes in the absorbance difference spectrum, ΔAbs(420/402), of Figure 3.8a are plotted against time. The reaction conditions were as in Figure 3.8a, except 50mM formate (final) was added to the enzyme and incubated for 30 minutes. The arrow indicates point of cyanide addition.

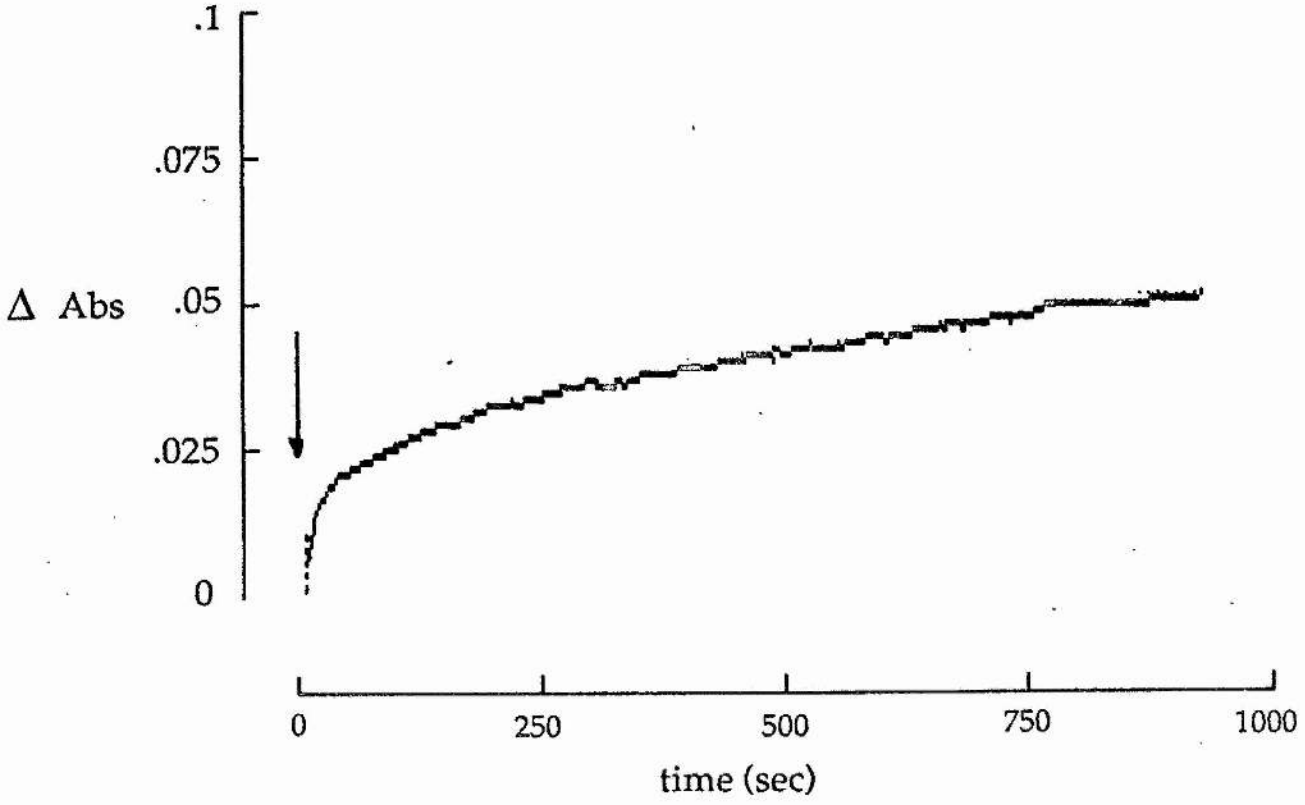
.1
.075
Δ Abs
.05
.025
0
0
250
500
750
1000
time (sec)

3.2.4.3 *Formate*

The EPR spectrum of resting cytochrome *c* oxidase exhibits a "g'=12" signal (Brudvig *et al.*, 1981). Formate converts the enzyme to a slow form (Moody & Rich, 1991) and shows a characteristic g'=12 signal (Cooper *et al.*, 1991). The "g'=12" signal is thought to be the result of a $S = 2$ spin system from the binuclear centre (Brudvig *et al.*, 1981). However, $S = 2$ spin systems need not necessarily result in an EPR signal in the g'=12 region and indeed a resonance, if even present, might equally appear elsewhere in the EPR spectrum [Salerno,J.C., personal communication]. Both the "resting" and the formate-inhibited enzymes exhibit an additional higher field resonance at g=2.9. When the enzyme is fully oxidised the g=2.9 signal is partially obscured by the low-spin haem *a* signal found at g=3 (Boelens & Wever, 1979). Progressive power saturation studies on the g'=12 and the g=2.9 signals were shown to behave similarly (Cooper *et al.*, 1991). This led Cooper and colleagues to suggest both resonances originated from the binuclear centre when in a $S = 2$ spin state. The half reduced enzyme, obtained either by rapidly freezing dithionite reduced resting enzyme or reducing the formate-inhibited enzyme with dithionite, still exhibit these signals. The preceding finding was taken as strong evidence to support the conclusion that electron transfer to the binuclear centre is required before the enzyme reverts to the "pulsed" state.

In Section 3.2.4.2 cyanide binding to cytochrome *o* was examined. It was shown that treatment of the purified enzyme

with formate decreased the rate of cyanide binding (*c.f.* Figure 3.8). If this was the result of a conversion from a "pulsed-like" cytochrome *o* to a "resting" form, as occurs in the mammalian cytochrome aa_3, it might be possible to observe a "g'=12" resonance. To this end, purified cytochrome *o* was treated with 10mM formate for 1 hour prior to freezing in an epr tube. Figure 3.9 shows a wide field scan recorded at low temperature and high power, conditions under which the g'=12 signal should be at its most intense (Cooper *et al.*, 1991; Brudvig *et al.*, 1981). A very broad signal, not seen in the control, is observed centred at approximately g=12. However, in the half-reduced, formate-treated enzyme, there was no signal observed in the g=3 region despite the low-spin haem b (g=3) being fully reduced and therefore diamagnetic (not shown). However, a formate induced high field signal (g=2.9) has been observed by others in the fully oxidised enzyme (W.J. Ingledew, personal communication).

3.2.5 *Effect of HOQNO on EPR spectra*

Figure 3.10 shows a wide field scan of oxidised EPR spectrum of RG145 membranes in the g=3 region. Addition of 2-n-heptyl-4-hyroxyquinoline *N*-oxide (HOQNO), an inhibitor to the quinone binding site, causes lineshape changes to the low-spin g_z (3.01) resonance. The quinol binding site is likely to be located within the membrane bilayer and a shift in the EPR peak position of the low-spin haem component, in the presence of HOQNO, implies proximity between quinone

Figure 3.9

EPR spectrum of purified cytochrome o in presence of formate

Shown is a low field scan of cytochrome o (30μM), pH 7 (50mM BES) treated with 5mM formate for 30 minutes prior to being frozen at 77K and scanned. g-values are indicated above spectra. The spectrometer settings were; temperature, 5K; time constant, 1 second; microwave power, 60mW; field modulation intensity, 10 gauss p.p. The gain used was 2.5 x 10^5 in the g=12 region, 2.5 x 10^4 in the g=6 region and 5 x 10^4 in the high field region (g=3).

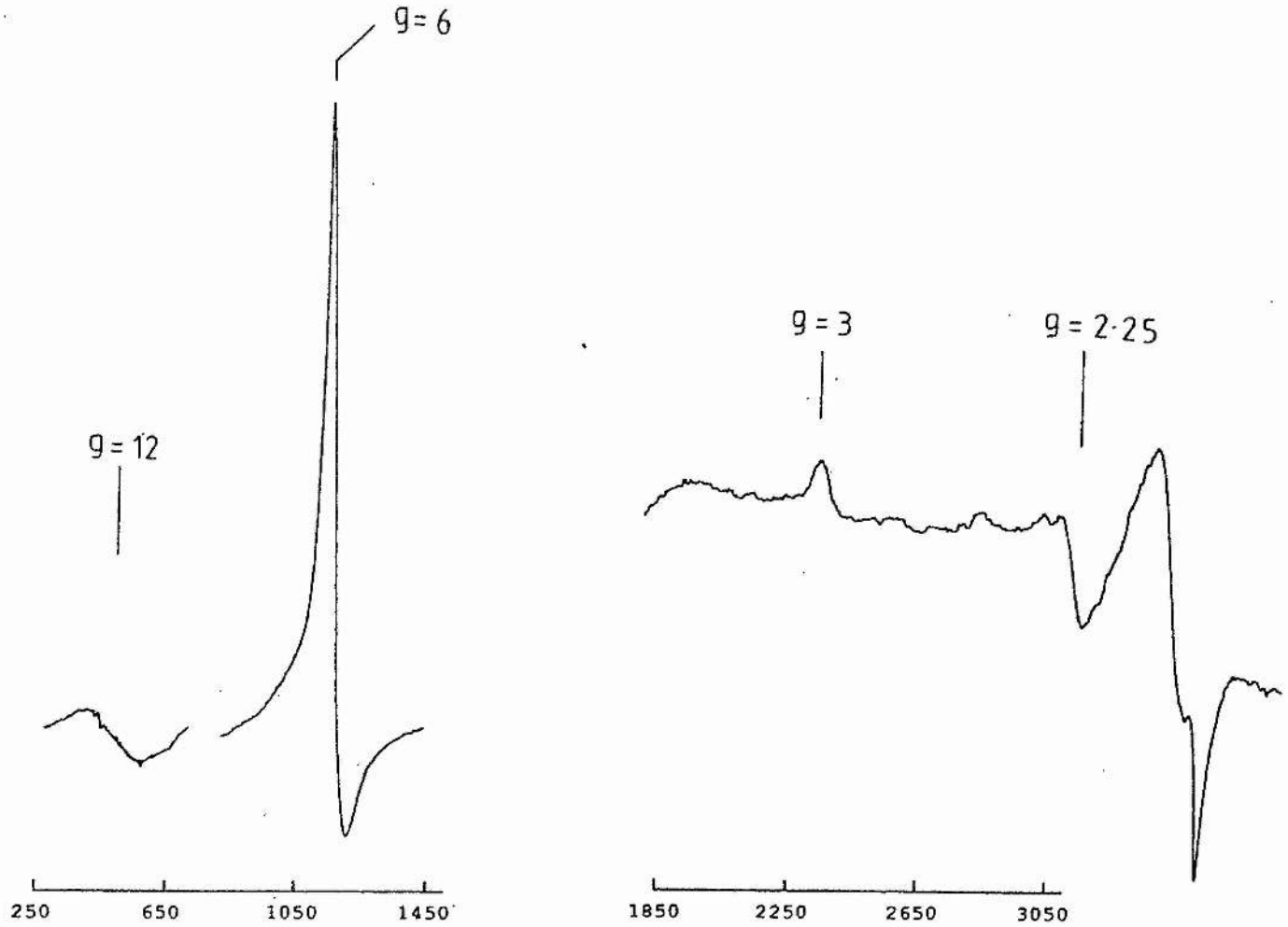
g = 6
g = 12
250
650
1050
1450
g = 3
g = 2·25
1850
2250
2650
3050

Figure 3.10

Effect of HOQNO on low-spin g_z (3.01) signal of cytochrome o in membranes

The effect of the quinone binding site inhibitor, HOQNO, on the EPR spectrum of cytochrome *o*, is presented. A suspension of RG145 membranes (~20mg protein ml^{-1}) was oxidised with hydrogen peroxide (1-2µl, 0.05% solution) in the EPR tube. Trace (a) shows the oxidised spectrum and trace (b) shows the spectrum of oxidised cytchrome *o* treated with inhibitor (20µM). HOQNO was dissolved in ethanol. Spectra were recorded at 14K and the g-values are indicated above spectra. Spectrometer settings; gain 4 x 10^5; time constant, 1 second; microwave power, 18mW; field modulation intensity 10 g.p.p.

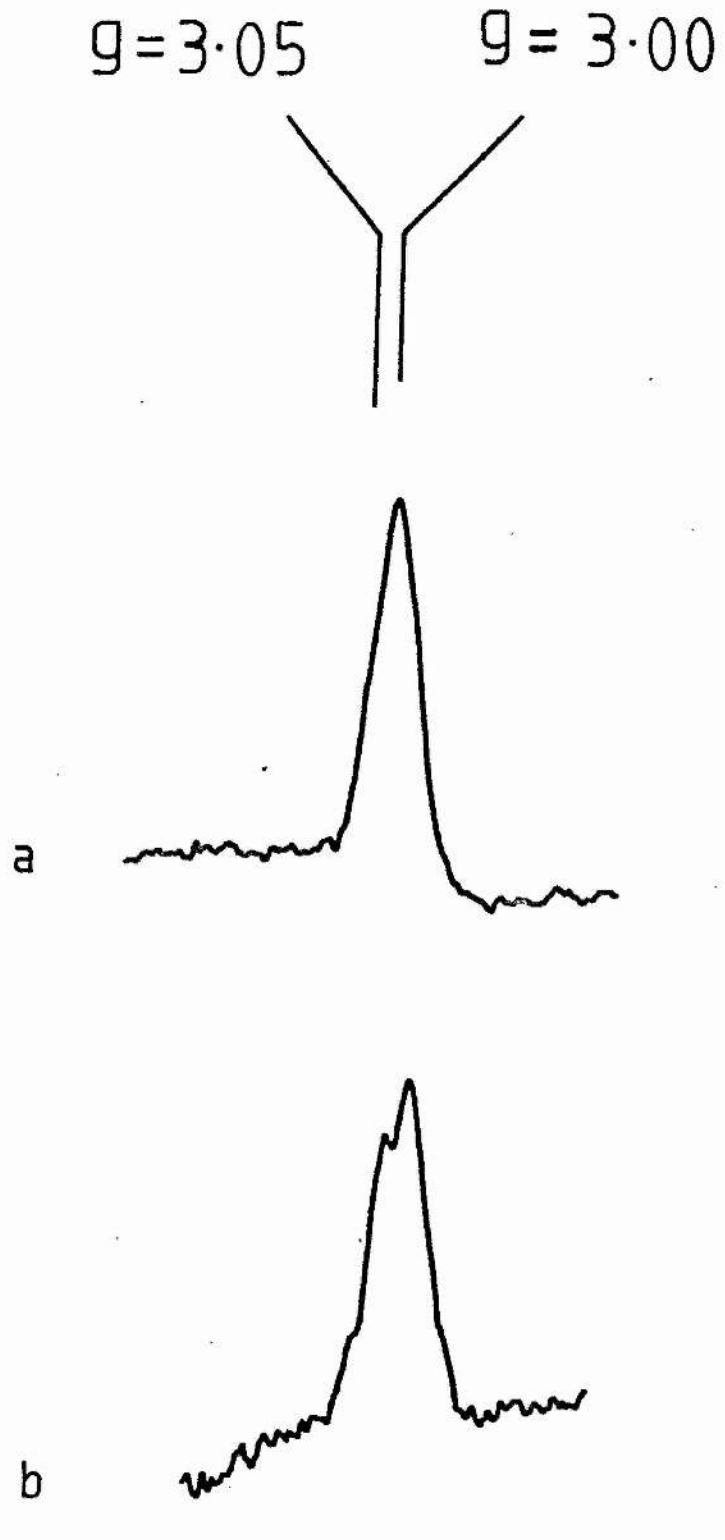
g=3·05
g= 3·00
a
b

binding site and low-spin haem.

3.2.6 *The nitrosyl adduct of cytochrome o*

3.2.6.1 *Formation of nitrosyl adduct to cytochrome o by treatment with nitrite*

The ability of reduced haemoproteins and copper-containing proteins to 'bind' nitric oxide has proved fortuitous as nitric oxide adducts of these metalloproteins possess a paramagnetic delocalised electron ($S = {}^1/_2$) with characteristic anisotropic EPR spectra. Nitric oxide ligation to the sixth coordinate position of a high-spin haemoprotein results in a six coordinate low-spin species. Unlike many ligands to the sixth coordinate of high-spin ferrohaem, nitrosylferrohaem is EPR detectable and can act as a probe to the catalytic site of these enzymes. Conversely, nitric oxide ligation to reduced high-spin haem results in the loss of the optical spectrum of the reduced haem. The delocalised electron conferring the paramagnetic properties is mainly associated with the d_z2 orbital of iron and NO (Kon & Kataoka, 1969). Cytochrome *o* reduces nitrite to form nitric oxide which ligates to the ferrous haem *o* centre;

$$NO_2^- + 2H^+ + e^- \text{------>} NO + H_2O; \quad E_{m,7} = +350mV$$

It is useful to note, at this stage, that a solution of nitrite exists as an equilibrium mixture of nitrite (NO_2^-)

and nitrous acid (HO-N=O; pK_a=3.37). In a study of the reactions of cytochrome *bd* with nitrite, Rothery (1989), argues that it is nitrous acid which is the reactive species in this alternative quinol oxidase. At this time it is not known whether cytochrome *o* reduces nitrite or nitrous acid to form the nitrosylferrohaem *o* complex.

Although some enzymes found in *E. coli* possess nitrite reductase activity and can bind and ellicit characteristic nitrosyl EPR spectra around g=2, the relative concentrations of these components will be small compared to that of cytochrome *o* in an amplified strain grown aerobically. In addition, some non-haem iron redox components, such as those found in the Photosystem II reaction centre of spinach chloroplasts, results in the formation of an intense g=4 signal ($S = {}^3/_2$) (Petrouleas & Diner, 1990). Membranes of RG145 treated with nitrite possessed no additional resonance in this region which might be attributable to such a spin system (not shown).

To date there has been no extensive characterisation of the nitric oxide binding properties of cytochrome *o* either from *E. coli* or from other sources. However, quite extensive data has resulted from haem-NO studies on cytochrome *bd* (Moodie, 1990; Rothery, 1989), haemoglobin (Morse & Chan, 1980; Henry & Banerjee, 1973), myoglobin (Morse & Chan, 1980; Hori *et al.*, 1990; Hori *et al.*, 1981) and cytochrome *c* oxidase (LoBrutto *et al.*, 1983; Barlow & Erecinska, 1979; Mascarenhas *et al.*, 1983; Brudvig *et al.*, 1980; Morse & Chan, 1980; Ohnishi *et al.*, 1982; Stevens & Chan, 1981).

The formation of the nitrosylferrohaem *o* (haem *o*-NO) complex is rapid in cytochrome *o* treated with nitrite, with optical changes taking place within 6 minutes of addition of nitrite to lactate reduced membranes (Figure 3.11). Comparable fast nitric oxide binding is observed in cytochrome *bd*, and assigned to haem *d*-NO, whereas slower spectral changes (over hours) have been attributed to nitric oxide binding to haem b_{595} (Rothery, 1989; Moodie, 1990).

Initial attempts at forming the haem *o*-NO (nitrosylferrohaem *o*) complex in membranes obtained from strain RG167 proved unsatisfactory, resulting in poor and uncharacteristic nitrosylferrohaem EPR spectra. The reason for this is unclear, particularly in view of the apparently normal carbon monoxide and reduced *minus* oxidised difference spectra obtained from these membranes (not shown). The *E. coli* strain RG145 was used in all subsequent studies and the anomalous behaviour of RG167 was not further investigated.

Nitrosylferrohaem *o* samples for EPR investigation were prepared by the addition of 15mM sodium nitrite to a suspension of *E. coli* membranes (RG145) pretreated with 15mM sodium lactate so as to anoxically reduce the membranes. The samples were incubated for 10 minutes, allowing complete formation of the nitrosylferrohaem *o* signal, before being rapidly frozen in freezing mixture and finally transferred to liquid nitrogen. The nitrosylferrohaem signal (g=2) is relatively slow relaxing and is best observed at higher temperatures (i.e. > 25K) in order to avoid the possibility

Figure 3.11

Optical reduced-plus-nitrite minus reduced difference spectra of membranes of E. coli strain RG145

A time course of spectral changes between 400nm to 600nm optical range after addition of nitrite (15mM) to lactate reduced membranes of RG145 (~ 6mg protein ml^{-1}) is shown. Lactate was added to two stoppered cuvettes containing membranes in 50mM K_2HPO_4, pH 7.5, buffer and left for 10 minutes to create anoxic conditions. To one cuvette, the nitrite solution was added, via a capillary hole, to initiate reaction. A reduced *minus* reduced difference spectrum was recorded as a baseline prior to nitrite addition (dotted line). Spectra are shown at set times after nitrite addition: a, 10 seconds; b, 7 minutes; c, 25 minutes; d, 120 minutes. Each spectra took approximately 7 minutes to complete. Spectra were recorded at room temperature on a split-beam spectrophotometer. Relative gain shown on spectra. The bar represents absorbance change at relative gain x1 (~400-480nm). The relative gain of the photomultiplier is increased (x2.5) for all spectra in the region ~480-600nm.

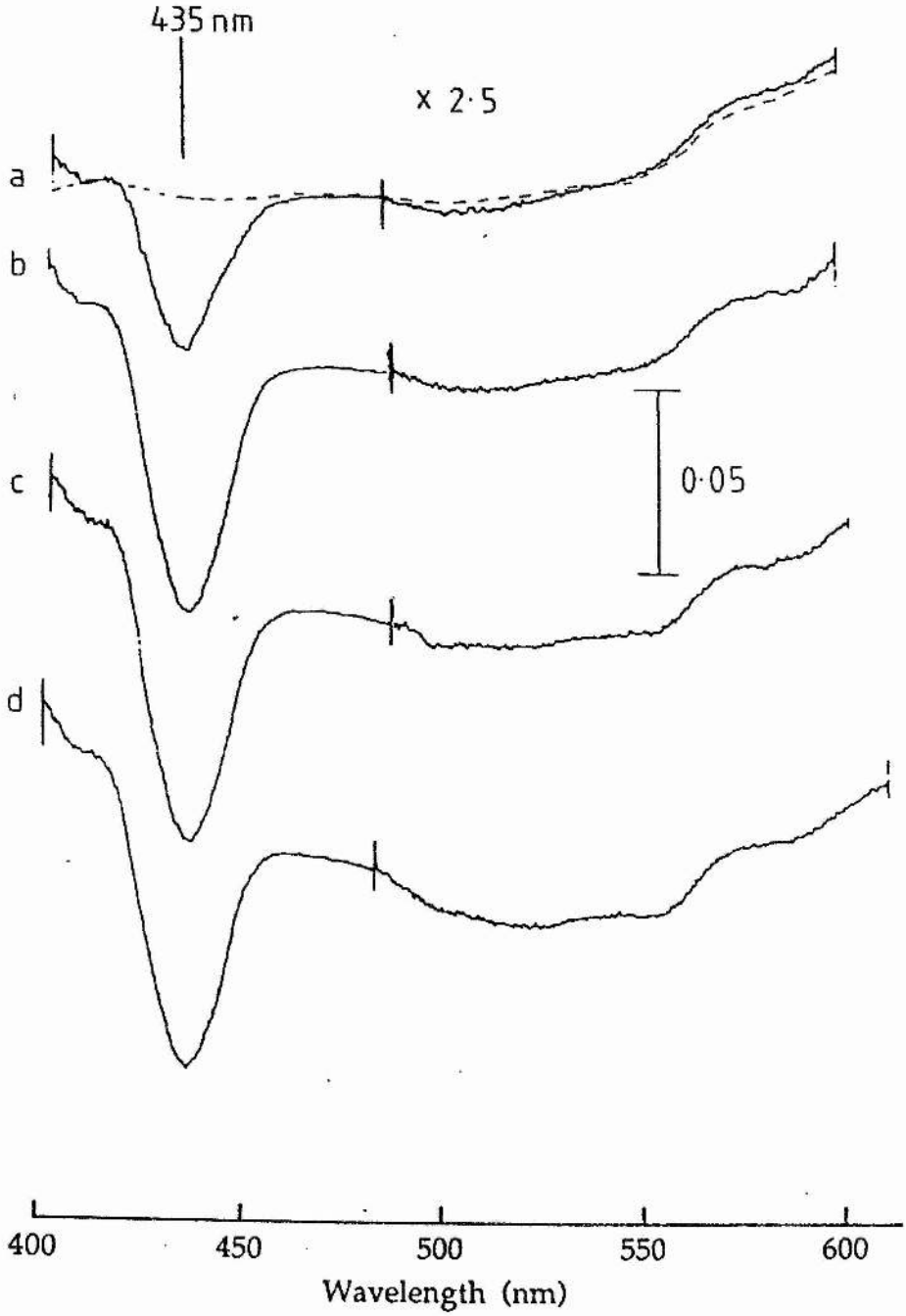
435 nm
x 2·5
a
b
c
d
0·05
400
450
500
550
600
Wavelength (nm)

of saturating the spectra (the technique of progressive saturation will be used to advantage in Chapter 5).

Figure 3.12 shows a typical nitrosylferrohaem *o* spectrum from cytochrome *o* exhibiting rhombic symmetry. The principal g-values are observed at g=2.09, 2.00 and 1.98. These have been assigned to g_x, g_z (split into a triplet of hyperfine structure) and g_y, respectively, in accordance with orientation data obtained from multilayer preparations of cytochrome *o* (see Chapter 5) and by comparison with cytochrome aa_3 (Blokzijl-Homan & van Gelder, 1971; Kon & Kataoka, 1969; Barlow & Erecinska, 1979). Often, EPR investigations into nitrosyl adducts of haemoproteins reveal the presence of rather more complex spectra, composed of at least two distinct signals, Type I and Type II (Yonetani *et al.*, 1972). Morse & Chan, (1980) further investigated the relationship between these signals in both model haem compounds and haemoproteins and concluded that they arose from at least two conformations in thermal equilibrium (see below). At lower temperatures, Type I spectra predominate. On increasing the temperature the Type II species becomes progressively dominant. It is believed that Type I and II spectra result from a displacement of the haem iron atom from the porphyrin plane when ligated to nitric oxide.

Type I Type II

Figure 3.12

EPR spectrum of the nitrosylferrohaem o complex: haem o-NO

The EPR spectrum of the nitrosyl haem adduct to reduced cytochrome *o* is shown. Membranes of RG145 ($35mgml^{-1}$; 50mM BES, pH 7.0) were anoxically reduced in the presence of 15mM lactate at room temperature. The haem *o*-NO species was produced by adding 10mM sodium nitrite to the samples. g-values are indicated above the spectrum. Spectrometer settings were: temperature, 35K; microwave power, 8.7 mW; field modulation intensity, 5 gauss (p.t.p.).

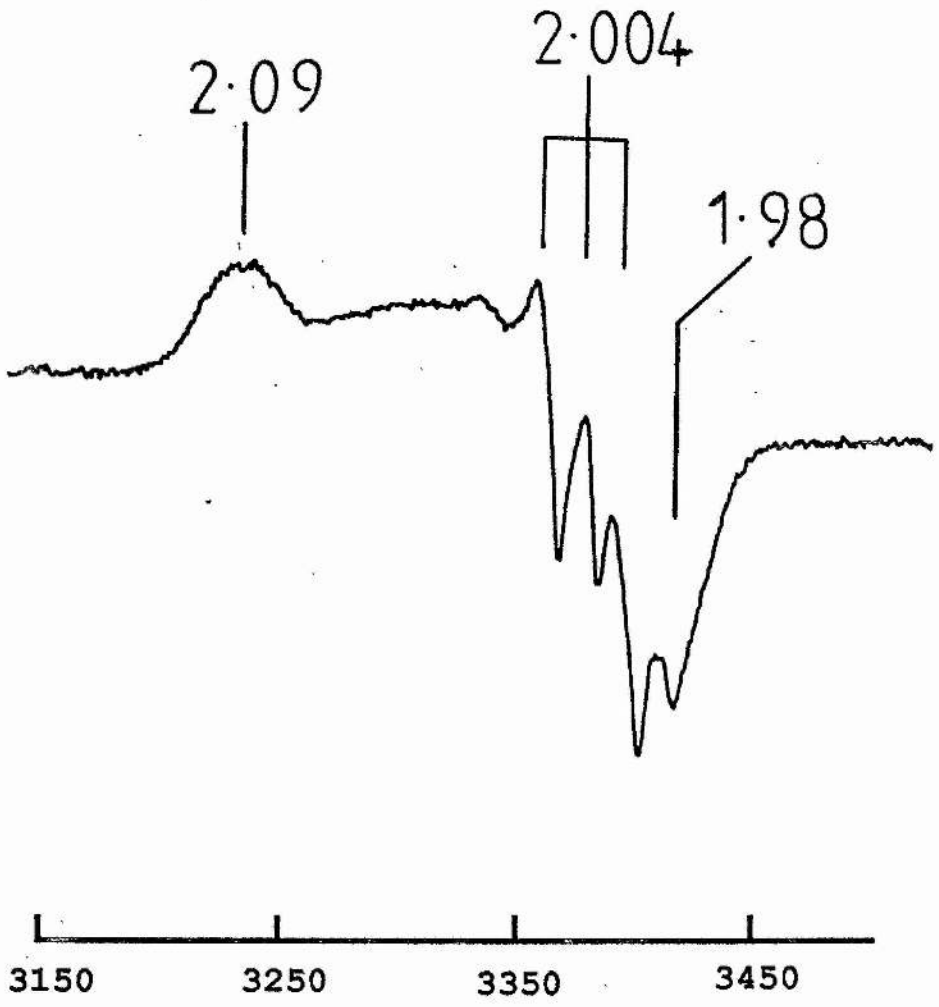
2·09
2·004
1·98
3150
3250
3350
3450

In Figure 3.13, the effect of temperature on the EPR spectra of nitrosylferrohaem *o* is shown. It is clear that the EPR lineshape of nitrosylferrohaem *o* is temperature independent over this range. Thus, cytochrome *o* should be classed as a Type I nitrosyl compound based on its spectral shape and the arbitrary definitions proposed by Yonetani *et al.*, 1972; Type I ($g_y < 1.96$) and Type II ($g_y > 1.97$).

Cytochrome *c* oxidase also forms a Type I nitrosylferrohaem complex and, like cytochrome *o*, appears to be temperature independent (Morse & Chan, 1980). Cytochrome *bd* exhibits both Type I and II spectra with a characteristic temperature dependence for each type (Rothery, 1989; Moodie, 1990). An additional haem-NO signal results from the ligation of NO to haem b_{595} which forms slowly with time (Moodie, 1990).

[One should note that the temperature independence of the nitrosylferrohaem adduct of cytochrome *o* may not be wholly due to an interaction with Cu_o. Cytochrome *c* peroxidase (which does not possess an analogous copper centre) also exhibits a Type I EPR spectrum over a wide temperature range (Yonetani *et al.*, 1972), although, hydrogen bonding has been suggested to account for the stabilisation of Type I over Type II in this system (Morse & Chan, 1980)].

Figure 3.13

Temperature dependence of the haem o-NO spectrum

EPR spectra of the nitrosyl haem adduct of reduced cytochrome *o* are shown. Membranes of RG145 ($35mgml^{-1}$; 50mM BES, pH 7.0) were anoxically reduced in the presence of 15mM lactate at room temperature as in Figure 3.12. Spectra are shown at the temperatures indicated in the figure. The g-values of the haem *o*-NO species are indicated above the spectra. The spectra are slightly saturated because of the high microwave power setting. Spectrometer settings were: microwave power, 91 mW; field modulation intensity, 20 gauss (p.t.p.).

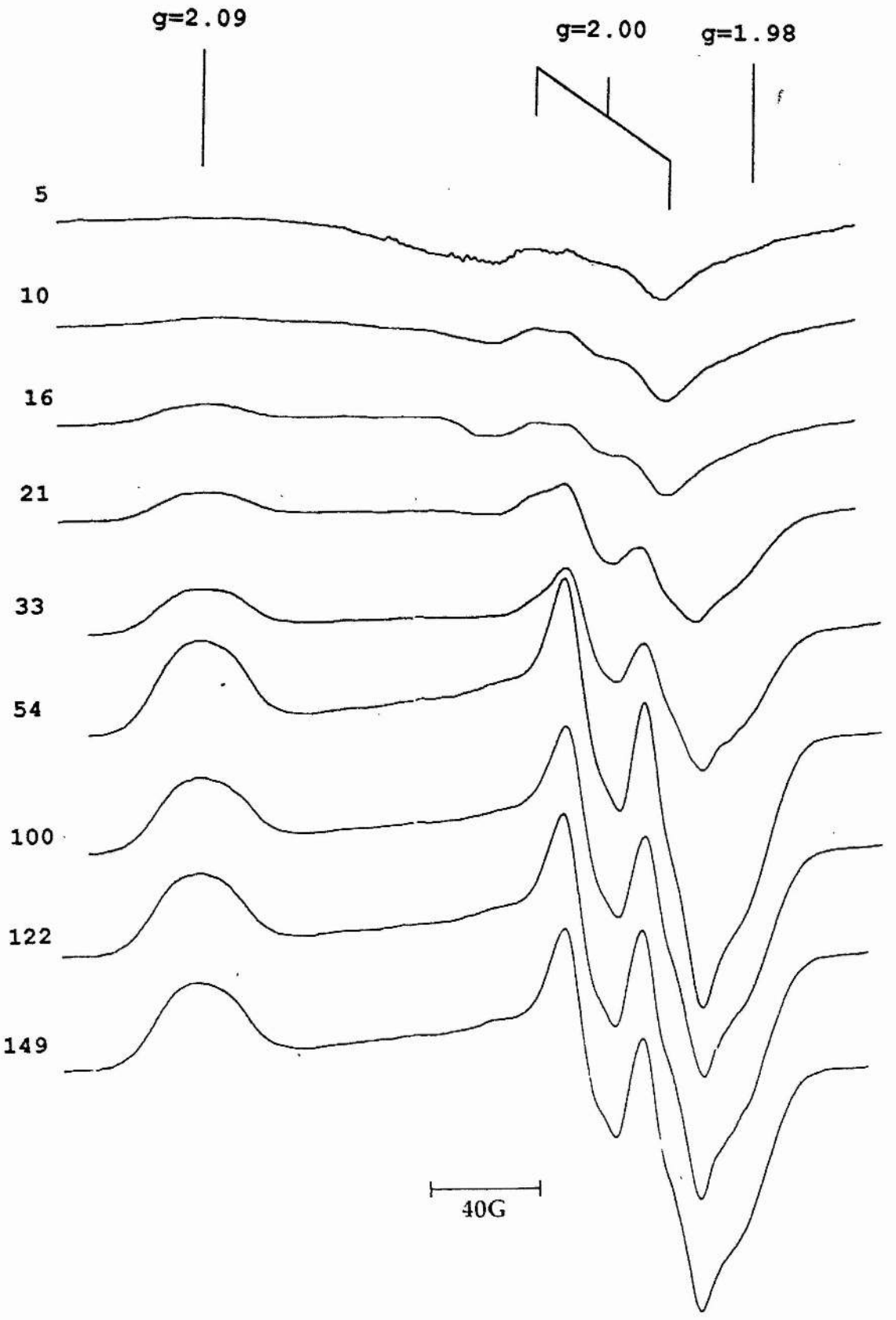
g=2.09
g=2.00
g=1.98
5
10
16
21
33
54
100
122
149
40G

3.2.6.2 *Hyperfine and superhyperfine structure of the nitrosylferrohaem complex*

In Figure 3.14a hyperfine splitting can be seen in the central g_z region. This is made up of a triplet. The hyperfine splitting constant, A_z, appears to be around 21 Gauss (2.1 mTesla). This value is close to that expected for nitrosyl complexes of cytochrome *c* oxidase and other haemoproteins of Type I (Morse & Chan, 1980). The hyperfine structure manifests as a result of interaction of the delocalised electron with the exogenous nitrosyl ^{14}N atom (I = 1) (Kon & Kataoka, 1969). It should be possible to further resolve each triplet of hyperfine into another triplet set of superhyperfine (the result of an interaction with two non-equivalent nitrogen nuclei (I =1)): thus a triplet of triplets should be observed. Analysis of the z absorption component in Figure 3.12 suggests that the superhyperfine structure has coalesced into three. The lack of resolved superhyperfine, even at high gain, low field modulation (1 Gauss p.t.p.) and non-saturating conditions, could suggest that the proximal (endogenous) ligand is not nitrogenous. However, an absence of superhyperfine is not definitive for such an assumption, as many haemoproteins with nitrogen atoms as the fifth-coordinate ligand can also lack such splittings (e.g. myoglobin, Yonetani *et al.*, 1972; Henery & Banerjee, 1973 see also Lukat *et al.*, 1988). Moodie, 1990, also failed to detect superhyperfine in the alternative quinol oxidase of *E. coli*, cytochrome *bd*, but this is most probably explained in terms of spectral overlap between

Figure 3.14

The effect of urea on the spectrum of haem o-NO in membranes

RG145 membranes (~25mg protein ml^{-1}) were reduced with lactate (15mM) for 5 minutes prior to the addition of 10mM sodium nitrite (^{14}N) and left for 10 minutes to form nitrosyl complex and frozen at 77K. (A) Sample as prepared above. (B) pre-incubated with 1M urea for 1hr before treatment with lactate. g-values are indicated above spectra and field position shown at bottom of figure (in gauss). Spectrometer settings; temperature, 50K; gain 8 x 10^4; time constant, 0.5 seconds; microwave power, 19mW; field modulation 1 g.p.p.

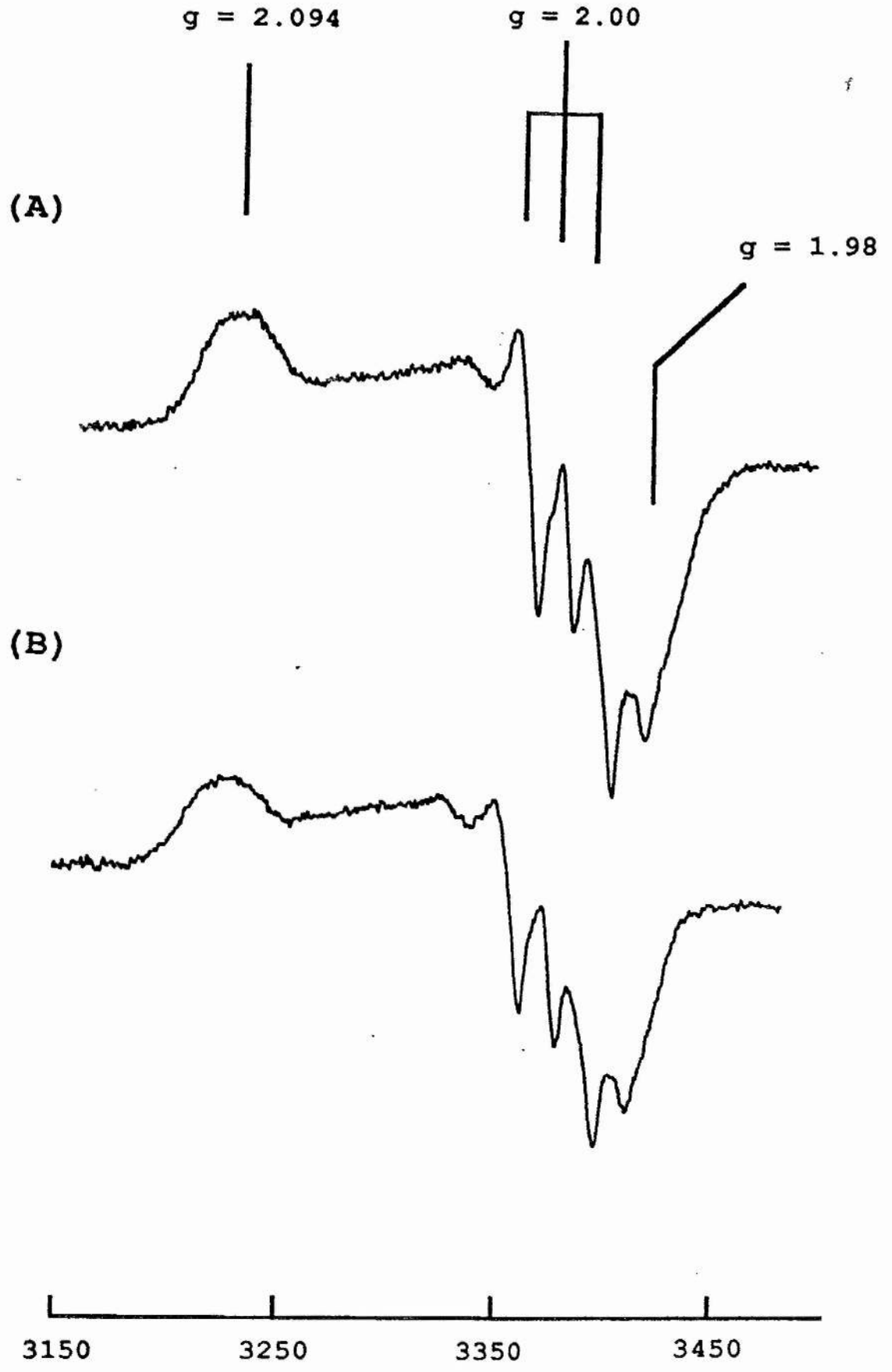
g = 2.094
g = 2.00
(A)
g = 1.98
(B)
3150
3250
3350
3450

nitric oxide adducts to both the haem *d* and haem b_{595} centres at the reaction centre (Moodie, 1990).

Treatment with 1M urea failed to improve the resolution of the hyperfine of the nitrosylferrohaem signal (Figure 3.14b).

3.2.6.3 *Isotopic Substitution*

Isotope substitution (^{15}N sodium nitrite) was used to study the effect on the x, y and z absorptions (g_x, g_y and g_z, respectively). Unfortunately resolution in the g_x and g_y was too poor to observe any significant changes in these regions compared to spectra obtained from haem o–^{14}NO. However, the central g_z region became a doublet of hyperfine consistent with this feature resulting from the delocalised electron interacting with the ^{15}N nuclei ($I = {}^1/_2$) from the nitrosyl ligand (Figure 3.15). The hyperfine splitting constant in this case was 29 Gauss. An increase in splitting is consistent with the higher magnetogyric ratio for the ^{15}N atom.

3.2.6.4 *Reactions with Hydroxylamine*

Treatment of oxidised cytochrome *o* with hydroxylamine (NH_3^+OH) results in the formation of a g=2 signal identical to that formed with nitrite (Figure 3.16). At room temperature, and in anaerobic conditions, the signal remains stable. The saturation behaviour of both signals confirm that formation of the nitrosylferrohaem complex, either by treatment with nitrite or hydroxylamine, results in the

Figure 3.15

EPR spectra of (^{15}N) haem o-NO in membranes of E. coli

RG145 membranes (~25mg protein ml^{-1}) were treated as in Figure 3.14(a), except the ^{15}N isotope of sodium nitrite was used for the formation of nitrosyl species. g-values are indicated above spectra and field position shown at bottom of figure (in gauss). Spectrometer settings were the same as found in Figure 3.14

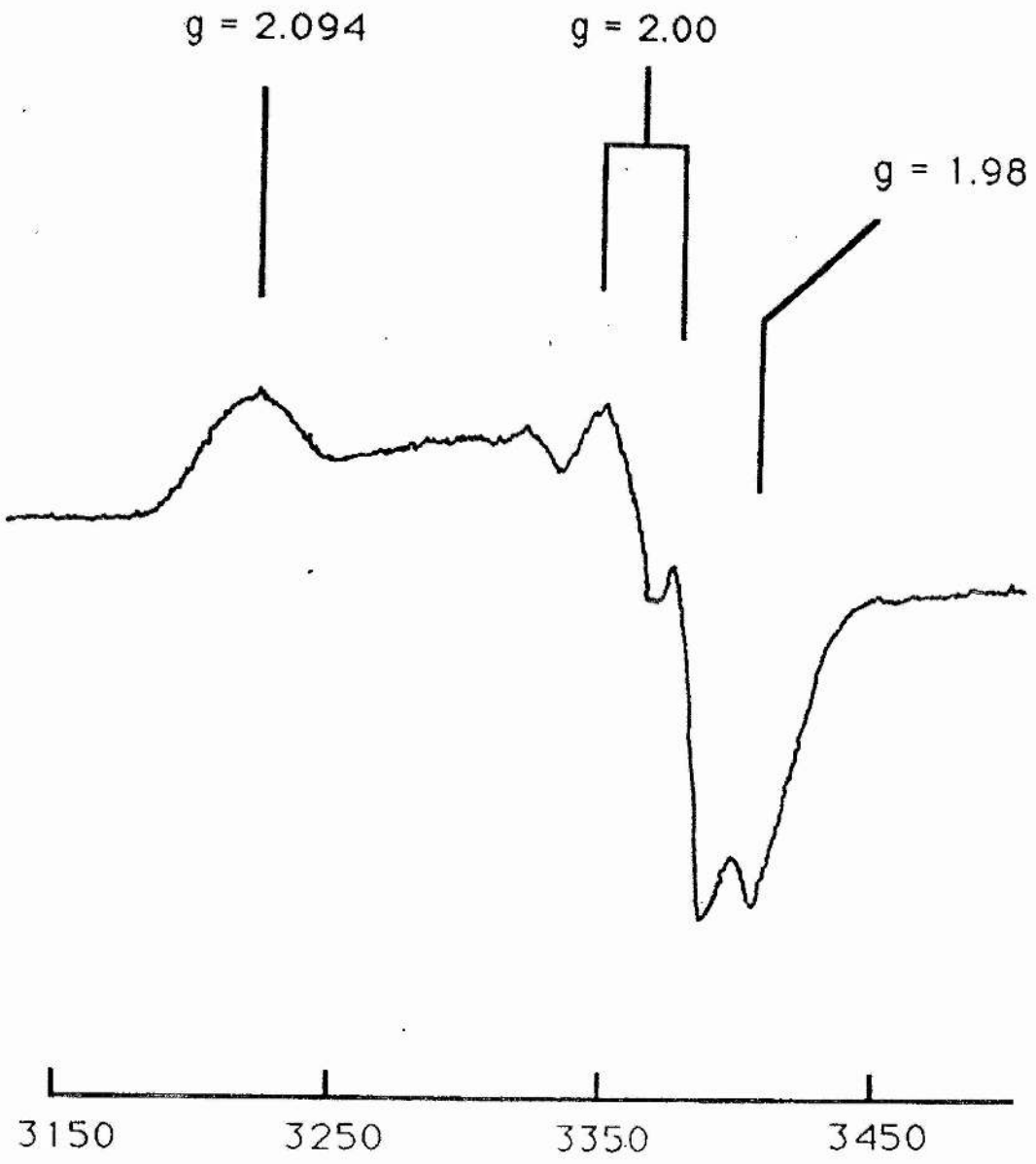
g = 2.094
g = 2.00
g = 1.98
3150
3250
3350
3450

Figure 3.16

EPR spectra of membranes treated with hydroxylamine

A suspension of RG145 membranes (~30mg protein ml^{-1}) was treated with hydroxylamine (final concentration, 250μM) and left, at room temperature, for 20 minutes, before being frozen in liquid nitrogen (77K). Spectra were recorded at 35K. g-values, for the hydroxylamine formed nitrosyl ferrohaem *o* adduct, are indicated above spectra and field position shown at bottom of figure (in gauss). Spectrometer settings; gain 8 x 10^4; time constant, 0.5 seconds; microwave power, 19mW; field modulation 5 g.p.p.

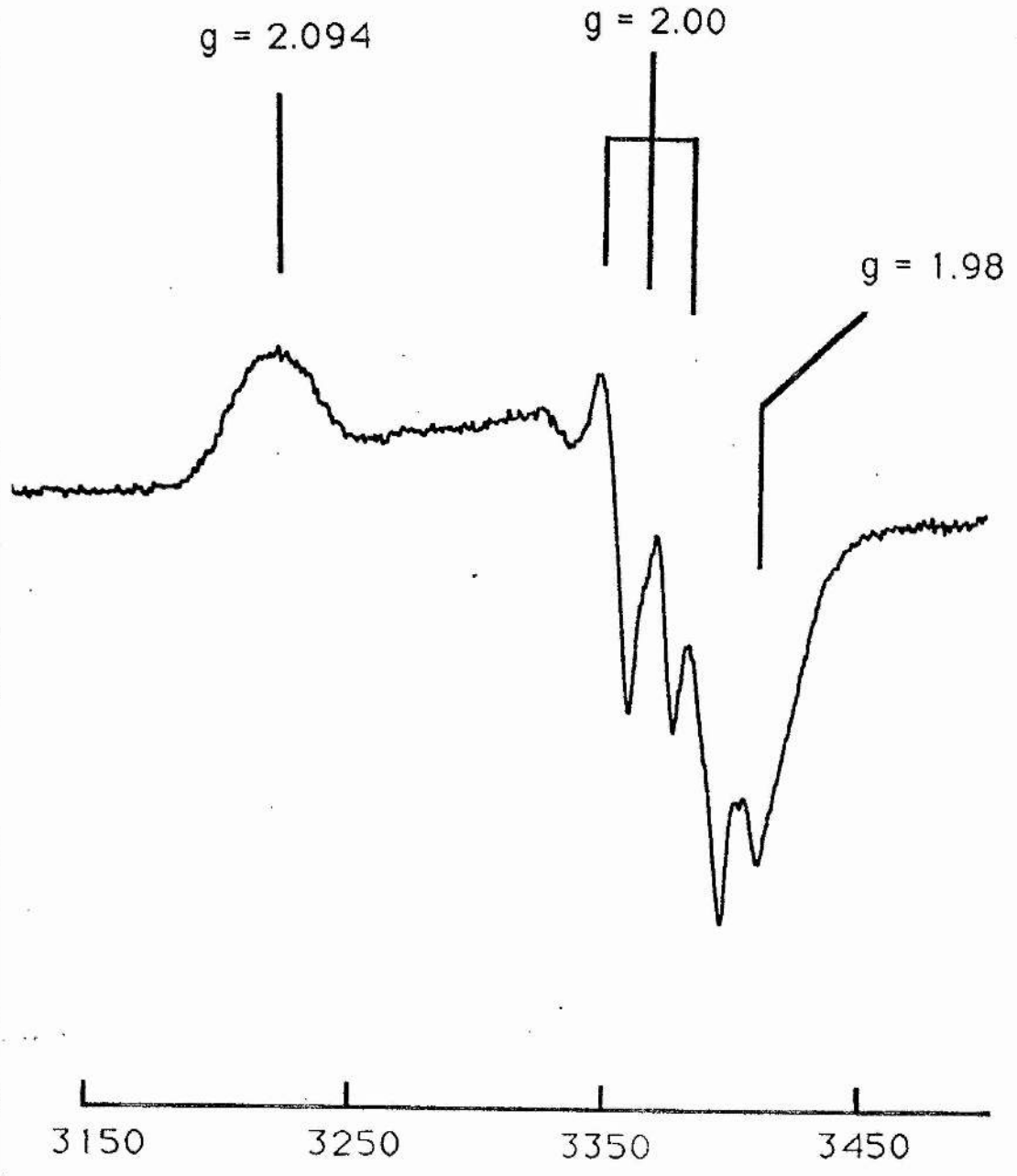
g = 2.094
g = 2.00
g = 1.98
3150
3250
3350
3450

formation of the same compound, Figure 3.17. As with the nitrosyl EPR spectra formed by treatment with nitrite, no superhyperfine was observed. Examination of the low-spin haem *b* (g=3) signal of hydroxylamine treated membranes confirm cytochrome *o* to be in the mixed valence state. Addition of dithionite to this species abolished the g=3 signal without any loss of the g=2 nitrosyl signal (not shown).

Other haemoproteins do not appear to react with hydroxylamine to give a nitrosylferrohaem signal (Blokzijl-Homan & van Gelder, 1971).

The coordination chemistry and reactions of hydroxylamine are complex and highly dependent on, amongst other parameters, the relative stoicheiometry of added hydroxylamine and metalloprotein (see Wieghardt, 1984 for more detailed discussion on this topic). An approximate 3:1 ratio of hydroxylamine to protein was used to obtain the spectra found in figure 3.16. The nitrosyl complex is formed by a two electron oxidation of hydroxylamine to form nitroxide which goes on to bind the haem centre.

Figure 3.17

Saturation profiles of haem o-NO formed by treatment with hydroxylamine or nitrite

The saturation profiles of the g_x (2.09) signal of the nitrosylferrohaem *o* signal formed either by treatment of lactate (15mM) reduced membranes of *E. coli* strain RG145 (~35mg protein ml^{-1}) with nitrite (5mM); (closed triangles), or by treatment of oxidised membranes with hydroxylamine (~0.25mM, final); (open triangles). To achieve saturation, samples were run at 18K. Other spectrometer settings; time constant, 1 second; field modulation intensity, 10 G (ptp).

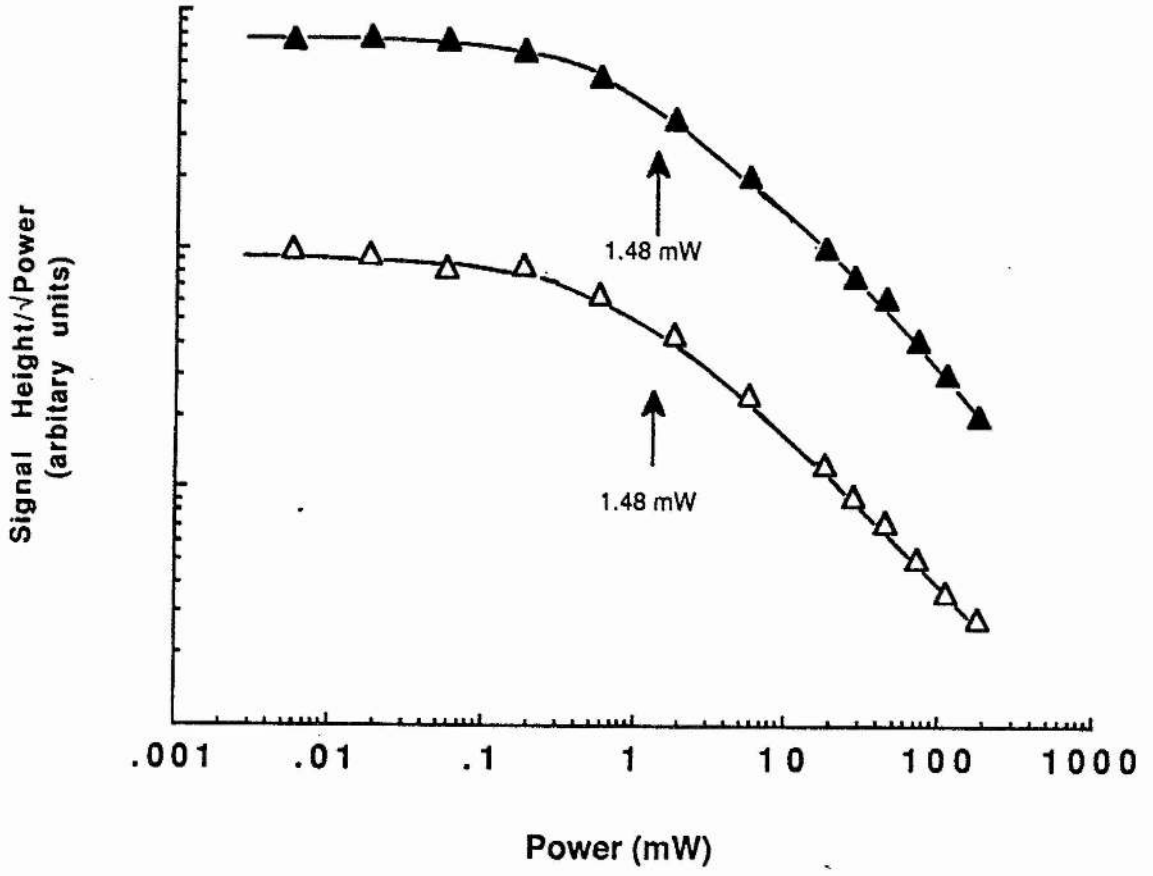
Signal Height/√Power
(arbitary units)
1.48 mW
1.48 mW
.001
.01
.1
1
10
100
1000
Power (mW)

3.3 Conclusion

The purified preparation of cytochrome *o* used herein, obtained from a strain containing a multicopy plasmid, has proved to be a reliable source of the enzyme for further study. It has a high catalytic turnover (430 mol e- sec^{-1}mol haem o^{-1}) and possesses four subunits by SDS-PAGE analysis. In addition, the optical spectra and redox behaviour of the EPR spectra of this preparation are identical to those reported from membrane sources.

It is clear that copper is an essential component of a functional enzyme and is required for growth through the aerobic respiratory chain of this strain. Future studies incorporating zinc in place of Cu_o will help establish the precise nature of the role played by Cu_o in this enzyme; in addition it will provide complementary information on the nature of Cu_B in the mitochondrial cytochrome *c* oxidase where ligand replacement is not possible. Furthermore, zinc replacement should provide direct evidence that antiferromagnetic spin-coupling between the high-spin haem *o* centre and Cu_o is responsible for the bell-shaped redox data observed in EPR studies.

The reaction between the reduced enzyme and carbon monoxide shows relatively slow binding kinetics which is proposed to be the result of carbon monoxide binding to Cu_o after photolytic release from haem *o*. It may also be possible to accommodate a second carbon monoxide molecule within the reaction site when Cu_o is occupied by the

photolysed carbon monoxide molecule. Because bound carbon monoxide has no unpaired electron it ligates to haem in a linear fashion. It is therefore possible that the reaction site pocket may allow two carbon monoxide molecules to reside within it. In support of this, haem *d* and haem b_{595} of the cytochrome *bd* complex in *E. coli* are both thought to be able to bind carbon monoxide (Moodie, 1990). In cytochrome *bd*, haem b_{595} could have an analogous function to the copper centre of cytochrome *o*. In cytochrome *o* the binding of a second carbon monoxide molecule is a slower process but might be favoured over the reassociation of the photolysed carbon monoxide bound at the Cu_o centre. This fact may account for the biphasic reassociation kinetics observed in cytochrome *o* where the slowest process might be due to the more difficult binding of a second carbon monoxide molecule at haem *o* when there is a carbon monoxide bound to Cu_o, possible through steric hindrance.

Evidence of ligand binding to both centres supports models in which dioxygen forms a bridged compound at the reaction site. This assumption is consistent with direct observations of Cu-CO stretching frequencies using low temperature FTIR reported by Alben *et al.*, (1981) after photolysis of the carbon monoxide-inhibited cytochrome *c* oxidase. From their studies it was concluded that Cu_B was the initial acceptor of ligands, including dioxygen. However, this seems an unnecessarily restrictive model; there is no evidence to suggest either centre is the primary ligand acceptor. Indeed, carbon monoxide, and therefore

dioxygen, might equally bind to the high-spin centre first. In cytochrome *o*, further evidence in support of a bridging model comes from temperature dependence studies of the nitrosylferrohaem *o* signal. The lack of a temperature dependent nitrosyl Type I/Type II transition in cytochrome *o* infers a higher degree of stability than is present in other nitrosylferrohaem species in which a bimetallic reaction site does not exist (and where the EPR spectra are susceptible to temperature). It is interesting to speculate on the role played by Cu_o in this stabilisation. An interaction between the oxygen moiety of the nitrosylferrohaem *o* complex and Cu_o would, in theory, serve to *fix* the imidazole-haem-NO distances and inhibit Type I/Type II transitions (Morse & Chan, 1980). A nitroxide bridging species has already been identified in cytochrome *c* oxidase (Stevens *et al.*, 1979a).

It is attractive, in the context of determining the catalytic stages of dioxygen binding and reduction, to identify coordination between nitroxide and both centres at the reaction site. In contrast to carbon monoxide, nitroxide and dioxygen possess an unpaired electron when bound at the haem centre which creates a bent molecule (Edwards *et al.*, 1988) which may facilitate bridging between metal centres.

A model for the reduction of molecular oxygen by cytochrome *o* is presented in Chapter 6.

Conformational states?

The question, is cytochrome *o* similar to cytochrome *c*

oxidase, in having more than one conformational state? cannot be unequivocally answered. What is likely is that conformational changes are required for a proton pumping activity, such as that observed in cytochrome *o* (Puustinen *et al.*, 1989), but in order that transitions be linked to this activity they must be shown to be kinetically competent. Given the dependency of the fast/slow ratio on the purification procedure and the absence of slow form in the membrane bound oxidase, it is far from clear whether the fast/slow transition in cytochrome *c* oxidase has any functional relevance. Although cyanide binding to cytochrome *o* has been demonstrated to be biphasic, this phenomenon does not appear to be related to the cyanide binding behaviour of cytochrome *c* oxidase, principally because the amplitude and rates are not affected by redox cycling. Since it has been shown that both the mitochondrial and *E. coli* oxidases pump protons the conformational changes related to the fast/slow transition in cytochrome *c* oxidase are not likely to be relevant to this activity. Further kinetic resolution of the reaction between cyanide and cytochrome *o* is required before we can distinguish between whether two populations of cyanide binding site or a single population undergoing an optical transition, is responsible for the observed biphasic kinetics.

In those parameters examined e.g. cyanide binding kinetics and EPR spectral features, formate appears to induce a form of the cytochrome *o* enzyme which has some similarity to cytochrome *c* oxidase under similar conditions.

It is therefore possible that cytochrome *o* can be made to form a "slow" conformation but there is no evidence that it forms this state during purification, as with cytochrome aa_3.

To what extent can we assume the nature of the axial (proximal) ligand to be nitrogenous?

On the basis of EPR studies of the nitrite treated enzyme, the identity of the axial (proximal) ligand remains ambiguous because of poorly resolved superhyperfine, diagnostic of an imidazole residue at this position. It is possible to explain the lack of observed superhyperfine by a "freezing" of the ferrohaem-to-base distances in a multiplicity of states, tending to average out the splitting at the haem iron atom. However, the hypothesis above, in which the Type I nitrosylferrohaem spectra of cytochrome *o* is stablised by an interaction with Cu_o, would appear to contradict this. This is because it is difficult to envisage a model whereby both the intercentre distances are variable (lack of hyperfine) whilst the nitroxide ligand remains bridged between the haem and the copper moieties (thermal stability) unless the interaction between Cu_o and the oxygen atom of the nitrosyl adduct is extremely weak.

Sequence (see Section 1.4) comparisons between subunit I from known cytochrome *c* oxidases and *cyo*B (the subunits thought to contain the redox active centres of cytochrome *o*) show there to be six totally conserved histidine residues (Lemieux *et al.*, 1991). Point mutagenesis of these conserved

imidazole bases provides the only evidence at this time that one of these residues binds the high-spin haem *o* centre (Lemieux *et al.*, 1991).

In the future ^{15}N-rich histidine could be used during growth in an attempt to incorporate this isotope into the endogenous (axial) ligand position. It might then be possible to observed perturbations in the lineshape of the EPR spectrum of the nitrosylferrohaem *o* species.

CHAPTER FOUR

Optical and potentiometric analysis of purified cytochrome o

4.1 Introduction

In common with cytochrome aa_3, cytochrome *o* of *E. coli* contains two haem prosthetic groups (*a*-type haem in the former and protohaem IX-like haem in the latter) and copper (Kita *et al.*, 1984a). There remains in the literature, however, some confusion as to the copper-haem stoicheiometry in cytochrome *o* but more recent EPR and optical evidence argues in favour of there being only one copper per complex (*c.f.* Kita *et al.*, 1984a; Georgiou *et al.*, 1988a; Salerno *et al.*, 1990 and this chapter). This is in contrast to (at least) two copper components known to exist per cytochrome aa_3 monomer.

Further confusion lies in the lack of a definitive assignment of the optical bands in the α region to either of the two *b*-type haems found in cytochrome *o*. Difficulties in resolving the optical bands, and therefore the redox behaviour of this enzyme, have in the past been compounded by the use of strains with wild-type expression of cytochrome *o* in a high background of other *b*-type and *c*-type haems in the membranes and the expression of the alternative quinol oxidase, cytochrome *bd*. In those studies with purified enzyme preparations, the ligand binding haem component (haem *o*) has been alternatively identified with either the absorbance peak at 555nm (Kita *et al.*, 1984a) or 564nm (Withers & Bragg, 1990) (see below). It is also reported that the α band of cytochrome *o* is relatively insensitive to carbon monoxide ligation (Kita *et al.*, 1984a;

van Wieklink *et al.*, 1982). In support of this, the optical nitrite difference spectra presented in Chapter 3, revealed little perturbations except in the Soret region. Photochemical action spectra (see Poole, 1988) and multi-order finite difference spectra in the presence of carbon monoxide (Kita *et al.*, 1984a; Scott & Poole, 1982) remain equivocal and have failed to positively identify either band with haem *o*.

To date conclusive evidence for the presence of a cytochrome *o*-type oxidase is taken from the carbon monoxide difference spectra in the Soret region, photo-relief of carbon monoxide-inhibited respiration and established kinetic competence (Haddock *et al.*, 1976) of the carbon monoxide binding moiety to act as an oxidase (*c.f.* Chapter 3) (Poole *et al.*, 1979a & b). This chapter will attempt to characterise the redox behaviour of the α band absorbance(s) arising from cytochrome *o*, taking advantage of a purified enzyme preparation from the amplified strain RG145 (*cyo*$^-$ *cyd*$^-$ which possesses a multicopy *cyo*$^+$ plasmind).

As discussed above, the reduced *minus* oxidised difference spectrum of purified cytochrome *o* contains a broad α band (more clearly resolved into two distinct peaks at lower temperature; Chapter 3, Figure 3.5a). The origin of this duplex may come from two separate haem components (i.e. haems *b* and *o*), but equally, may arise from a single haem with a split absorption band. Until this problem has been addressed complete and accurate analysis of potentiometric data by optical methods will prove problematical.

Perhaps the clearest characterisation, to date, of the redox behaviour of the haems of cytochrome *o* is provided by low temperature EPR spectroscopy, previously described by Salerno *et al.*, (1990,1989) and confirmed in the purified enzyme (Chapter 3). The data from these experiments can be summarised as follows (citing the published oxidation-reduction potentials of Salerno *et al.*, (1990)). A high-spin (g=6.0) signal, attributable to haem *o*, was shown to give a bell-shaped titration curve (see Chapter 3). The low potential region of the curve can be fitted with two n=1 components with mid-point potentials of +160mV and +250mV. The high potential region can be fitted with a single n=1 transition and is suggested to be due to the loss of the high-spin signal resulting from antiferromagnetic spin coupling between the observed high-spin resonance (haem *o*) and a copper centre (Cu_o), as the latter goes oxidised. The low-spin signal, haem *b* (g=3.0 and 2.25), was also shown to give a titration curve which was fitted with two components, $E_{m,7}$'s of +160mV and +250mV. However, no loss of low-spin signal intensity was observed at high potential. In the presence of carbon monoxide, the g=6.0 signal disappeared, consistent with its assignment to haem *o*, whilst the low-spin haem *b* potential shifted in the reduced direction, taken as evidence for haem-haem interaction of the sort shown to exist in cytochrome aa_3 (Leigh *et al.*, 1974; Wilson *et al.*, 1972).

In the present optical study analysis of the α band of purified cytochrome *o* (room temperature) showed two peaks

with λ_{max} at 558nm and 564nm. Potentiometric analysis of these peaks revealed unusual behaviour in the presence of carbon monoxide and the results were suggestive of an anticooperative interaction between haem centres, consistent with EPR data from membrane preparations (Salerno *et al.*, 1990) and purified cytochrome *o* (Chapter 3).

Also reported in this chapter is a more detailed examination of the optical spectrum of cytochrome *o*. A new absorbance in the reduced spectrum, detected in the near-infrared region, is reported. This absorbance may be analogous to the charge transfer resonances (band III) of haemoglobin and myoglobin (Iizuka *et al.*, 1974). In addition, carbon monoxide caused a spectral shift in a trough thought to be associated with the high-spin (ferric) haem *o* (Bolgiano *et al.*, 1991). In the absence of carbon monoxide the trough had a λ_{min} around 632nm but upon addition of carbon monoxide this shifted to 643nm.

Detailed analysis of these data, coupled with analysis of the effect of carbon monoxide on the potentiometry of the optical bands, is presented and their significance discussed.

4.2 Results & Discussion

4.2.1 *Optical spectra*

Figure 4.1 shows the reduced *minus* oxidised difference spectra of a) purified cytochrome *o*, b) purified beef heart cytochrome *c* oxidase and c) solubilised succinate-cytochrome *c* oxidoreductase (mainly bc_1 complex). Spectra were scanned in the visible to near-infrared region of the spectrum. Also shown are expansions (x10) of the region between 650nm to 900nm for the enzyme complexes. Features include a broad absorbance in the oxidised form of the cytochrome *c* oxidase (indicated by a broad trough in the reduced *minus* oxidised difference spectrum) centred around 830nm (Figure 4.1b) which is due to copper (Cu_A). Of note is the absence of any such feature in the spectrum of purified cytochrome *o* (Figure 4.1a). However, the x10 expansion in Figure 4.1a clearly shows an absorption band with λ_{max} around 758nm. No comparable feature is seen in the spectrum of cytochrome *c* oxidase, however this does not preclude the possibility that a similar feature could be swamped by the trough associated with Cu_A. The spectrum of succinate-cytochrome *c* oxidoreductase, Figure 4.1c, is shown for comparison; it is a *b*-type haem containing complex which does not contain copper. The spectrum of succinate-cytochrome *c* oxidoreductase is featureless beyond 600nm and shows neither a trough around 830nm nor a peak around 758nm.

The reduced *minus* oxidised difference spectrum of cytochrome *o* also reveals a trough, centred at 632nm,

Figure 4.1

Comparison of reduced minus oxidised optical difference spectra from different purified enzyme complexes.

Sodium dithionite reduced *minus* potassium ferricyanide oxidised difference spectra are shown of (A) purified cytochrome *o* complex extracted from *E. coli*, strain RG145, (0.7μM final enzyme concentration in cuvette); (B) beef heart cytochrome *c* oxidase (1μM) and (C) beef heart succinate cytochrome *c* reductase (1μM). *Insets* show x10 expansions from 650 - 900nm for each enzyme. An oxidised spectrum was stored by microcomputer and subtracted from a scan of the sample after reduction with solid dithionite. All spectra were recorded at room temperature. Cytochrome *c* oxidase was preincubated with catalase to remove bound peroxide from enzyme.

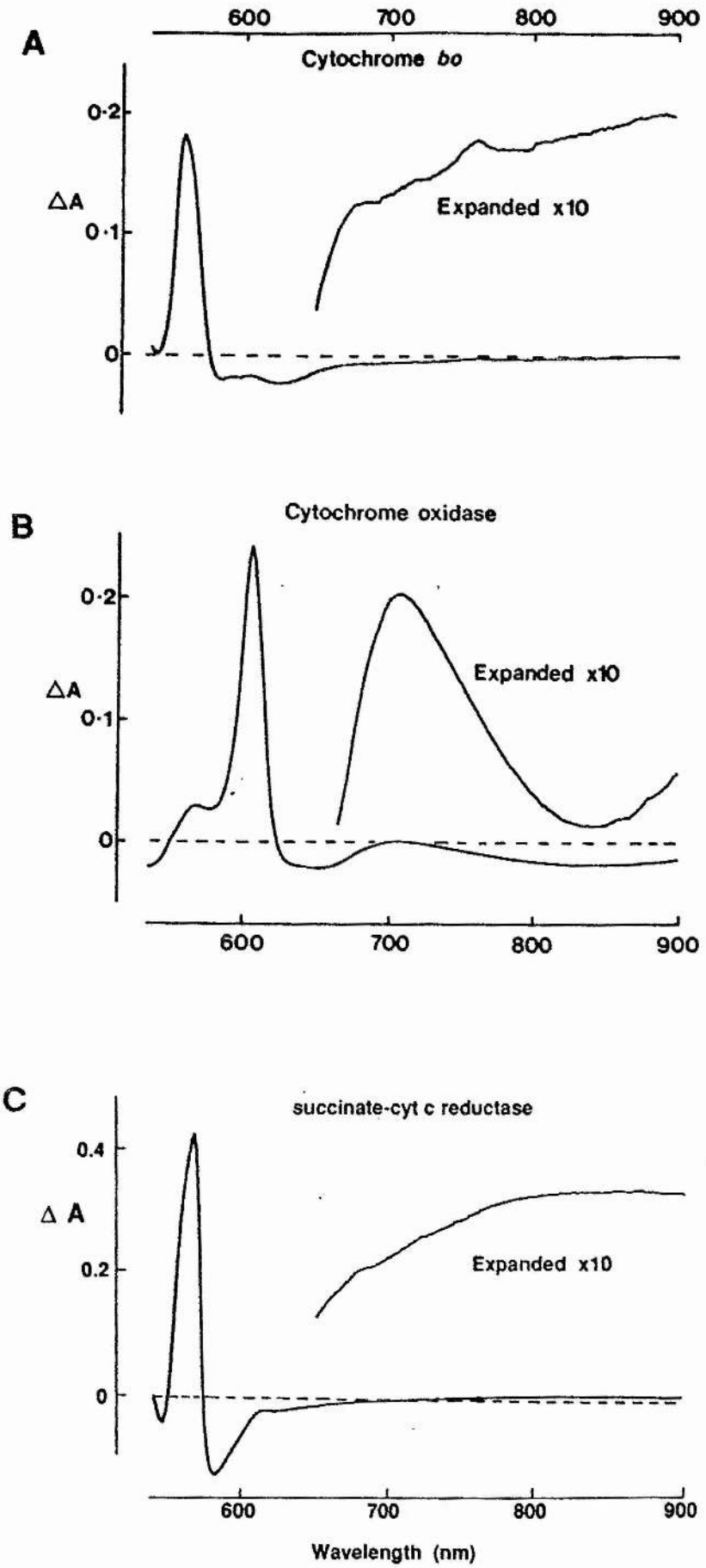
A
600
700
800
900
Cytochrome bo
0·2
ΔA
0·1
0
Expanded x10
B
Cytochrome oxidase
0·2
ΔA
0·1
0
Expanded x10
600
700
800
900
C
succinate-cyt c reductase
0.4
Δ A
0.2
0
Expanded x10
600
700
800
900
Wavelength (nm)

believed to be associated with the high-spin (ferric) haem *o* (Wood, 1984; Bolgiano *et al.*, 1991).

4.2.2 *The effect of peroxide*

Stoicheiometric additions of hydrogen peroxide were made to purified cytochrome *o* to produce the peroxide binding spectrum shown in Figure 4.2. When hydrogen peroxide was added in excess, the peroxide binding spectrum of cytochrome *o* remained unchanged, as evidenced by the difference spectrum also shown in Figure 4.2 (*broken line*). This is in marked contrast to observations in the cytochrome aa_3 system where the presence of excess hydrogen peroxide causes the "peroxy" form of cytochrome aa_3 to convert to the ferryl-oxo intermediate [$Fe^{4+}=O^{2-}$] (Chan *et al.*, 1988; Witt & Chan, 1987). Whilst the peroxy state has a characteristic α-band absorbance at 606nm, the ferryl state is identified by an α-band absorbance at 580nm. Thus, a trace of stoicheiometric-H_2O_2 *minus* excess-H_2O_2 produces a difference spectrum in cytochrome *c* oxidase. The finding that excess hydrogen peroxide did not elicit a change in the binding spectra of cytochrome *o* is potentially very informative. Cytochrome *c* oxidase is a single electron acceptor in which one might expect four electronic reduction states of dioxygen under appropriate conditions. The so called peroxy intermediate is a $2e^-$ reduction state and the ferryl intermediate is a $3e^-$ state (Section 1.6; see also Orii, 1988 and references found therein). It is, as yet, unclear whether a ferryl intermediate is produced in cytochrome *o*,

Figure 4.2

Peroxide binding spectra of cytochrome o in visible region

A room temperature light absorption spectrum of peroxide bound cytochrome *o*, is presented. The solid line indicates the spectrum from cytochrome *o* after a stoicheiometric addition of hydrogen peroxide *minus* the ferricyanide oxidised spectrum. The oxidase concentration was approximately 0.6μM final concentration in 50mM phosphate buffer, pH 7.0. The broken line shows the difference spectrum of the x50 excess hydrogen peroxide treated oxidase *minus* the spectrum of the oxidase treated with a stoicheiometric hydrogen peroxide addition. The relative gain is indicated. A slight baseline shift is observed below 600nm. The protein concentration and buffer system were the same as for the solid line spectrum, above.

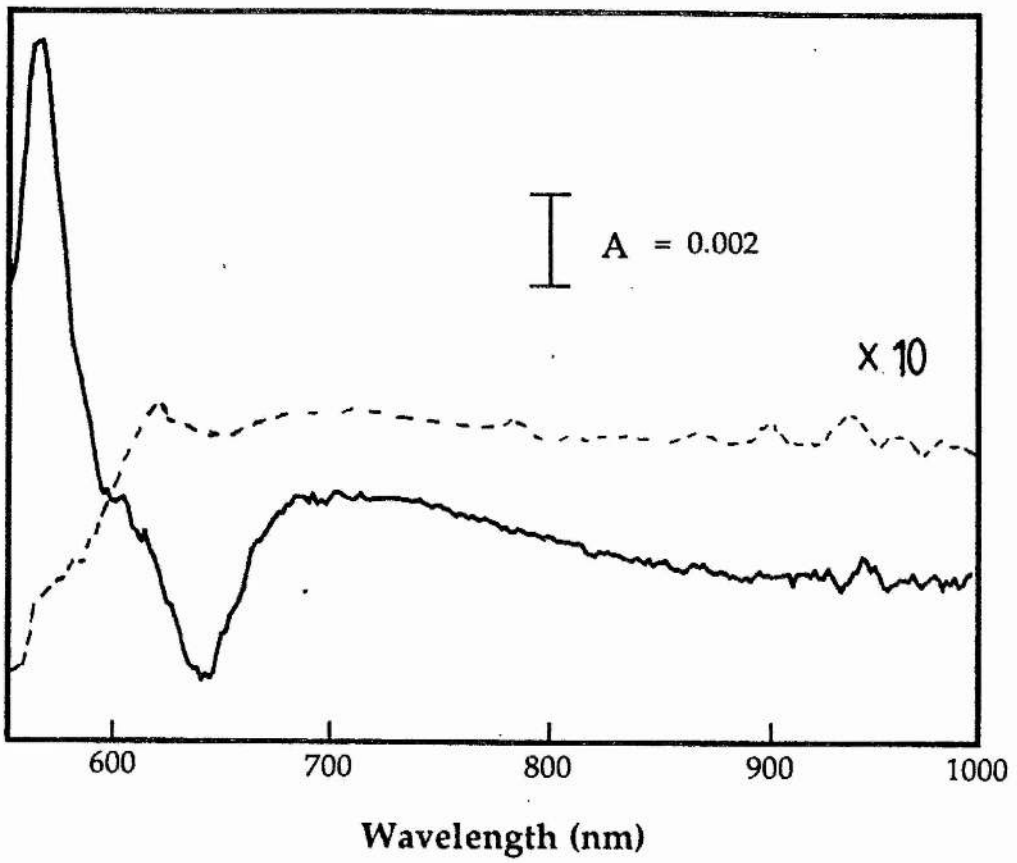
A = 0.002
X 10
600
700
800
900
1000
Wavelength (nm)

but if not, as these preliminary optical studies indicate, it may well be a function of the electron donor for cytochrome *o*, ubiquinol ($2e^-$). With a two electron donor system, cytochrome *o* might only exist in the two or four electron reduced state with oxygen. During turnover, this would mean that 50% of the enzyme population would be in the two electron reduced or peroxy state. Preliminary unpublished results appear to agree with this (P.R. Rich, personal communication). This has important consequences for models for the chemistry of dioxygen reduction and may indicate a departure from the mechanism employed by cytochrome *c* oxidase (see Chapter 1, Figure 1.5). It also questions the importance of the ferryl intermediate in vectorial proton pumping, at least for cytochrome *o*, as suggested by Wikstrom (1989) for cytochrome *c* oxidase. The use of rapid transient analysis techniques in resonance Raman spectroscopy on the reaction between dioxygen and cytochrome *o* will identify a ferryl intermediate, if present (e.g. Han *et al.*, 1990a & 1990b).

4.2.3 *The effect of carbon monoxide on the optical spectrum of cytochrome o*

Carbon monoxide binding to cytochrome *o* was confirmed by the difference spectrum in the Soret region showing a peak at 415nm and a trough at 432nm, in agreement with reported results in the literature (Caster and Chance, 1955,1959). This has already been reported in Chapter 3. Carbon monoxide difference spectra (reduced-*plus*-CO *minus*

reduced) in the region of 500nm to 600nm showed two additional peaks at 530nm and 568nm and troughs at 550nm and 580nm (see Figure 3.5b).

Figure 4.3 shows the difference spectra obtained from purified cytochrome *o* between 600nm and 800nm in the presence and absence of carbon monoxide. The reduced *minus* oxidised difference spectrum reveals a feature centred around 758nm (Figure 4.3, *upper trace*). The ratio of the Soret/758nm bands is approximately 1000, which would make the extinction coefficient of this feature about 0.145 $mM^{-1}cm^{-1}$ assumming 100% of the haem contributes to this feature (calculated from the ε_λ Kita *et al.*, 1984a). The 758nm band is quenched by the addition of carbon monoxide (Figure 4.3, *lower trace*) and subsequently regenerated by prolonged aggitation in the presence of dithionite and absence of carbon monoxide. The carbon monoxide bleaching can also be reversed by light, in parallel to other carbon monoxide binding characteristics, (not shown). Membrane fragments obtained from strain RG145 also show a peak at 758nm which confirms this feature is real and not an artifact of the purification procedure. The absorbance associated with the membrane bound form of the enzyme is also quenched by carbon monoxide as well as other inhibitory ligands known to bind to the reduced form of high-spin haem (not shown).

The optical spectra of myoglobin and haemoglobin have been extensively studied with the result that the optical bands of these proteins have been well characterised.

Figure 4.3

The effect of carbon monoxide on the 758nm absorbance.

Spectra of purified cytochrome *o*, reduced with solid dithionite, were scanned in the near infrared region from 700nm to 900nm, in the presence and absence of carbon monoxide. Loss of the 758nm band is seen in the carbon monoxide-inhibited oxidase (*lower trace*). Spectra were recorded at room temperature, in 50mM phosphate buffer, pH7.5, the protein concentration was 3μM, final.

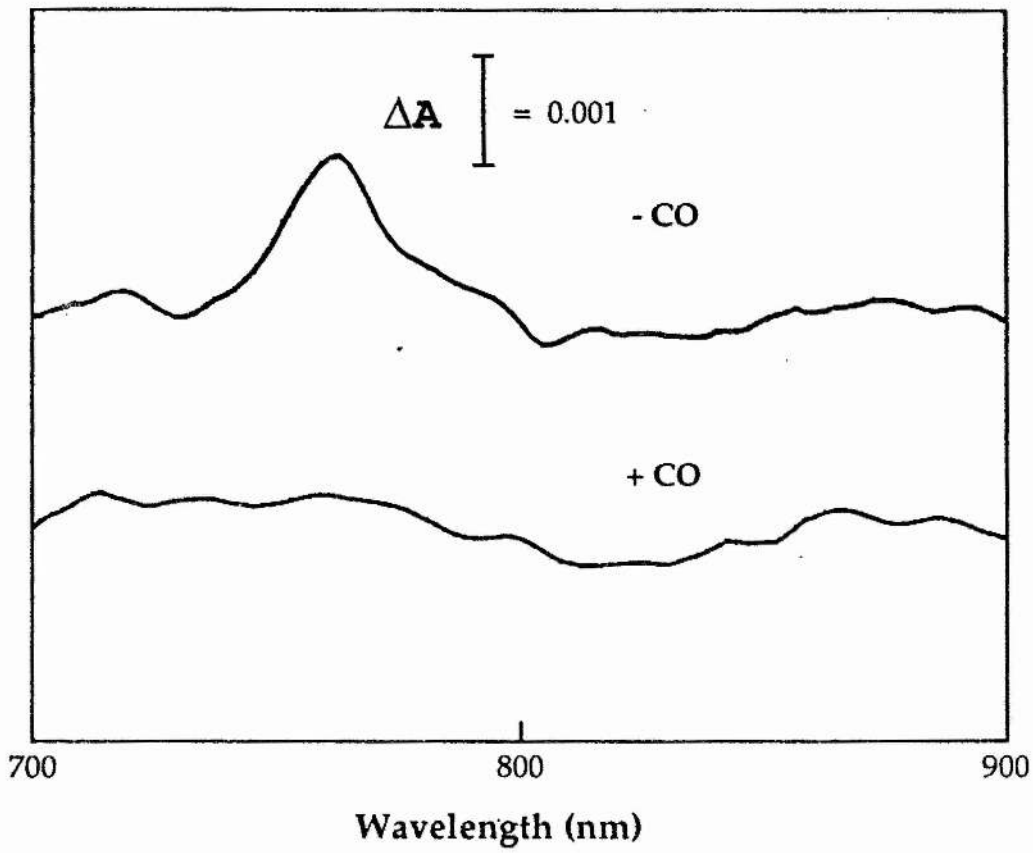
ΔA
= 0.001
- CO
+ CO
700
800
900
Wavelength (nm)

Absorbance spectra in the near infrared region of myoglobin, Mb(Fe^{2+}), show an absorbance peak at 758nm (Iizuka *et al.*, 1974) which is sensitive to the conformational state of the haemoprotein (Xie & Simon, 1991; Ansari *et al.*, 1985; Campbell *et al.*, 1987; Sassaroli & Rousseau, 1987; Fiamingo & Alben, 1985; Chavez *et al.*, 1990). This absorbance arises from a charge transfer transition between the porphyrin π system and the iron π system [$a_{2u}(\pi)$ ---> d_{zy}] (Eaton *et al.*, 1978). The Mb(Fe^{2+})-CO form is also reported to have an absorbance in this region but this broadens markedly on increasing the temperature (almost negligible above 50K). In this respect, we would expect to see a near infrared absorbance feature disappear in the carbon monoxide-inhibited cytochrome *o* at room temperature. This is what is observed (see Figure 4.3, *lower trace*). Photolysis of the Mb(Fe^{2+})-CO species gives rise to the reduced, unliganded, species. However, at sufficiently low temperature (4.2K) the 758nm band of myoglobin is shifted to 772nm signifying a conformational difference between the reduced form (R, ground state) and the reduced form created by photodissociation (R*) (Iizuka *et al.*, 1974). No red shift has so far been observed in the photodissociated cytochrome *o* enzyme. This is possibly because at 77K, the lowest temperature at which photolysis experiments have so far been attempted (not shown), the photolysed enzyme can relax to the reduced ground state. Lower temperature (<50K) photolysis experiments are required to identify the cytochrome *o* enzyme in the ligand bound conformation but in

the non-liganded state (R*).

Future studies might also benefit from coupling mutagenesis experiments on putative endogenous ligands to the high-spin haem *o* with optical studies in the near infrared region.

Carbon monoxide also causes a red shift in the high-spin trough at 632nm, this is shown in Figure 4.4. In the presence of carbon monoxide the trough (inverted by computer manipulation and shown as a peak in figure) broadens with a shift in the λ_{max} to 643nm (lower trace). Since the 632nm absorbance is thought to be due to a ferric (Fe^{3+}) haem species it is not expected to be present in the carbon monoxide-inhibited enzyme (Fe^{2+}-CO). The "corresponding" high-spin ferric haem absorbance in cytochrome *c* oxidase (655nm) is abolished by carbon monoxide.

4.2.4 *Redox behaviour of the α band*

Optical titrations were performed at pH 6, 7 and 8 and the two peaks in the α band (λ_{max} 556nm and 564nm) associated with cytochrome *o* were deconvoluted using 576nm as the reference wavelength. The titration curves for each peak can be seen in Figure 4.5a. Each curve contained two separable components which fit well with two n=1 processes. Each transition showed approximately -60mV/pH unit dependance over the pH range, (Figure 4.5b). At pH 7.0 the feature centred at 564nm gave $E_{m,7}$ values of +249mV for the

Figure 4.4

The effect of carbon monoxide on the high-spin trough.

Shown are difference spectra of cytochrome *o* in the 600nm and 700nm optical region. For the purposes of this diagram, the trough has been inverted by subtracting a fully reduced spectrum from a sample spectrum. The upper trace is of the enzyme in the absence of carbon monoxide and is essentially an oxidised *minus* reduced spectrum. It can be seen that an oxidised (ferric) absorption feature is centred at 632nm. The lower trace was produced by treating the sample with carbon monoxide and represents the carbon monoxide-inhibited spectrum *minus* the fully reduced. The lower trace shows the trough shifted ~10nm (λ_{max} 643nm) towards the red and broadened by carbon monoxide. Conditions were the same as those for Figure 4.3, except, final protein concentration was 0.9μM.

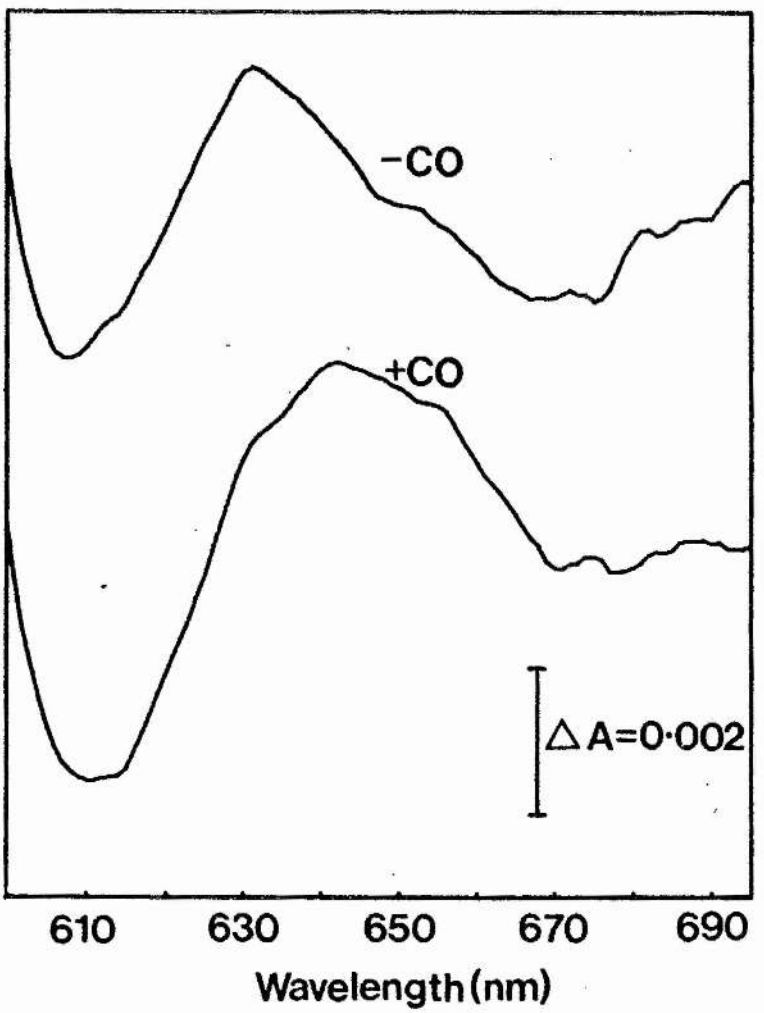
-CO
+CO
ΔA=0·002
610
630
650
670
690
Wavelength (nm)

Figure 4.5a

Redox titrations of the alpha band.

Shown are the absorbance changes of the 558nm (A) and 564nm bands (B) relative to 576nm. Plotted are titrations at different pH's; (squares) pH 8; (circles) pH 7; (triangles) pH 6. Each curve was fitted with two non-interacting n=1 components, the higher potential component in each accounting for approx. 60% of the total absorbance. Redox titrations were performed as described in the Methods section. The mid-point potentials of these components, at pH 7, are +250mV, +105mV for the 564nm band and +240mV, 90mV for the 558nm band. The buffer systems used are described in Materials & Methods Chapter.

a

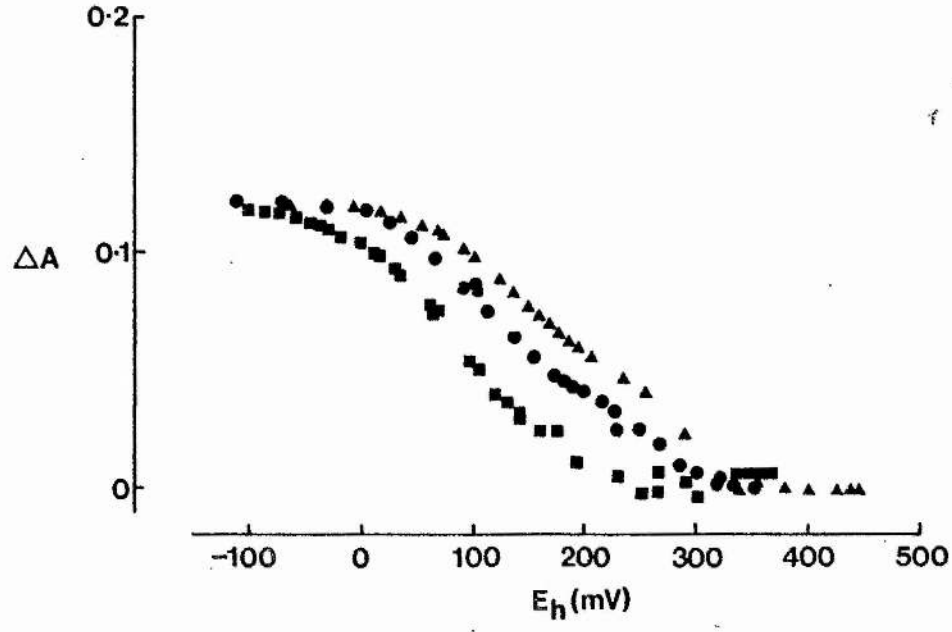
0·2
ΔA
0·1
0
−100
0
100
200
300
400
500
E_h (mV)

b

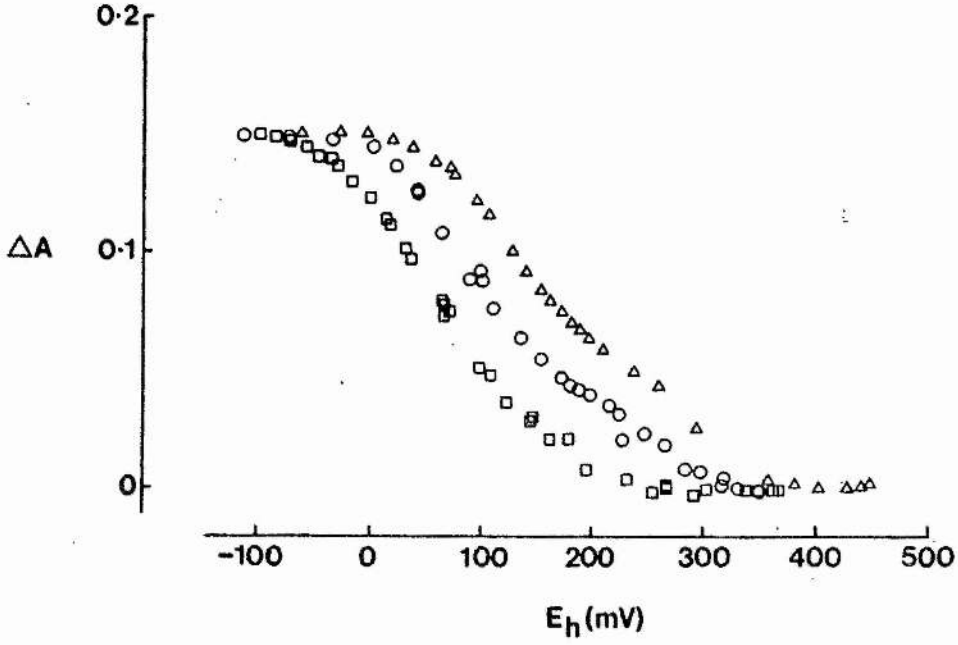
0·2
ΔA
0·1
0
−100
0
100
200
300
400
500
E_h (mV)

Figure 4.5b

pH dependence of redox features in the α band

The pH dependence of the mid-point potentials of the redox components in Figure 4.5a, are shown. In (A), the redox mid-points of the high (closed triangles), and the low (open triangles), potential components of the 558nm band, are plotted against pH. (B) plots the high and low potential components, (closed and open circles, respectively) of the 564nm band. The straight lines show the theoretical -60mV/pH unit dependence.

A

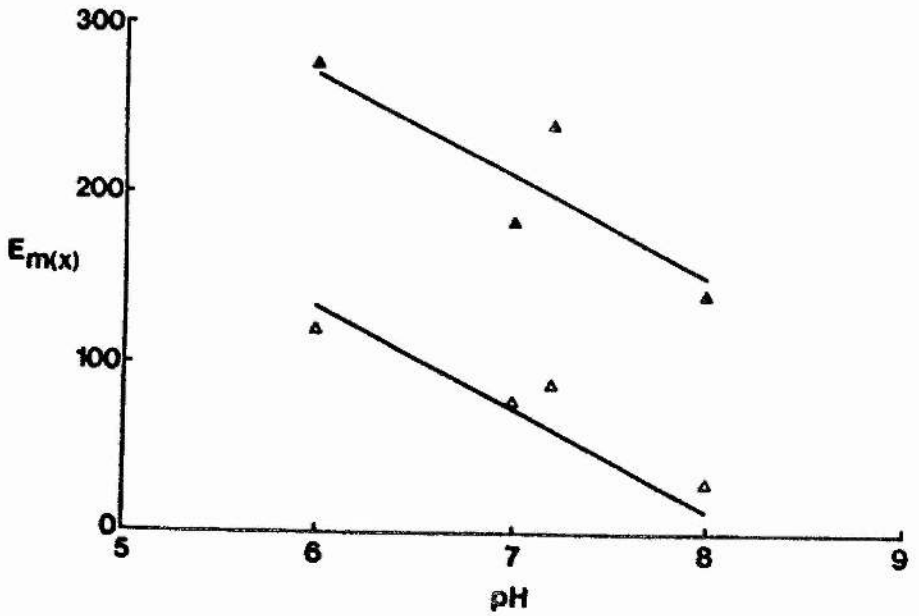

B

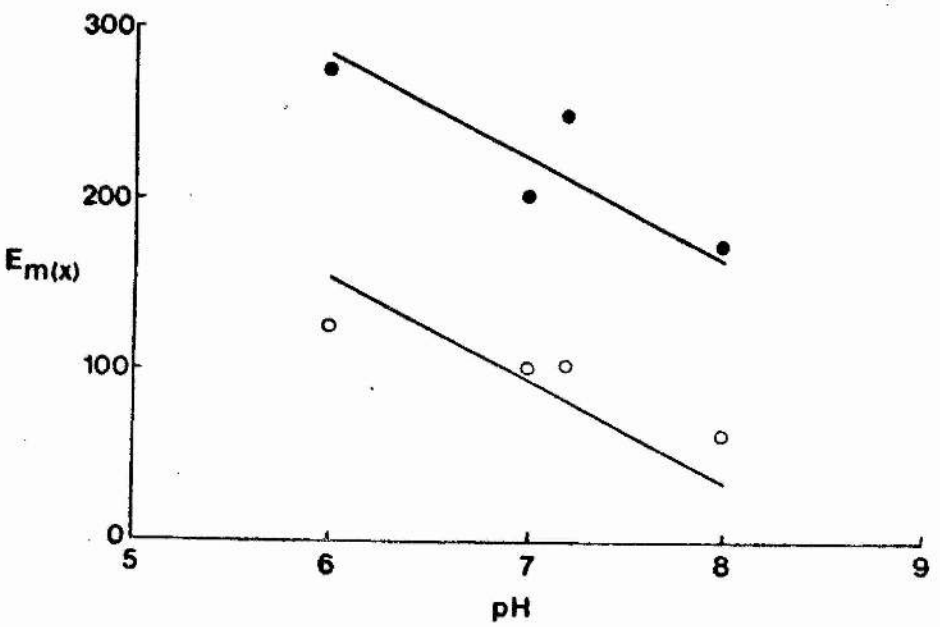

high potential wave and +103mV for the low potential wave, contributing to 40% and 60% of the total absorbance change, respectively. The feature centred around 558nm gave $E_{m,7}$ values of +239mV(40%) and +87mV(60%). The high potential transition for both peaks is similar to that reported in EPR studies on the purified enzyme in Chapter 3 and in membrane preparations (Salerno *et al.*, 1990; Salerno *et al.*, 1989; Bolgiano *et al.*, 1991). However, the low potential wave is somewhat lower than those reported by these authors. This disparity is perhaps due to these data coming from a detergent solubilised purified enzyme, not the membrane bound, complex. Furthermore, in view of the low temperatures at which the EPR data, from Salerno and colleagues, was obtained, a temperature dependance of the mid-point potentials may exist due to electron redistribution at low temperature.

4.2.5 *The effect of carbon monoxide on the redox behaviour of the α band*

In order to observe the effect of carbon monoxide on the potentiometry of various optical features in the visible spectrum redox titrations were performed, as described in Chapter 2, under a positive pressure of carbon monoxide. Figure 4.6 shows data obtained from a redox titration performed at pH 7.0. Under these conditions the 558nm band (A) titrates with two n=1 components with $E_{m,7}$ values of +155mV(40%) and +110mV(60%). The 564nm band (B) also titrated with two n=1 transitions ($E_{m,7}$ of +80mV(60%) and

Figure 4.6

The effect of carbon monoxide on the redox behaviour of the α band

Shown in (A) is the redox behaviour of the 558nm band in the presence of carbon monoxide. The higher potential component, seen in Figure 4.5a (A), shifts to a lower potential whilst the relative contribution remains the same (40%). The overall absorbance also remains the same. The mid-point potentials in the presence of carbon monoxide are +160mV and +80mV (pH 7.0). The 564nm band is similarly affected, (B), the mid-point potentials for this band are +155mV and +110mV. In both graphs the dotted lines indicate the individual n=1 curves used to produce the Nernstian redox curve (solid line).

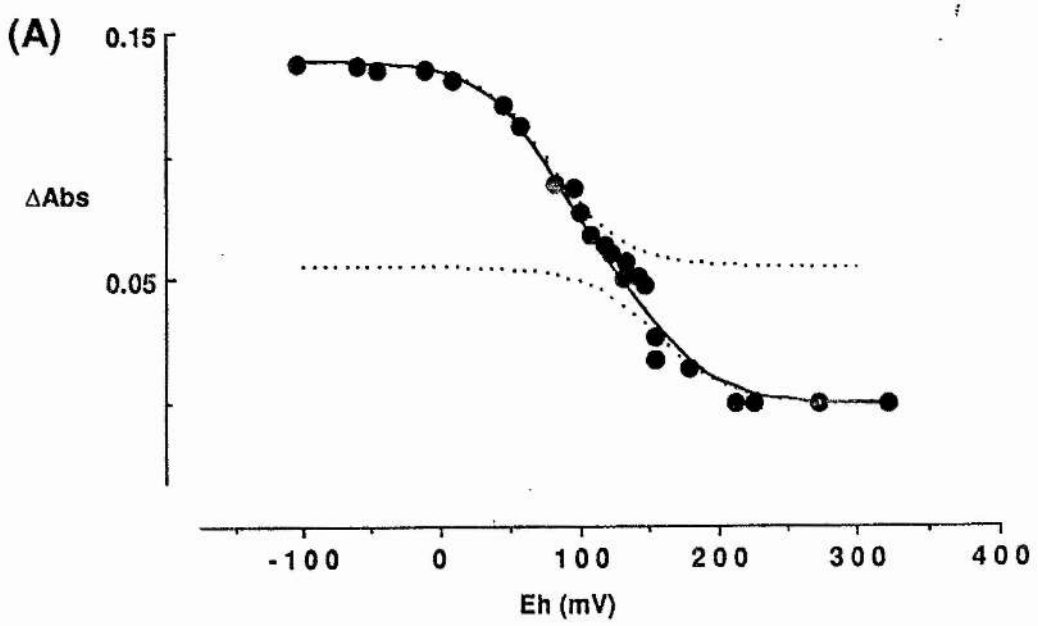
(A)
0.15
ΔAbs
0.05
-100
0
100
200
300
400
Eh (mV)

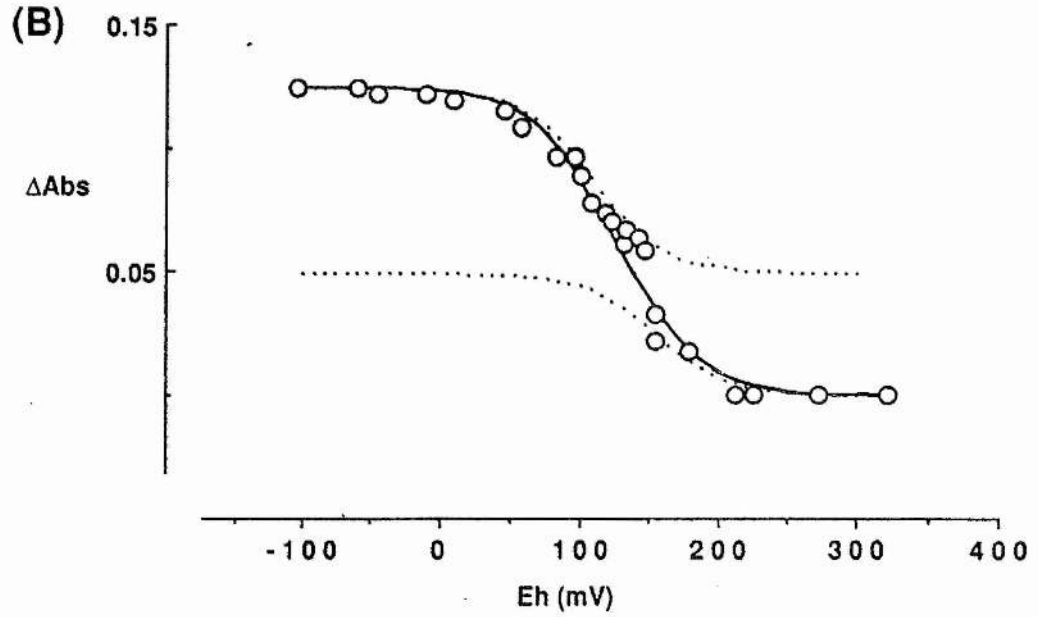
(B)
0.15
ΔAbs
0.05
-100
0
100
200
300
400
Eh (mV)

+157mV(40%)). The composite Nernst curve, obtained from the individual n=1 curves (dotted lines), is given (solid line).

Many ligand binding components have been identified by virtue of their redox behaviour in the presence of carbon monoxide. Carbon monoxide is known to bind to ferrous haem, forming a stable carboxyferrohaem complex consequently elevating the mid-point potential (more oxidised) of those component(s) able to undergo carbon monoxide ligation. By comparing the data in Figure 4.5 & 4.6 it is seen that the overall absorbance for both peaks, whether carbon monoxide is present or not, remains the same which is suggestive of the high-potential component, observed in the absence of carbon monoxide, being shifted into the low-potential component rather than being shifted to a more positive value outwith the redox potential range of the titration. It would also be consistent with the anomalous behaviour of cytochrome *o* with carbon monoxide (Kita *et al.*, 1984a). If haem *o* were to contribute significantly to the α band, the results from cytochrome *o* would be somewhat surprising, assuming carbon monoxide binds to the reduced haem *o* centre. On the basis of these data, it is proposed that both bands in the α region originate from the low-spin haem *b* centre (see Conclusion).

In an optical study on a purified preparation, Kita *et al.* (1984a) found that cytochrome *o* titrated as a single component with $E_{m,7.4}$ of +125mV, although the redox range was not wide enough to eliminate the possibility of other components. Unfortunately the redox behaviour of the carbon

monoxide-inhibited enzyme was not determined in this study.

In a more recent report, Withers and Bragg (1990) (see also Sedgwick & Bragg, 1988; Withers & Bragg, 1987) identified three optical components at 553.5-554.75, 557.5 and 563.5-564nm (the variation was dependent on the origin of preparation) by higher order derivative spectra of purified cytochrome *o*. Potentiometric titration of the α band indicated the presence of three redox components with mid-point potentials +260mV (22%), +127mV (49%) and -58mV (29%). The mid-point of the +260mV component was shifted to a more oxidised potential in the carbon monoxide-inhibited enzyme and was taken to be consistent with this component binding carbon monoxide in the reduced form.

The results presented in this study are at variance with the results of Withers & Bragg (1990). The significance of this cannot be ascertained as further analysis of their data is hampered by a lack of absolute absorbance values for their published titrations. However, it should be noted that the presence of a major low potential component ($E_{m,7}$ of -58mV;20%) identified in their purified preparation (not seen in the study presented herein) is difficult to reconcile with our current understanding of the oxidase. Indeed, it is difficult to envisage a role for this component in a ubiquinol oxidase ($E_{m,7}$(UQ) of +70mV, although $E_{m,7}$(MQ) of -74mV, (from Ingledew & Poole, 1984) and it may be due to damaged haem.

A detailed study of the redox components present in membrane fragments of a strain containing amplified

expression of cytochrome *o* has recently been reported (Bolgiano *et al.*, 1991). Based on computer analysis of area and surface optical titration data, Bolgiano *et al.* (1991) identified two redox components with $E_{m,7}$= +58mV and +227mV in the α band. Experiments were not carried out in the presence of carbon monoxide.

4.2.6 *Redox behaviour of other optical features of cytochrome o*

Figure 4.7 shows the results of a redox titration performed on the 758nm band seen in Figure 4.3 (pH 7.0). The size of the feature makes analysis difficult and subsequent determination of oxidation-reduction potentials should be treated with caution. With this proviso, these data were fitted with two n=1 components and found to give $E_{m,7}$ values of +300mV and +120mV, split 50:50. On the basis of the interactive model proposed, it is anticipated that the mid-point potential of the high-spin haem *o* would be split into two phases. The redox behaviour of the band III-like transition of cytochrome *o* is thus consistent with its assignment to haem *o*.

High-spin ferric haem usually possesses a broad absorbance in the 450nm to 650nm region (Wood, 1984). Although haem *o* does not absorb strongly, if at all, in the 560nm region, its presence is manifest in the optical spectrum in the form of an absorbance in the ferric state. In cytochrome *o* this absorbance is centred around 632nm and

Figure 4.7

Redox titration of the near infrared absorbance at 758nm

A titration of the 758nm signal was performed at pH 7.0. The feature titrated biphasically and could be fitted with two theoretical n=1 components, $E_{m,7}$ of +300mV and +120mV. Each component contributed to approximately half the total absorbance. A reduced sample was used as a baseline spectrum which gives rise to the apparent negative light absorption values in the data.

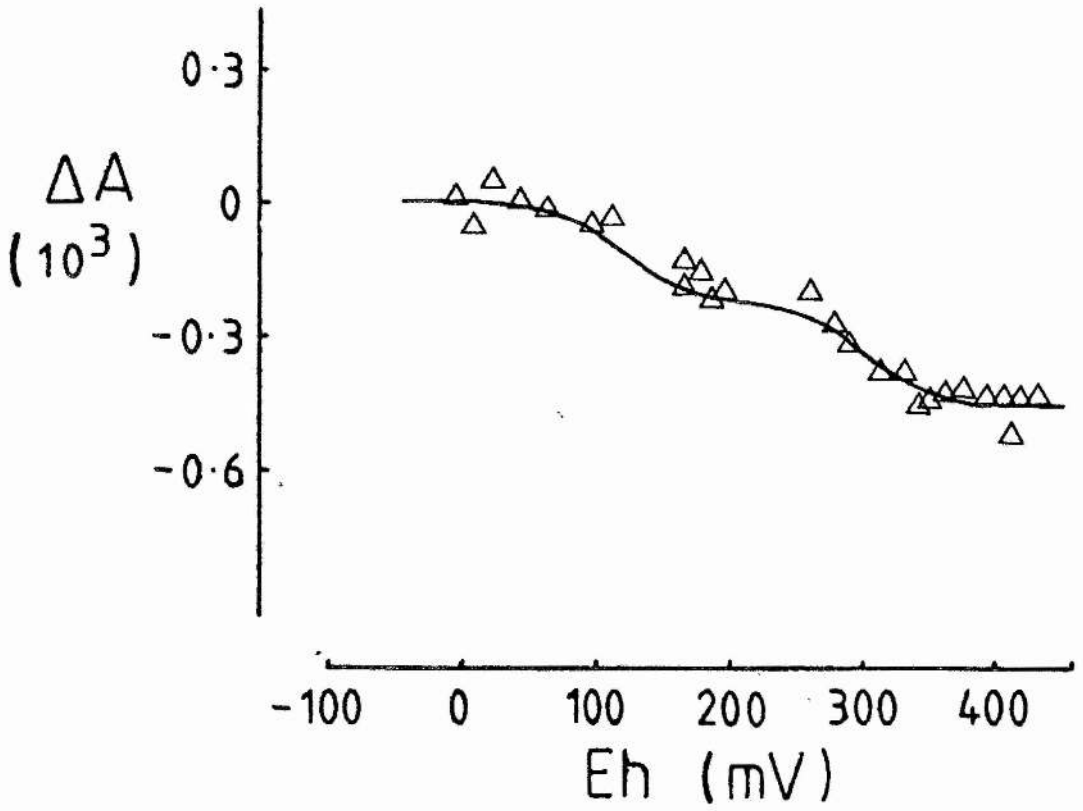
0·3
ΔA
(10³)
0
-0·3
-0·6
-100
0
100
200
300
400
Eh (mV)

has previously been attributed to high-spin ferric haem *o* in membranes of RG145 (Bolgiano *et al.*, 1991; λ_{min} 635nm). Potentiometric analysis of this feature showed it to titrate with a $E_{m,7}$ of +285mV (Figure 4.8). A more complex redox behaviour is reported (λ_{min} 635nm) by Bolgiano *et al.* (1991) in membrane preparations but this could be explained in terms of baseline shifts and changes in peak position.

In cytochrome *c* oxidase, a high-spin charge transfer band of ferric haem a_3 appears at 655nm (Mitchell *et al.*, 1991 and references found therein). Mitchell *et al.* (1991), have described the redox chemistry of this feature and point out that, although present as a trough in the fully reduced *minus* oxidised difference spectrum, the feature only exists when both centres (a_3 and Cu_B) of the binuclear site are fully oxidised. Consequently they observe a very high mid-point potential for this feature (ca. +400mV; n=1) (*c.f.* data in Figure 4.8). Inhibitors of respiration, such as carbon monoxide and azide, abolish the absorbance in cytochrome c oxidase, indicating the feature is influenced by the redox state of the binuclear site. Cyanide, which produces a ferric low-spin haem a_3, also abolishes the cytochrome *c* oxidase feature revealing the sensitivity of this feature to spin-state.

There are two obvious differences between the 632nm band of cytochrome *o* and the 655nm band in cytochrome *c* oxidase, which are; (i) although the cytochrome *o* absorbance titrates as a simple n=1 process, the apparent mid-point potential is relatively low (+285mV) and as a consequence

Figure 4.8

Redox titration of the 632nm "high-spin" trough

A redox titration (pH 7.0) was performed on the ferric haem feature characterised by a λ_{min} at 632nm. The data is of the optical signal intensity of this feature (obtained from inverted spectra *c.f.* Figure 4.4) plotted against potential. The signal titrates as a single n=1 transition with an Em,7 of +285mV. However, the end-point for these data is poor due to difficulties obtaining high oxidising potentials with reasonable additions of ferricyanide.

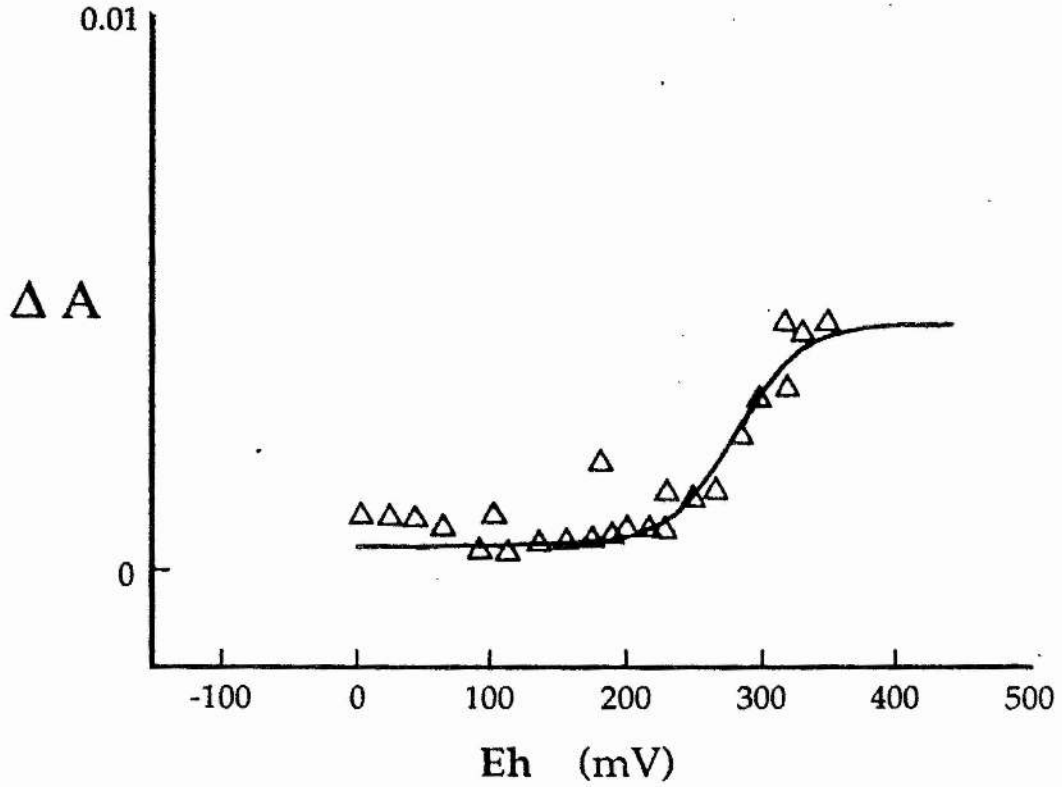
0.01
Δ A
0
-100
0
100
200
300
400
500
Eh (mV)

the absorbance must exist before the binuclear site is fully oxidised (Cu_o; $E_{m,7}$ ~ +350mV) and (ii) the feature is not abolished in the carbon monoxide-inhibited enzyme, only red-shifted. The reason for these differences is unknown but it seems obvious that the 632nm aborbance in cytochrome *o* is not due to a simple high-spin ferric haem component. It may represent a redox dependent intermediate spin state of the haem *o* centre.

4.3 Discussion

It is clearly shown that the light absorption spectrum of purified cytochrome *o* is deviod of any feature similar to the broad trough associated with the Cu_A centre in cytochrome *c* oxidase, (Figure 4.1a & b). Indeed, EPR investigations of membrane bound and purified preparations of cytochrome *o* have failed to detect a copper signal of sufficient magnitude to suggest the presence of copper in stoicheiometric amounts (Salerno *et al.*, 1990; Kita *et al.*, 1984b; Puustinen *et al.*, 1991). Previous reports of copper/iron ratios approaching one (Kita *et al.*, 1984a) have recently been revised downwards (unpublished reference in Chepuri *et al.*, 1990a). The optical evidence against there being a copper centre analogous to Cu_A of cytochrome *c* oxidase is compounded by the lack of sequence conservation between *cyo*A (subunit II, cytochrome *o*) and COII (subunit II, cytochrome aa_3) within the region thought to contain the putative ligand binding site for Cu_A (Chepuri *et al.*, 1990a).

A new absorption band present in the reduced form was identified in the near-infrared spectrum with a λ_{max} at 758nm. This feature was bleached by carbon monoxide and is analogous to the band III charge transfer absorbances identified in haemoglobin amd myoglobin. This feature may be useful in the future as a true marker of the redox state of

the high-spin centre (haem *o*). Identification of this band takes on an increased importance since it has been shown that ferrous haem *o* does not significantly absorb in the visible spectrum (discussed below). In addition, the only other feature in this region, the "632nm" band, does not parallel the redox behaviour of haem *o* expected if it was merely an indicator of the ferric state, (*c.f.* Figure 4.5). Preliminary potentiometric data from the 758nm band confirms the haem-haem interaction (discussed below) which is known to exist between the haem centres of cytochrome *o* (Salerno *et al.*, 1989,1990 and Chapter 3)

Potentiometry and model

From the redox data presented herein, both the 558nm and the 564nm band titrate essentially together which suggests that both peaks originate from one centre, haem *b*. This, in itself, is not conclusive proof. However, the assumption is further validated when the redox data obtained from the carbon monoxide-inhibited enzyme are considered. As mentioned, carbon monoxide should bind to, and stabilise, the ferrous haem *o*. If haem *o* contributed to the α band one would expect the potential of an optical component to be shifted far out to the right (more oxidised). The data herein, show that, far from being shifted to a more oxidising potential, the mid-point of the high potential component, for both the 558nm and the 564nm band, was shifted to a more reducing value. It is noteworthy, that the overall absorbance from both peaks remained the same, making

it unlikely that carbon monoxide caused a shift in the mid-point potential of a component outwith the range of the redox titration. Based on an EPR redox study, Salerno *et al.*, 1990, proposed an anticooperative model to account for the redox behaviour of the haem components in *in situ* cytochrome *o*. It is proposed that such a model can adequately account for the redox behaviour of the optical absorption in the α band of cytochrome *o*. Clearly, the α band does not titrate as a simple Nernstian n=1 process and the separation of the titration data into two redox waves must be due to an interaction between the absorbing centre (low-spin haem *b*) and another centre. The identity of the second centre can be speculated upon in view of the redox behaviour of the α band in the presence of carbon monoxide. The most likely candidate must be high-spin haem *o* which will bind carbon monoxide and remain trapped in the reduced form. Thus, the redox data, under such conditions, will be due to the real mid-point potential of haem *b* plus the interaction strength/potential due to the site-site effects with reduced haem *o*. The magnitude of this interaction is approximately -100mV at pH 7.0 (room temperature). It is possible that some proportion of this interaction is due to Cu_o of the binuclear site, however, our understanding of the dependence of spectral behaviour of cytochrome *o* on the redox state of all the centres (including perhaps bound quinone) is inadequate to allow more detailed analysis at this time. Figure 4.9 details a proposed interactive scheme between haem centres which accounts for the redox behaviour

Figure 4.9

Interactive model between haem o and haem b

A cooperative redox model is shown for the two haem centres of cytochrome *o*. The high-spin, ligand binding, haem *o*, is represented by a **o** and the low-spin haem b is represented by **b**. The redox state of each centre is indicated and the mid-point potentials which would be observed for each possible transition, shown. Δ indicates the redox interaction strength (mV) and is ca. -100mV for cytochrome *o* at room temperature (pH 7.0). No account of the possible interactions between the copper (Cu_o) centre, at the bi-nuclear reaction site, or any interaction from other species, such as bound quinone (if present), has been taken in this scheme. E_b and E_o are the real mid-point potentials for haem *b* and haem *o*, respectively. These are observed when the appropriate centre is in the reduced state.

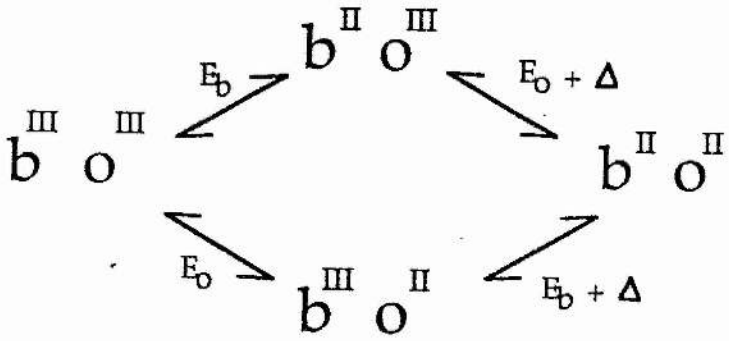
$b^{II}\ o^{III}$
E_b
$E_o + \Delta$
$b^{III}\ o^{III}$
$b^{II}\ o^{II}$
E_o
$b^{III}\ o^{II}$
$E_b + \Delta$

of EPR and optical data (after Salerno *et al.*, 1990).

If haem *o* contributed to the α band, as suggested by Withers & Bragg (1990), a more improbable explanation would be required to explain the data from the α band. In this, a redox component from both peaks would be shifted to a value outwith the measured range; an increase in the extinction of the remaining absorption (presumably haem *b*) would then be necessary to explain the lack of signal diminution in the presence of carbon monoxide. Whilst a conpensatory change in the extinction of a haem, not directly undergoing carbon monoxide ligation, may be possible, it seems extremely unlikely.

Recently, it has been proposed that, under certain conditions i.e. in an amplified strain where protoporphyrin IX synthesis is limiting, cytochrome *o* inserts an *o*-type haem in place of protoporphyrin IX at the low-spin six coordinate site (M. Wikstrom, personal communication, 1992). This will create two populations of cytochrome *o*, one incorporating a mole of haem *b* and a mole of haem *o* per mole of enzyme and another with two moles of haem *o*, one low-spin and the other high-spin, per mole of enzyme. This hypothesis can be used to explain the existence of two transitions in the redox data from the carbon monoxide-inhibited enzyme (Figure 4.6) when, strictly speaking, the cooperative interactive model predicts a single n=1 curve. The two potential waves in Figure 4.6 can be ascribed to the mid-point potentials of six coordinate low-spin haem *o* and low-spin haem *b*.

It is established that cytochrome *o* contains both high- and low-spin components, as identified by low temperature EPR spectroscopy (Salerno *et al.*, 1989, 1990; Hata *et al.*, 1985) and resonance Raman analysis (Uno *et al.*, 1985). The present data suggest that little or no contribution to the α band is made by haem *o*. That this might be the case is not necessarily surprising. The optical spectra of cytochrome *o* exhibit neither truly high-spin nor truly low-spin characteristics. These anomalies include; (i) a continuous absorbance in the ferric state between 500nm and 600nm characteristic of high-spin (Kita *et al.*, 1984a; Bolgiano *et al.*, 1991), (ii) a peak near 640nm in the oxidised state characteristic of high-spin (Figure 4.4 & Bolgiano *et al.*, 1991), (iii) the shape and temperature dependance of carbon monoxide difference spectra are more reminiscent of low-spin (see Wood, 1984; Poole, 1988) and (iv) a Soret/α band ratio of <30 & >10 in carbon monoxide difference spectra more characteristic of an intermediate spin state (data not shown, but see Wood, 1984). Many of these anomalies might be explained, in part, by the lack of a significant contribution in the α band by haem *o*.

Chapter Five

Magnetic Intracomplex Interactions and Spatial Organisation between Centres of the Cytochrome o complex

5.1 Introduction

Obtaining knowledge of the spatial organisation of the redox active centres involved in the cytochrome *o* complex is one important step towards an understanding of the mechanism of catalytic action of the enzyme; it also serves to set useful constraints on models proposed. The aim of the following study was to characterise the intramolecular organisation of the redox active centres of cytochrome *o* using EPR spectroscopy and extended X-ray absorption fine structure (EXAFS).

It is well established that the addition of exogenous paramagnetic rare earth cations, such as nickel (Ni^{2+}), gadolinium (Gd^{2+}) and dysprosium (Dys^{3+}), enhance the spin-lattice relaxation rate, $1/T_1$, of intrinsic paramagnetic redox centres, resulting in a relief of the microwave power saturation parameter ($P1_{/2}$) in a concentration dependent manner. This effect is quantifiable and has been successfully used to establish the asymetric distribution of redox centres within the respiratory chain (Case & Leigh, 1979; Blum *et al.*, 1983; Blum *et al.*, 1981; Rothery, 1989; Ohnishi *et al.*, 1989 and references found therein). In membrane preparations of *E. coli* with amplified expression of cytochrome *o*, both low-spin haem *b* and haem *o*, the latter as the paramagnetic nitrosylferrohaem complex (haem *o*-NO; see Chapter 3), show a dipolar interaction with added Dys(III)EDTA (Dys-EDTA). In the following study Dys-EDTA has been used to determine the sidedness and

spatial relationship between the redox active, EPR visible, centres in cytochrome *o*.

In addition, a study on oriented multilayers of membrane fragments treated with nitrite is also presented and the angular magnetic field dependence of the anisotropic haem *o*-NO (g = 2) spectrum is related to the structure of cytochrome *o*.

Characterisation of the redox active centres of proteins such as cytochrome *c* oxidase has been greatly hampered by the possibility of site interactions manifesting themselves in spectral perturbations and redox effects. A complete description of the copper centres of cytochrome c oxidase has particularly proved difficult for the following reasons. Optically the copper centres of this oxidase possess weak transitions. Additionally, one of the coppers is rendered "EPR silent" through a spin-coupled interaction with haem a_3. The second copper, Cu_A, although EPR-visible, is atypical and lacks the hyperfine structure of either a Type I or Type II copper (Cu^{II}) (see Powers *et al.*, 1979). X-ray Absorption Spectroscopy (XAS) is responsive to both copper centres and their redox state. Unfortunately, there are associated problems in the analysis of X-ray absorption data from species with multiple equivalent absorber sites. These will be the subject of more detailed discussion later in this chapter. Extended X-ray Absorption Fine Structure (EXAFS) data from purified cytochrome *o* (which has a simpler complement of metal centres) is examined in the light of

published results from cytochrome *c* oxidase.

Some of the information contained within this chapter has been reviewed elsewhere (Ingledew & Bacon, 1991).

5.2 Results & Discusion

5.2.1 *Interactions between Dysprosium and Redox centres of cytochrome o*

As was shown in Chapter 3, reduced cytochrome *o* reacts with nitrite to form the haem *o*-NO complex with a characteristic EPR spectrum around g = 2 (see Figure 3.12). Nitrosylferrohaem complexes are relatively slow relaxing and best observed at relatively high temperature and low microwave powers. The saturation behaviour of this species can be more usefully described by the parameter $P1_{/2}$. Figure 5.1 shows the effect of increasing microwave power on the spectrum of membranes reduced with lactate and treated with nitrite. A power profile of this effect can be obtained by plotting the intensity of the signal as a function of the square root of the microwave power *versus* the incident microwave power. Such a profile, obtained from features in Figure 5.1, is illustrated in Figure 5.2 and is quantitatively described by (Barber *et al.*, 1982):

$$S = k \ (P \ / \ [1 + {}^{P}/_{P1_{/2}}]^{0.5b})^{1/2} \qquad \text{.....5.1}$$

where S is the observed signal height; *k* is a constant relating to the concentration of species under investigation and b is a constant relating to the degree of inhomogeneous line broadening.

The descriptive parameter $P1_{/2}$ is the microwave power required for half saturation such that the following

Figure 5.1

EPR spectra of nitrosylferrohaem o species of membranes from E. coli strain RG145 at 1.6 and 16mW

EPR spectra of RG145 membranes (~45mg protein ml^{-1}), treated to form the nitrosyl haem *o* adduct (see Figure 3.12), are shown at (a) 1.6mW and (b) 16mW (76K). Principal g-values are indicated above spectra. The signal intensity increases on increasing incident microwave power. The relationship between signal height and power is shown as a double log plot in Figure 5.2. Spectrometer settings; gain, 8 x 10^4; time constant, 0.5 seconds; field modulation intensity, 5 gauss (peak to peak).

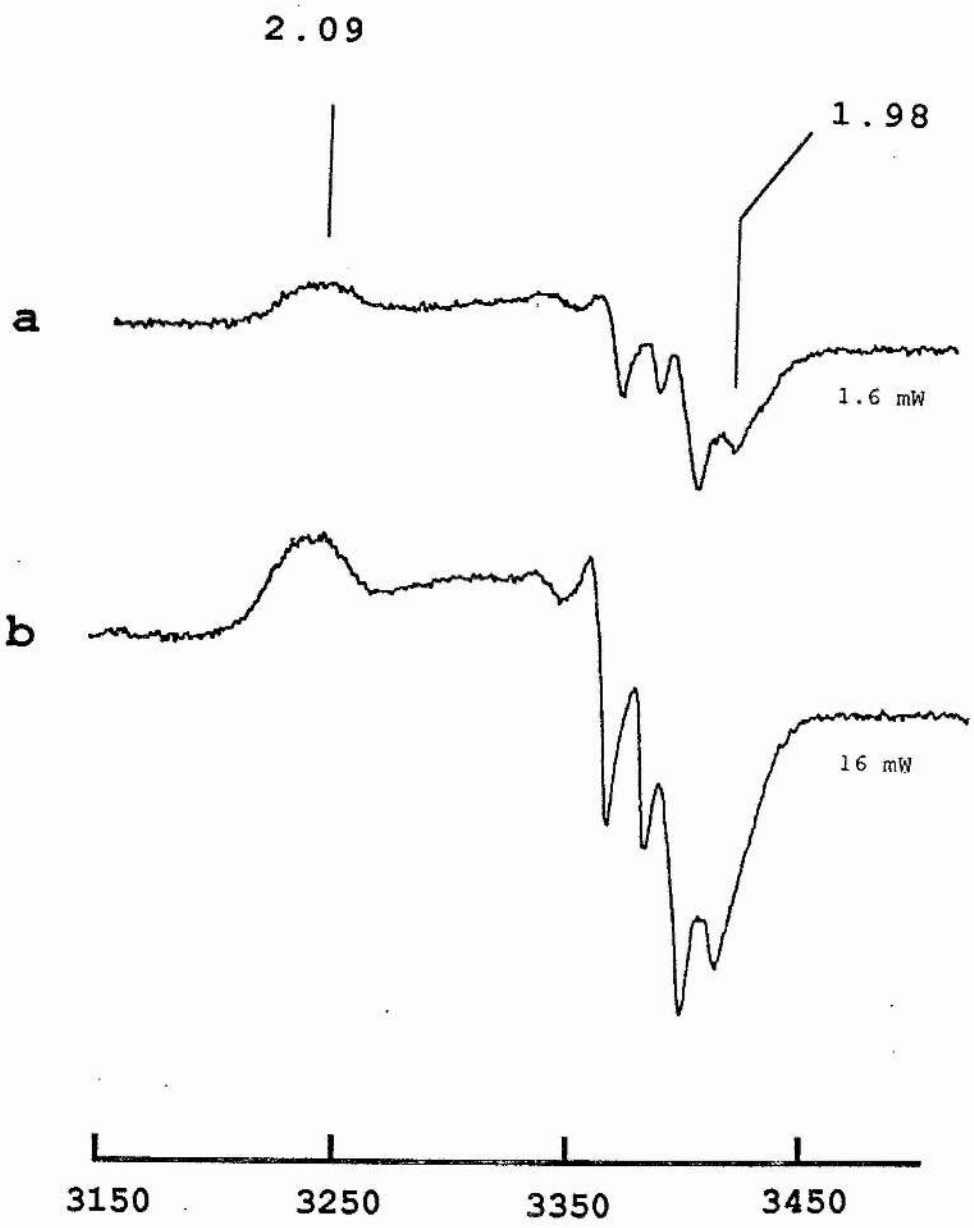
2.09
1.98
a
1.6 mW
b
16 mW
3150
3250
3350
3450

Figure 5.2

Saturation behaviour of EPR features in membranes of E. coli strain RG145

The effect of microwave power on (a), the three major features of the haem *o*-NO EPR spectrum; g_x (Δ), g_z (open squares), g_y (closed triangles) and (b), low-spin ferric haem *b* g_y (3.01) feature (closed circles), are presented. Haem *o*-NO samples were prepared as described before and data was obtained at 18K. The low-spin data was obtained at 8K in the oxically oxidised (H_2O_2) EPR spectrum of membranes. Approximate protein concentration, 35mgml^{-1} in 50mM BES/KOH, pH 7.0, buffer solution. $P^1/_2$ values are indicated above profiles. Other spectrometer settings: field modulation intensity, 10 guass (p.t.p.); time constant, 1 second.

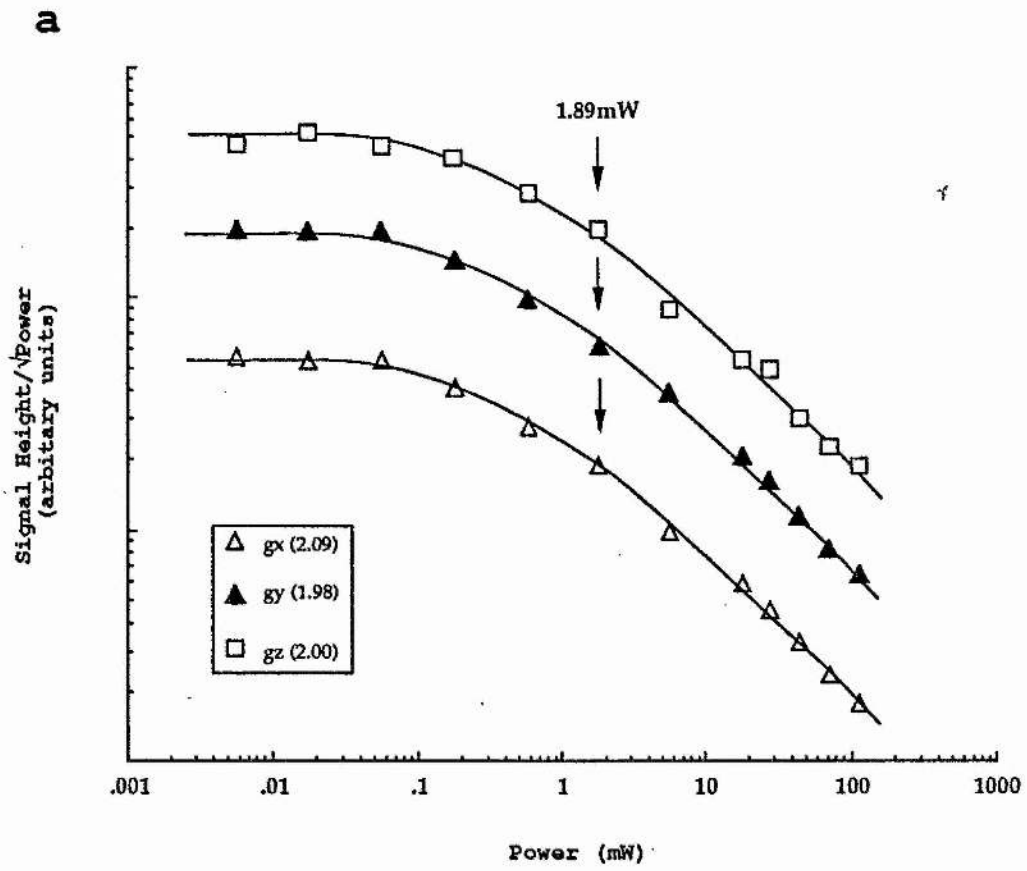
a
1.89mW
Signal Height/√Power
(arbitary units)
gx (2.09)
gy (1.98)
gz (2.00)
.001
.01
.1
1
10
100
1000
Power (mW)

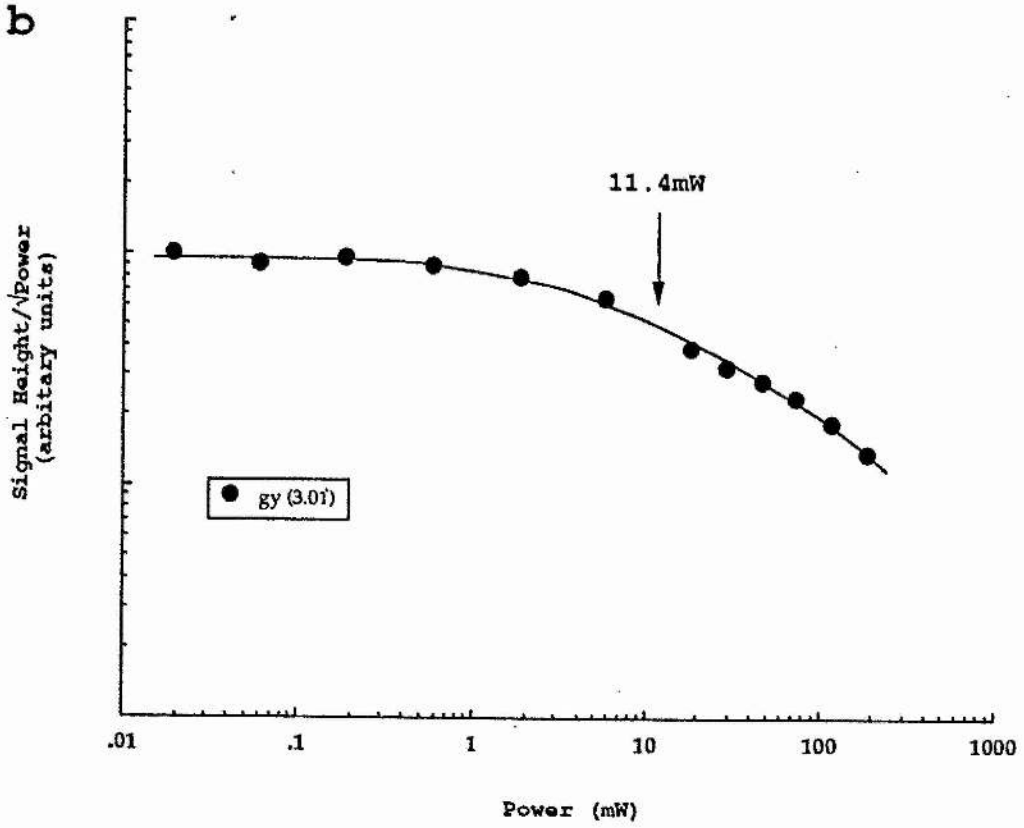
b
11.4mW
Signal Height/√Power
(arbitary units)
gy (3.01)
.01
.1
1
10
100
1000
Power (mW)

condition is met (Ohnishi *et al.*, 1982; Blum & Ohnishi, 1980):

$$\gamma^2 T_1 T_2 H1_{/2}{}^2 = 1 \quad \text{.....5.2}$$

where γ is the magnetogyric ratio; T_1 and T_2 are the spin-lattice and spin-spin relaxation times, respectively and $H1_{/2}$ is the microwave magnetic field corresponding to the $P1_{/2}$. By an extrapolation of the linear portion of the saturation profile described above (see Figure 5.2), to a point at which the observed signal height (here proportional to the SH/$\sqrt{}$power) is half the expected height (described by the theoretical linear portion), the $P1_{/2}$ can be determined.

The $P1_{/2}$ of a paramagnetic species is dependent on a number of factors including the spin-lattice relaxation time, T_1. For example, the spin-lattice relaxation rate ($1/T_1$) is highly dependent on how strongly the spin of an electron is "coupled" to the lattice (i.e. the molecular enviroment) (Knowles *et al.*, 1976). When a paramagnetic centre comes in close proximity to another, electrons, which have become excited by the absorption of microwave energy, dissipate that energy to the surrounding lattice in an enhanced manner. This effect results in a shortening of T_1, and from the relationship introduced in Equation 5.2 we see that $P1_{/2}$ is proportional to $1/T_1$.

From the studies of Blum and colleagues on soluble iron-sulphur proteins using a variety of dysprosium complexes with different charges, it is apparent that the

elicited effect of the exogenous paramagnetic probe is dependent on the overall charge of the probe complex rather than simply on concentration (Blum *et al.*, 1981; Blum *et al.*, 1983). Such findings are consistent with the probe interacting with specific binding sites rather than due to a simple dispersion effect. Equally, by increasing the ionic strength in experiments with myoglobin-NO it was shown that a higher probe concentration was required before the dependence of the parameter $P1_{/2}$ on the concentration became linear (Blum *et al.*, 1983), thus, strongly implicating the involvement of electrostatic interactions in binding at low concentrations.

However, as long as the dissociation constant, K_D, is significantly larger than the paramagnetic probe concentration (and the number of binding sites is large), the binding of the probe will be proportional to the concentration (Blum *et al.*, 1983). Blum *et al.* (1980,1981), in developing the work of Hyde and Rao (1978), suggested that the binding of each probe complex elicits an effect on the $1/T_1$ which is simply additive, thus $P1_{/2}$ shows a linear dependence on the concentration of the probe provided the term T_2, the spin-spin relaxation time, is assumed to be constant over the temperature range (see Eq. 5.2). Using a simple model system Blum and colleagues were able to present an equation for the calculation of the weighted average distance ($|r|$) between the dysprosium complex and the intrinsic species:

$$\Delta P1_{/2} = 4.12 \times 10^{8} \cdot |r|^{-6} \cdot \exp(-12.5/T) \quad .....5.3$$

where $\Delta P1_{/2}$ is a measure of the dependence of $P1_{/2}$ on the dysprosium concentration. It demonstrates that the interaction is highly weighted to distance ($|r|^{-6}$). However, this formulation depends on the binding sites being equivalent and can only estimate the effective radius between the relaxer and intrinsic centre, which will be slightly greater than the distance of closest approach (although as discussed above, this value will be heavily weighted towards that of closest approach since relaxation falls off by a term which varies by r^{-6}).

5.2.2 Dysprosium as a "relaxer"

The EPR spectrum of dysprosium is highly anisotropic with a major peak around g=14. Unfortunately, the resonance exhibits a high field "tail" which extends well into the g=2 region (Blum *et al.*, 1981). This is particularly significant when observing resonances of high-spin haem centres which occur at low field positions. In such cases the baseline is so affected by the underlying dysprosium signal that meaningful saturation data cannot be obtained when varying the probe concentration. Fortunately, the effect of the dysprosium ion on the paramagnetic haem *o*-NO complex (g=2) can be examined and it is this species which is used to determine the location of the five coordinate ligand binding haem (haem *o*) at the binuclear site; because of its field position, the effect of increasing the dysprosium ion

concentration on the low-spin haem *b* (g = 3) signal may be observed directly.

As mentioned above, some dysprosium complexes elicit their effect on the endogenous centre to a greater or lesser extent depending on the charge on the probe complex. In some reports $Dy(NO_3)_3$ was as potent a relaxer as Dys-EDTA (Ohnishi *et al.*, 1980), whilst in others the $Dy(NO_3)_3$ was more effective than the EDTA complex (Blum *et al.*, 1981). Dys-EDTA was used in this study because in general this complex gives the most effective enhancement of relaxation and because, although the binding characteristics are not fully understood, as long as the response is linear with respect to probe concentration, the results are quantitatively the same.

In order that equation 5.3 hold for cytochrome *o* the temperature dependence of the $\Delta P1_{/2}$ term must be determined. The temperature dependence of the parameter $\Delta P1_{/2}$ is a measure of the term $T_{1k} / (1 + \omega\ ^2T_{1k})$, where ω is the microwave frequency of observation and T_{1k} is the spin-lattice relaxation time of the dysprosium(III) complex (Hyde & Rao, 1978). The variation of the $\Delta P1_{/2}$ with temperature must be taken into account when estimating the distance between the dysprosium complex and the species under study. In other proteins to which this technique has been applied, the temperature dependence of $\Delta P1_{/2}$ fits a term which varies as exp(-12.5/T) (Blum *et al.*, 1983). Figure 5.3 shows the temperature dependence of the $\Delta P1_{/2}$ of

Figure 5.3

Variation of ΔP1/2 with temperature for the nitrosyl, and low-spin signals

$\Delta P^1/_2$ was obtained from the slopes of $P^1/_2$ versus Dys-EDTA concentration (Figure 5.2) at various temperatures. The data for haem *b* (closed symbols) and the nitrosylferrohaem *o* g_x (2.09) signal (open symbols) is presented. The graph is of $\Delta P^1/_2$ plotted as a function of inverse temperature. The slope shows that $\Delta P^1/_2$, for both species, varies by a term that is equal to k.exp(-12.5/T), where T is in Kelvin.

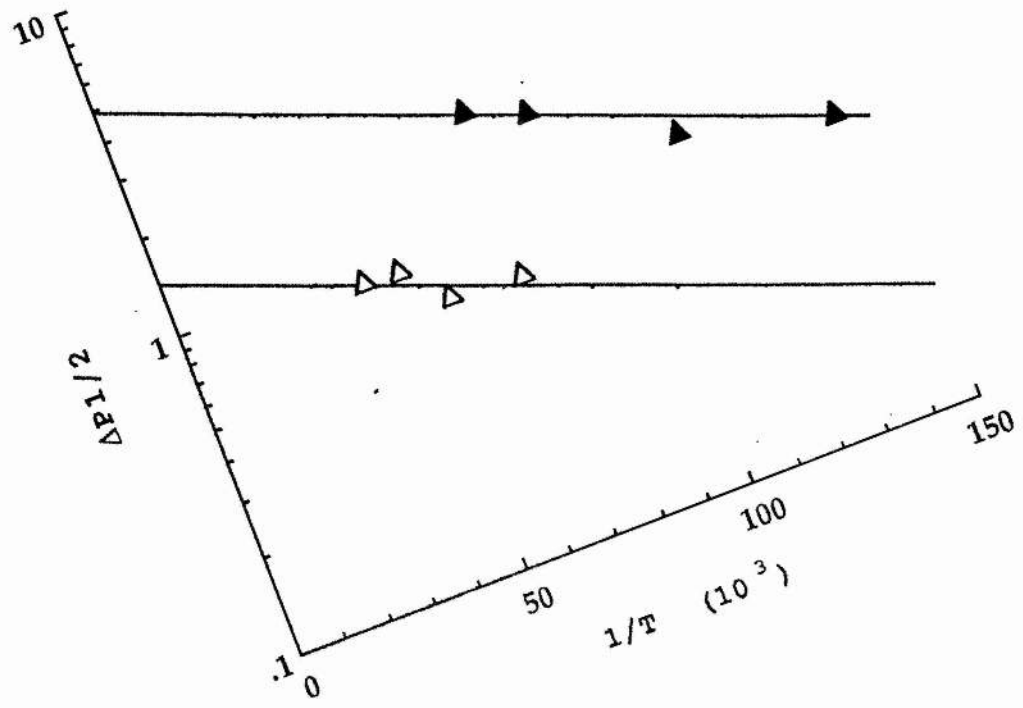
10
1
.1
0
50
100
150
1/T (10 3)
ΔB1/2

paramagnetic centres in cytochrome *o*. This, also, can be fitted to a term which varies as exp(-12.5/T). Thus, Equation 5.3 should be applicable to the centres of cytochrome *o*.

5.2.3 The effect of Dys-EDTA on EPR features in membranes.

Figure 5.4 shows power profiles of the haem *o*-NO complex (g_x = 2.09) in membranes in the presence of increasing concentrations of Dys-EDTA. The power profile obtained in the presence of 15mM La(III)EDTA (Lan-EDTA), a diamagnetic ion complex, is also shown for comparison. This is a useful control since Lan-EDTA and Dys-EDTA should bind in a similar fashion; the lanthium ion, however, will not enhance the spin-lattice relaxation rate (1/T) through dipolar interaction. It thus serves to separate any chemical effects from the magnetic. The results obtained with Lan-EDTA confirm that it is the presence of the paramagnetic dysprosium(III) ion which is responsible for the enhanced relaxation. The $P1_{/2}$ values obtained from Figure 5.4 (and those from the other principal g-values of the nitrosyl resonance, g_z (2.00) and g_y (1.98) (not shown) are replotted against Dys-EDTA concentration in Figure 5.5. It can be seen that all 3 features show a linear response to probe concentration and that all points lie on a line with similar slope, ($\Delta P1_{/2}$, $mWmM^{-1}$). The $\Delta P1_{/2}$ for the g_x, g_z and g_y signals at 20K are 0.78, 0.76 and 0.78 mWmM-1, respectively. Using the relationship found in Equation 5.3, the distances

Figure 5.4

Effect of Dys-EDTA on the power saturation profile of the nitrosyl signal

The effect of Dys-EDTA on the microwave power saturation profiles of the g_x (2.09) signal from nitrosylferrohaem *o* in membranes of *E. coli* strain RG145 are shown. These data are shown as a double log plot of signal height/√Power as a function of microwave power (mW). The concentration of Dys-EDTA used to obtain each profile is indicated in the figure (*inset*). 15mM Lan-EDTA was also used as a control, and this profile follows that of the 0mM Dys-EDTA sample. Experimental conditions were as for Figure 5.2a except; temperature, 20K.

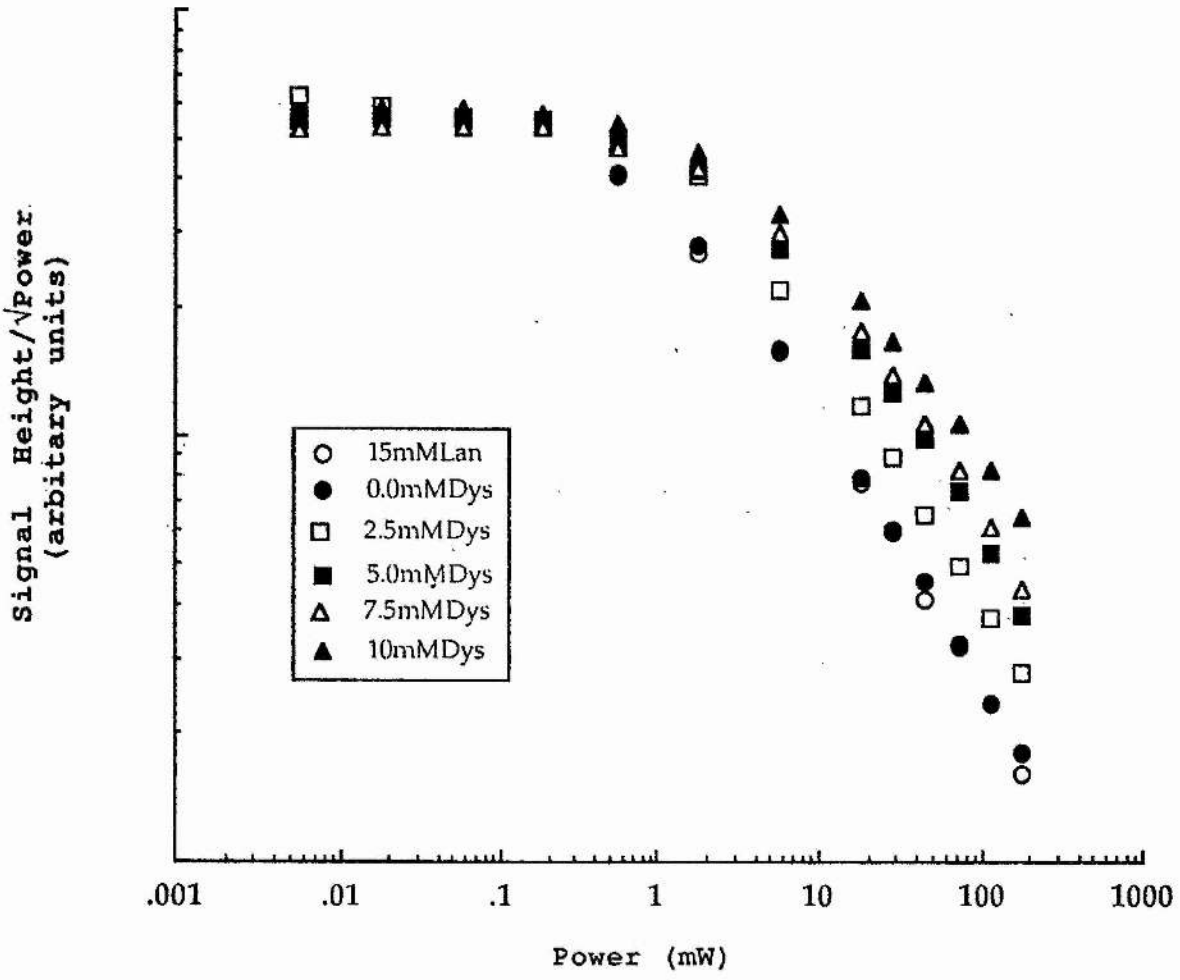
Signal Height/√Power
(arbitary units)
15mMLan
0.0mMDys
2.5mMDys
5.0mMDys
7.5mMDys
10mMDys
.001
.01
.1
1
10
100
1000
Power (mW)

Figure 5.5

Variation of $P^1/_2$ with Dys-EDTA concentration in membranes: haem o-NO

Saturation data for the major haem *o*-NO resonances is shown. $P^1/_2$ values are plotted for; g_x (2.09) (open squares); g_y (1.98) (open triangles); g_z (2.00) (closed squares), versus Dys-EDTA concentration. The slopes obtained for each resonance show that the $\Delta P^1/_2$ (the Dys-EDTA concentration dependence of $P^1/_2$; mW/mM) are approximately 0.78 for the three major resonances of the haem *o*-NO g-tensor (see Table 5.1). All experimental conditions were the same as those in Figure 5.4.

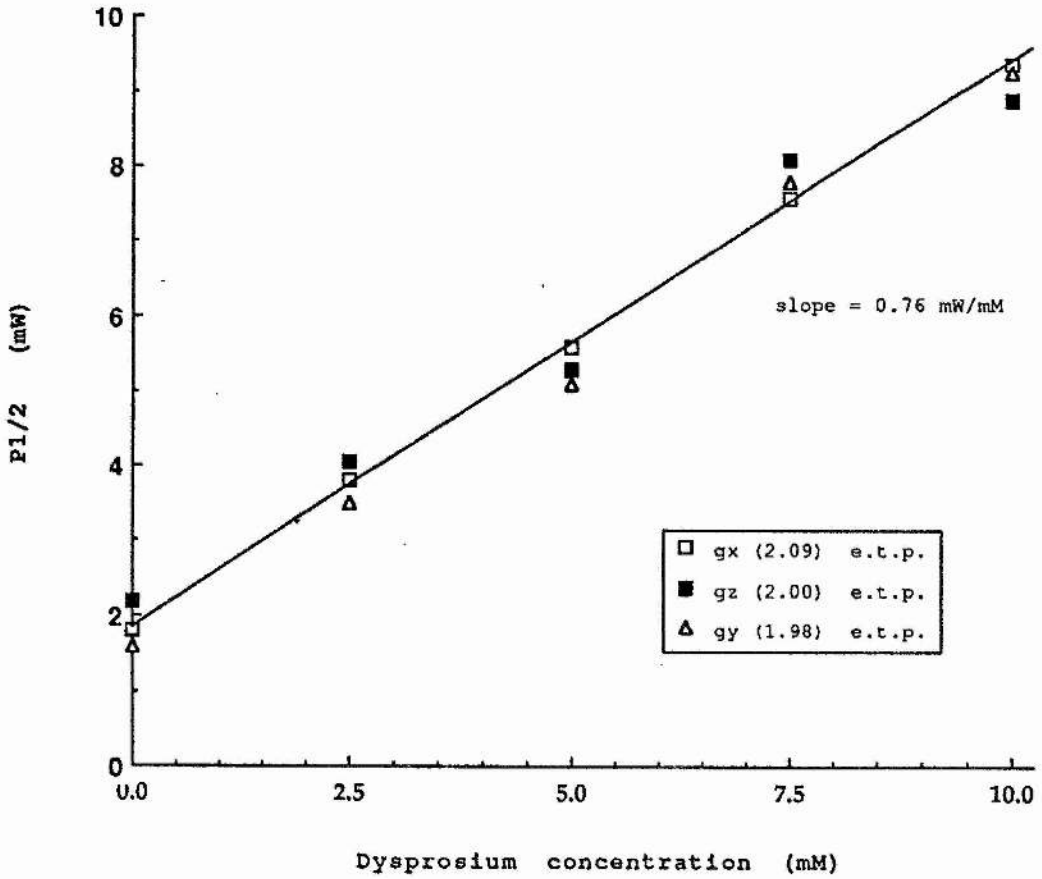
10
8
6
4
2
0
P1/2 (mW)
slope = 0.76 mW/mM
gx (2.09) e.t.p.
gz (2.00) e.t.p.
gy (1.98) e.t.p.
0.0
2.5
5.0
7.5
10.0
Dysprosium concentration (mM)

from the probe centre to the intrinsic centre are calculated to be 25.6Å, 25.7Å and 25.6Å, respectively. The radius of the Dys-EDTA complex (5Å) must also be taken into account when calculating distances, thus the above distance estimates are reduced by 5Å to give effective radii of approximately 20.6Å for all the principal g-values of the haem *o*-NO complex (haem *o*)

These data confirm that all three signals originate from the same species and that, broadly speaking, they can be treated as originating from a single distance within the membrane. This is useful in that only one resonance need be monitored when determining the depth of the high-spin centre within the membrane.

Figure 5.6 shows the effect of increasing Dys-EDTA concentration on the $P1_{/2}$ of the g = 3 signal attributed to low-spin haem *b* of cytochrome *o*. The $\Delta P1_{/2}$ for the g = 3 signal is 1.4 $mWmM^{-1}$ at 10K. From Equation 5.3 this corresponds to an effective radius of 15.9Å below the membrane/protein surface, after correction for probe radius.

5.2.4 The effect of Dys-EDTA on EPR features in sphaeroplasts.

In Section 5.2.3 the depth of centres within the membrane was determined. However, these experiments do not give information on the distribution or the sidedness of the centres with respect to the membrane. In order that this be determined for the high- and low-spin centres in cytochrome *o*, it is necessary to observe the effect of probe

Figure 5.6

Variation of $P^1/_2$ with Dys-EDTA concentration in membranes: haem b

Data for the low-spin haem *b* g_z (3.01) signal is presented. $P^1/_2$ (mW) values are plotted against the Dys-EDTA concentration (mM). The slope obtained from the data show $\Delta P^1/_2$ (the Dys-EDTA concentration dependence of $P^1/_2$; mW/mM) to be 1.4 for the low-spin centre (see Table 5.1). Experimental conditions were the same as those in Figure 5.2b, except; temperature, 10K.

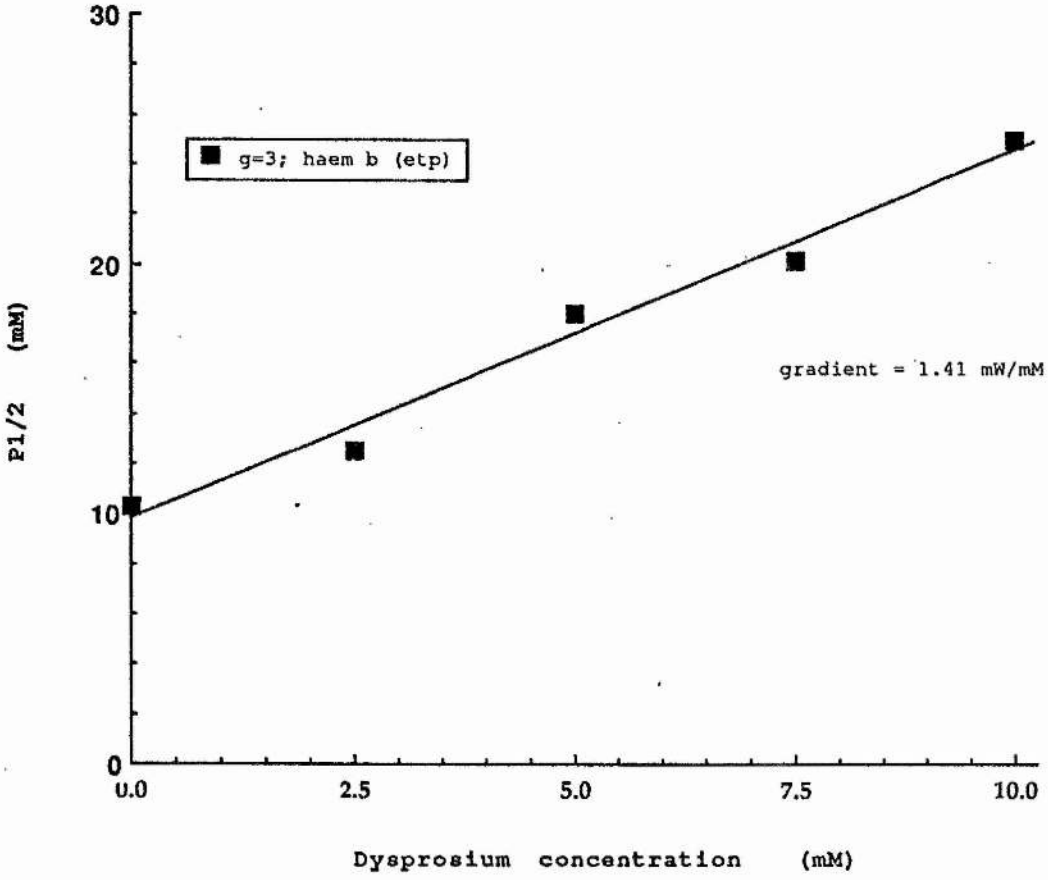
30
20
10
0
P1/2 (mM)
g=3; haem b (etp)
gradient = 1.41 mW/mM
0.0
2.5
5.0
7.5
10.0
Dysprosium concentration (mM)

concentration on the relaxation behaviour of features observed in sphaeroplasts. Sphaeroplasts are used because, unlike membrane particles, they provide a system in which access of the probe is limited to one side of the membrane only. Sphaeroplasts were chosen over whole cells in order to limit the effects of non-specific binding and permeability effects which might be encountered by the probe in crossing the periplasmic (outer) membrane of *E. coli*. Using sphaeroplasts offered the additional advantage of reducing the possibility of haem-NO signals arising from soluble nitrite reducing enzymes found in the periplasm which would significantly reduce the observed radius (see below).

Figure 5.7 plots the $P1_{/2}$ observed in sphaeroplasts for the low-spin haem *b* signal (g_z= 3) of cytochrome *o* as a function of Dys-EDTA concentration. The $\Delta P1_{/2}$ for the g = 3 signal is 1.35 $mWmM^{-1}$ (10K) which corresponds to an effective radius of 16Å, after correction for probe radius.

The dependence of the $P1_{/2}$ of the g_x (2.09) resonance of the haem *o*-NO complex on increasing Dys-EDTA concentration is also plotted in Figure 5.7. Comparing these data with those from Figure 5.5 it is obvious that Dys-EDTA is much less effective at relaxing the haem *o*-NO signal in sphaeroplasts than in membranes (c.f $\Delta P1/2$ (g=2.09) = 0.78 $mWmM^{-1}$ in membranes and approximately 0.11 $mWmM^{-1}$ in sphaeroplasts; the latter corresponding to an effective distance of ≥ 35Å). A similar comparison of the data from haem *b* shows that the probe is equally effective in either membrane or sphaeroplast preparations (see Figure 5.6). From

Figure 5.7

Variation of $P^1/_2$ with Dys-EDTA concentration in sphaeroplasts: haem o-NO and haem b

Data for the nitrosyl g_x (2.09) and low-spin haem *b* g_z (3.01) signals are presented. $P^1/_2$ (mW) values are plotted as a function of the Dys-EDTA concentration (mM). The slopes obtained from these data show $\Delta P^1/_2$ (the Dys-EDTA concentration dependence of $P^1/_2$; mW/mM) values to be 1.35 and 0.11 for the low-spin centre and haem *o*-NO signals, respectively (see Table 5.1). Experimental conditions were the same as those for respective ETP experiments found in Figures 5.5 and 5.6.

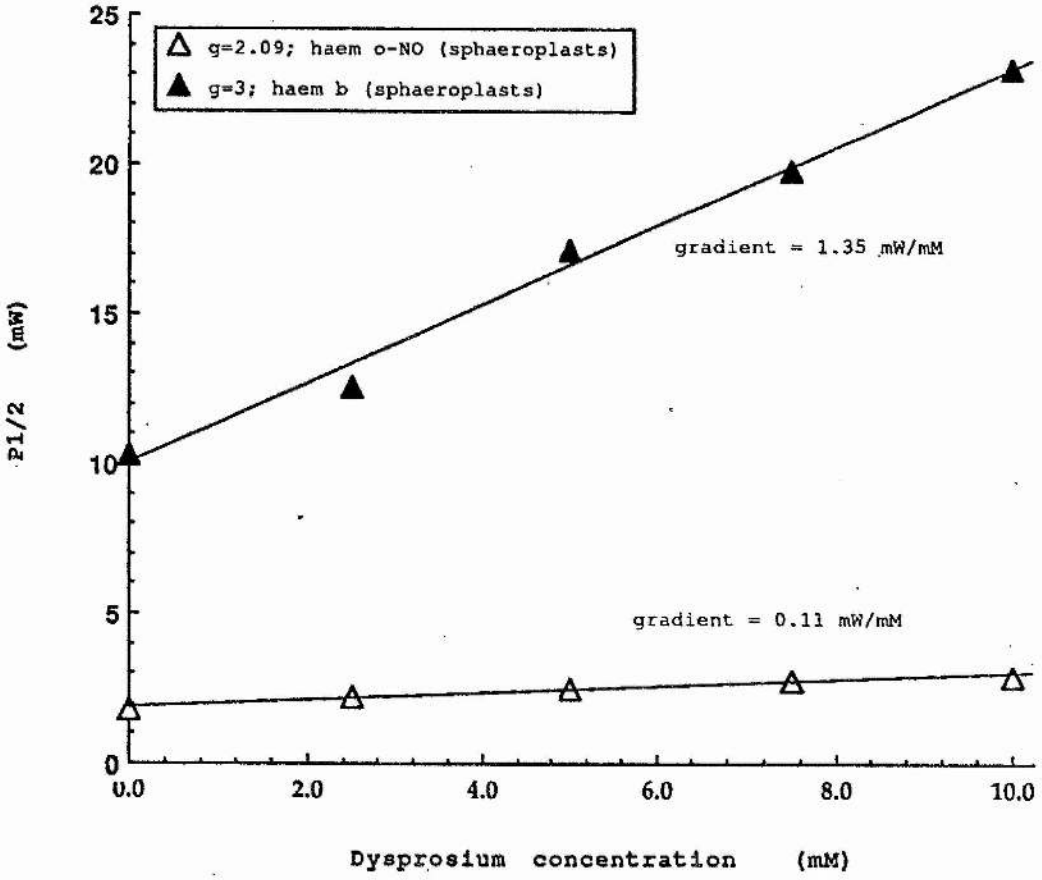
g=2.09; haem o-NO (sphaeroplasts)
g=3; haem b (sphaeroplasts)
gradient = 1.35 mW/mM
gradient = 0.11 mW/mM
P1/2 (mW)
25
20
15
10
5
0
0.0
2.0
4.0
6.0
8.0
10.0
Dysprosium concentration (mM)

Table 5.1

Distance measurements from studies with with Dys(III)EDTA on haem centres of cytochrome o

	ETP		Sphaeroplasts	
EPR resonance	$\Delta P1_{/2}$	|r|	$\Delta P1_{/2}$	|r|
Haem o-NO				
g_x (2.09)	0.78[a]	20.6Å	0.11	≥35Å
g_z (2.00)	0.76	20.5Å	--	--
g_y (1.98)	0.78	20.6Å	--	--
Haem *b*				
g_y (3.01)	1.4	15.8Å	1.35	16.02Å

Notes: [a]in $mWmM^{-1}$

this data it is concluded that haem *o* is buried too deeply within the membrane (w.r.t. the periplasmic aspect) to allow a significant dipolar interaction between the magnetic moment of the dysprosium complex and the intrinsic spin. The small ΔP1/2 might be due a real distance between the periplasmically located probe and intrinsic centre or simply due to a small amount of leakage of the probe into the cell.

It has been suggested that the Dys-EDTA complex, with an estimated diameter of 10Å, has access to the inner membrane of *E. coli* through the porin pores (11Å) (Rothery, 1989). One possible disadvantage of using sphaeroplasts over whole cells is assuring membrane integrity. However, as discussed above, the differences in the calculated distance of the haem *o*-NO signal, in membranes and sphaeroplasts, suggest that this is not a significant problem in this study.

5.2.5 *Orientation of the nitrosylferrohaem complex of cytochrome o*

The following section looks at the orientation of the nitrosyl ligand complex of cytochrome *o* (haem *o*-NO) in membranes. Oriented multilaminar arrays have been used to look at the orientation of prosthetic groups in a number of mitochondrial systems (Blasie *et al.*, 1978; Erecinska *et al.*, 1978; Blum *et al.*, 1978a; Erecinska *et al.*, 1977) and more recently applied to the study of the prosthetic groups of the terminal ubiquinol oxidases of *E. coli* (Salerno & Ingledew, 1991; Ingledew *et al.*, 1992).

The spectrum of the haem *o*-NO resonance, at two orientations relative to the incident magnetic field, is shown in Figure 5.8. It can be seen that when the magnetic field is parallel to the multilayer plane (||) the feature at 2.09 is approximately maximal. When the magnetic field is parallel to the membrane normal (⊥) the feature at 1.98 is maximal. The central absorbance at g = 2.01 is not well resolved and accurate determination of the signal height of the hyperfine structure is therefore difficult and not reported. A plot of the signal heights of the g = 2.09 and g = 1.98 signals, as a function of the angle between the magnetic field direction and the normal to the membrane plane, are shown in Figure 5.9. The resonances at g = 1.98 and 2.09 exhibit opposite orientation with respect to each other i.e. they are out of phase by 90°. Since the highest field resonance of the haem *o*-NO spectrum at g = 1.98 is maximal when the direction of the incident magnetic field is normal to the plane of the array, and from the data of Ingledew and Salerno (1991) (see later) we know the plane of the haem is parallel to this direction, it is likely that this resonance arises from an in haem-plane component of the g-tensor (by definition either the g_x or g_y axis). The fact that the lowest field feature, at g = 2.09, is out of phase by 90° to this resonance strongly suggests that this feature arises from the other in haem-plane axis. Neither feature can be unequivocably assigned to their respective axis on the basis of this data alone since the orientation of the g tensor x and y axes are not known within the plane of the

Figure 5.8

Electron paramagnetic spectra of nitrosylferrohaem o *in multilayers of membranes of E. coli:* g_x *(2.09) and* g_y *(1.98)*

EPR spectra shown in parallel (||) and perpendicular (⊥) orientations to the incident microwave magnetic field. g-values are indicated on spectra. Spectrometer settings were; temperature 25K, microwave power, 17mW, modulation amplitude, 10 gauss (p.t.p.).

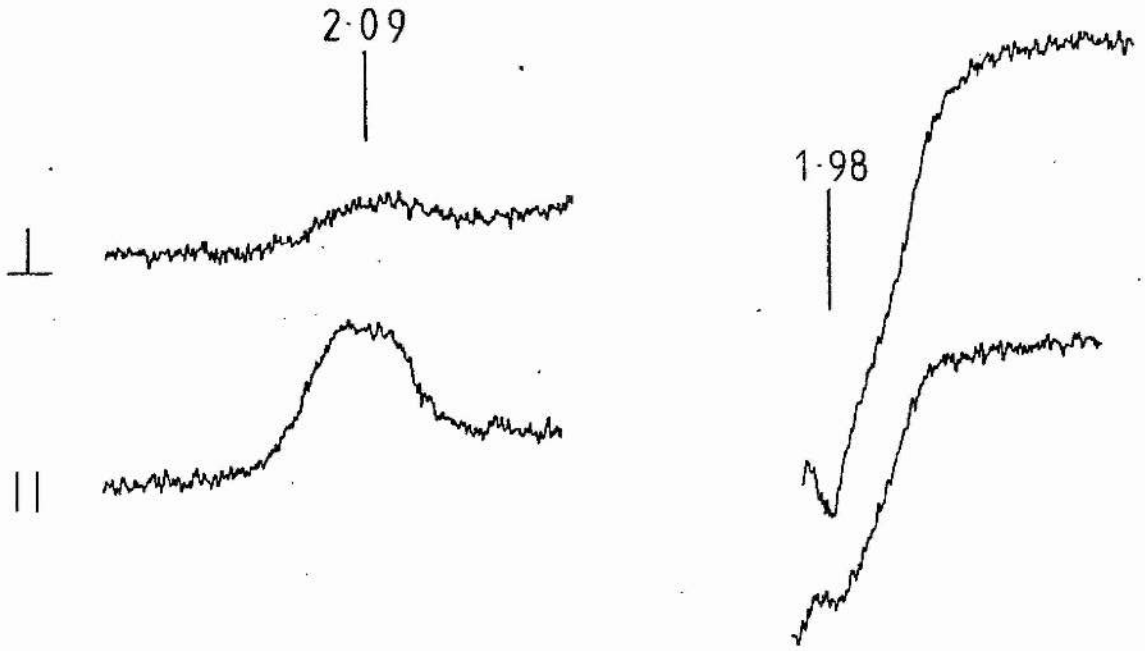
2·09
1·98
⊥
||

Figure 5.9

Plot of signal height against incident angle for multilayers

Shown are the angular dependence of signal amplitudes of the haem *o*-NO resonances; (closed symbols) g_x (2.09); (open symbols) g_y (1.98). Temperature and spectrometer settings as for Figure 5.8.

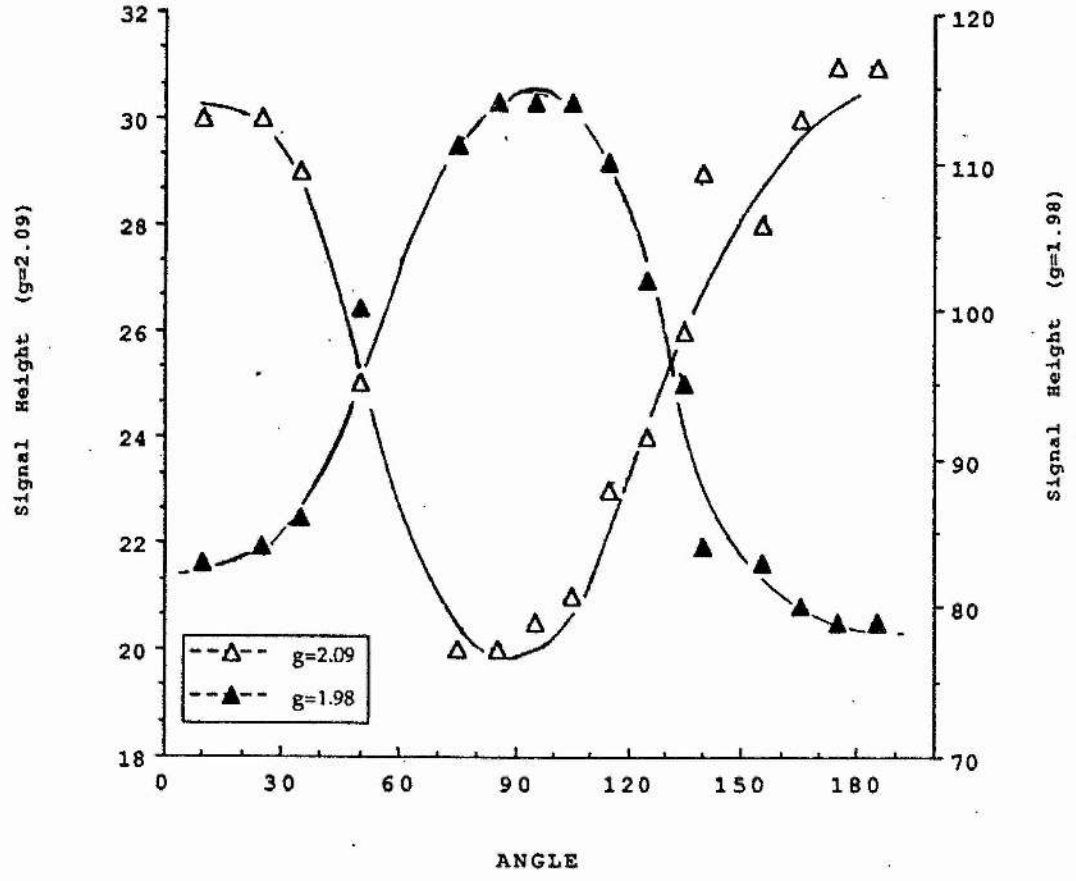
Signal Height (g=2.09)
Signal Height (g=1.98)
ANGLE
g=2.09
g=1.98
32
30
28
26
24
22
20
18
120
110
100
90
80
70
0
30
60
90
120
150
180

haem. The central absorbance feature (2.00) is assigned to the g_z axis of the g-tensor since this feature is closest to the g-value of a free electron and has been shown to contain hyperfine (Figure 5.1). These data are in broad agreement with the orientation data from avian mitochondria obtained by Barlow & Erecinska, (1979).

5.2.6 *Spin-spin interaction between haem centres*

Chapter 3 and 4 presented evidence for a haem-haem interaction between centres of the cytochrome *o* complex in the purified state. This was demonstrated by the redox behaviour of the high- and low-spin centres in low temperature EPR studies and the redox behaviour of optical components monitored in the α band. However, this in itself, is not proof of a spin-spin interaction between haem *b* and haem *o*; indeed, the redox effects discussed in Chapter 4 are likely to be a result of site-site interactions within the protein and do not, therefore, require close proximity. To date, no direct evidence of spin-spin interaction between the haem centres in cytochrome *o* has been reported.

Direct spin-spin interaction between haem *b* and haem *o* can be demonstrated by the enhanced relaxation of the haem *o*-NO signal in the presence of the faster relaxing paramagnetic low-spin haem *b*. The haem *o*-NO signal of cytochrome *o* is stable and can be observed at relatively high redox potentials. Membranes of *E. coli* strain RG145 were treated with 15mM nitrite and reduced with additions of saturated dithionite solution to form the haem *o*-NO

complex. This was carried out in a redox vessel in the presence of mediator dyes under anoxic conditions. By this method the ambient potential could be altered and samples taken at reduced potential, where low-spin haem *b* would be diamagnetic, and higher potential where haem *b* was paramagnetic (the redox state of haem *b* was confirmed by monitoring in the g = 3 region; not shown). In this way the saturation behaviour of the nitrosyl species could be monitored in the absence and presence of paramagnetic haem *b*.

Figure 5.10 shows the saturation behaviour of haem *o*-NO resonance (g_x=2.09) poised at (a) 0mV and (b) +290mV. At 0mV there is a less than 0.5% of haem *b* in the paramagnetic (oxidised) state since haem *b* follows a single n=1 Nernstian redox curve with a mid-point potential of +140mV when haem *o* is reduced. Under these experimental conditions, haem *o* is effectively trapped in the reduced state by ligation to nitric oxide (*c.f.* Figure 3.4a). The $P1_{/2}$ for the sample poised at 0mV is 1.96mW, which compares to 4.5mW for the sample poised at +290mV (20K). This is an enhancement of approximately 2.3 times when the enzyme possess a paramagnetic low-spin centre. A similar enhancement is observed for the g_y (1.98) signal (not shown).

This is the first unambiguous evidence for direct spin-spin interaction between the haem centres of cytochrome *o*. Unlike the site-site interactions reported in earlier chapters, dipole interactions of this sort can only be observed when two spins are in close proximity to one

Figure 5.10

The effect of haem b redox state on the saturation behaviour of haem o-NO

Shown are the microwave power saturation profiles of the g_x (2.09) resonance of haem *o*-NO in the presence and absence of a paramagnetic haem *b* centre. Profile (a); the membranes poised at 0mV. Profile (b); membranes poised at +290mV (see text for protocol). The P1/2 values were (a) 1.95mW and, (b) 4.5mW. All other experimental conditions were the same as those in Figure 5.2 except; temperature, 20K.

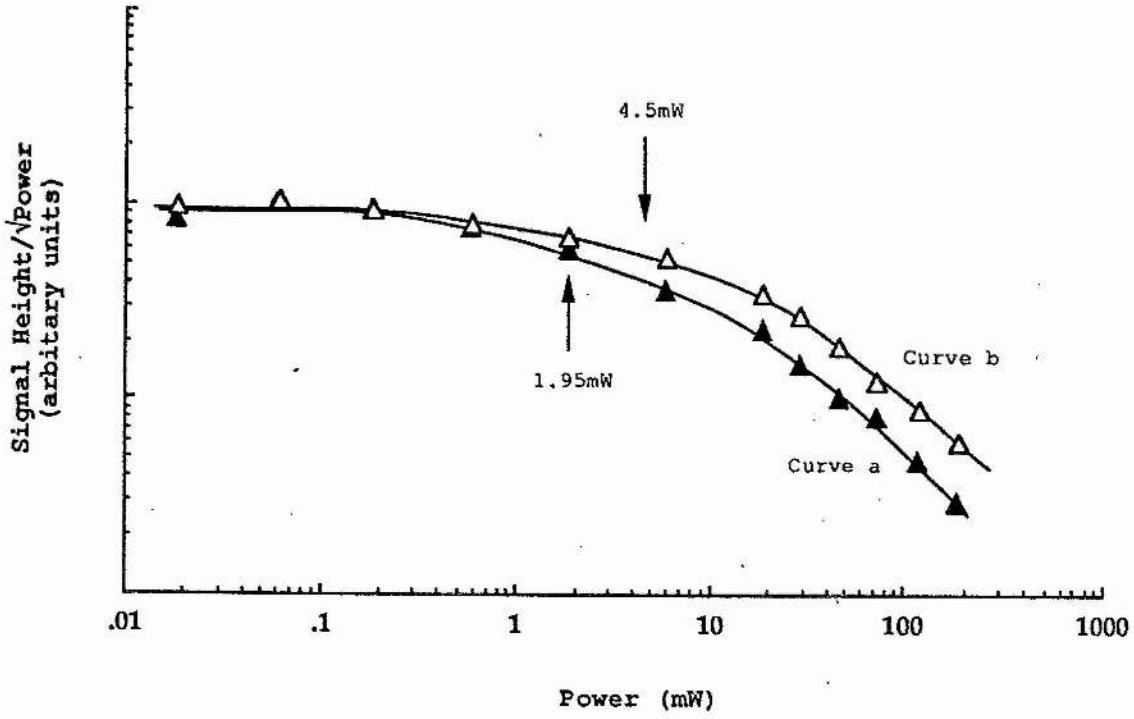
Signal Height/√Power
(arbitary units)
4.5mW
1.95mW
Curve b
Curve a
.01
.1
1
10
100
1000
Power (mW)

another. The strength of interaction can be used to estimate the distance between both centres. The calculation proceeds as follows (Ohnishi *et al.*, 1982):

The spin-lattice relaxation times for both the fast relaxing haem b species (T_{1f}) and the slow relaxing haem o-NO (T_{1s}) are estimated using the saturation parameter $P1_{/2}$. The relationship between $P1_{/2}$ and T_1 is given by Eq. 5.2. It is now important to determine the contribution to T_{1s} from a dipolar interaction with the paramagnetic haem *b*. This contribution is dependent on the g-values used in the estimation, such that the term Δw^2 (the difference between w_f - w_s) is calculated from g-values which correspond to a single direction in the enzyme. To proceed with this calculation it is important to have some knowledge of the relative orientation of the g-tensors participating in the interaction, i.e. the orientation of the haems. Recently, Salerno & Ingledew (1991) examined the orientation of the haem centres of cytochrome *o* using oriented multilayers. The angular dependence of the principal g-values corresponding to the x and y axes, that is the in haem-plane directions, of the low-spin g-tensor, were each found to be 10° from the multilayer (membrane) plane and normal, respectively. These findings are consistent with a model in which the haem(s) is held between membranes-spanning α helices. The high-spin centre was also found to be oriented in a similar fashion within the membrane. This motif is the simplest to envisage for a membrane spanning protein with multiple helical regions which span the membrane. However, it is interesting

to note, that the haem plane of the haems in Bovine cytochrome P-450 are parallel to the membrane plane, indicating that this structure is by no means universal (Blum *et al.*, 1978a).

Section 5.2.6 discussed the orientation of haem *o*-NO g-tensor. It was shown that the resonance at g = 1.98 corresponds to the in-haem-plane direction perpendicular to the membrane normal. The principal g-values for low-spin haem *b* occur at 3.0, 2.25 and 1.45 (e.g. Salerno *et al.*, 1990). The position of the low-spin haem *b* g-value which corresponds to the membrane normal direction can be calculated from the orientation data already established for the haems of cytochrome *o* by Salerno & Ingledew (1991). Since it is difficult to measure the saturation behaviour of intermediate g-values the $P1_{/2}$ for the g = 3.0 peak was used with the assumption that the $P1_{/2}$ will be the same at all values. The extent of relaxation limits the distance estimated between the two centres to approximately 14Å. This distance falls within the estimated range of Fe-Fe distances (12-16Å) calculated for cytochrome c oxidase (Ohnishi *et al.*, 1982).

5.2.7 Cu-EXAFS studies on purified cytochrome o

Much of our knowledge of the atomic structure of matter has primarily come from wave-diffraction techniques, principally X-ray crystallography. However, an increasingly useful alternative technique involves the analysis of X-ray absorption by individual atoms in an array (Stern, 1976).

More specifically, analysis of the "extended fine structure" of the characteristic X-ray absorption "signature" of an atom can be interpreted in terms of the atomic neighbourhood of the atom under study. The advantages of this technique over those employing wave-diffraction include freedom from requiring crystals with long range order, a problem very pertinent to those studying biological systems, where pure crystals are often not available.

X-rays are absorbed when they enter matter and collide with electrons in that matter. In some instances the X-ray photon energy is lost to the electron in the collision which results in the electron being lost from its atomic orbital. In this state the released electron is known as a photoelectron.

The energy of an x-ray photon is directly proportional to the frequency (Plancks' Law). Let us consider the second and first most tightly held electron clouds, L and K, respectively. When a photon of X-radiation collides with an atom it excites electrons from all shells. If the energy of the photon is sufficient to liberate an electron from its shell an absorption is observed. At low frequencies, that is low energies, electrons from the L shell are liberated. If the frequency is increased further a point is reached at which there is sufficient energy in the photon to liberate electrons from the more tightly held K shell. At this point the measured attenuation of the x-radiation exhibits a marked increase as the new mode of absorption becomes possible. The energy at which this occurs is known as the K

edge and is characteristic of the atom from which the electron is liberated. A similar effect is seen at the L edge.

The energy state of the free electron (photoelectron) can be represented by a forward moving wave whose epicentre originates from the atom. For an atom surrounded by other atoms the forward moving photoelectron wave will be scattered by the neighbouring atoms. This in turn produces smaller waves which result in constructive and destructive interference patterns depending on the relative phases of the coincident waves. It is this effect which gives rise to the fine structure of the K edge and which holds information on the atomic neighbourhood surrounding the atom under study.

In XAS it is the amplitude of the electron wave at the absorbing atom which is measured. Thus, by changing the frequency of the x-radiation source the relative phases of the incoming, scattered, photoelectron wave, and that of the outgoing photoelectron wave, are varied giving rise to the fluctuating absorption intensity observed.

For the case of copper the energy at which the K edge is observed occurs at approximately 9000 electron volts and the EXAFS are found at greater energy values than that (compare with Figure 5.12).

The technique of XAS has been used to characterise more fully the local atomic neighbourhood around centres of many metalloproteins, including cytochrome c oxidase (Hasnain,

1991, ed.). One factor, more than any other, which has hindered the analysis of copper XAS from cytochrome c oxidase, is the presence of (at least) two copper centres in the enzyme complex; one, Cu_A, is intimately associated with haem a, and the other, Cu_B, is found at the active site of dioxygen binding and reduction (see Section 1.5.1). Unfortunately, XAS cannot distinguish between similar metal centres, the data obtained from cytochrome *c* oxidase is therefore a composite spectrum arising from both copper centres in this enzyme. Although analytical deconvolution techniques (c.f. Scott *et al.*, 1988b and Powers *et al.*, 1979) and chemically modified enzyme preparations (in which Cu_A has been removed; Li *et al.*, 1987) have gone some way towards solving this and allowed reasonable assumptions of the atomic structure within the binuclear site to be made, there must always remain the possibility of structural preturbations within the enzyme resulting from the latter and misinterpretation of the data, from the former (see Scott *et al.*, 1988b). In cytochrome *o* these problems will not arise since this enzyme only possesses a single copper atom which is at the active site.

The problems of analysing XAS data from biological samples which contain multiple equivalent absorption site has been approached in two ways. The first, favoured by Powers and colleagues in studies on cytochrome *c* oxidase, uses a model (single) copper compounds with known absorption spectra and subtracts that from the composite spectra obtained from cytochrome *c* oxidase. Powers *et al.* have

claimed that a stellacyanin spectrum can be extracted from the XAS data from cytochrome *c* oxidase. The contention that stellacyanin is an appropriate model system, for one of the copper centres, is supported by sequence comparisons showing some identity between the copper binding site in typical Type I "blue" copper proteins and that found in subunit II of cytochrome *c* oxidase (Steffens & Buse, 1979). Using the above "site modelling" technique to analyse copper X-ray edge absorption spectra, Powers *et al.* proposed that the copper associated with the high-spin haem a_3 at the bi-metallic site i.e. Cu_B, is a Type I or "blue" copper site. Powers and colleagues further expanded their studies to include analyses of the copper (and iron) EXAFS of cytochrome *c* oxidase and compared these with composite spectra made from copper containing model compounds (Powers *et al.*, 1981). Figure 5.11 shows a schematic representation of bi-metallic site of cytochrome *c* oxidase based on available XAS data. The most striking feature of this model is the presence of a sulphur-containing bridge and a relatively long Cu-->Fe distance of 3.75Å.

Other investigators disagree with the "site modelling" approach used by Powers and colleagues arguing that any number of chosen model pairs can be used to produce the observed curves. The arguement against site modelling holds equally well when considering EXAFS data. A second alternative approach, favoured by Scott *et al.* (1981,1986), initially involves the fitting of XAS data to determine the "overall coordination" character of both copper sites (Scott

Figure 5.11

Schematic representations of the inferred structure of the cytochrome c oxidase reaction site

Based on XAS data, two major structural forms of the bi-metallic O_2 reaction site of cytochrome *c* oxidase are represented schematically (from Kumar *et al.*, 1988). In this scheme the possibility of the bridging sulphur ligand being a chloride ion is not shown (see text). Ligands to haem a_3, such as cyanide or peroxide, result in the loss of an interaction from a S(Cl) scatter in the Fe EXAFS data. Thus, these ligands are thought to displace the bridging ligand, although a sulphur scatterer is still observed in the Cu EXAFS data (Chance *et al.*, 1983).

Resting *aa* $_3$

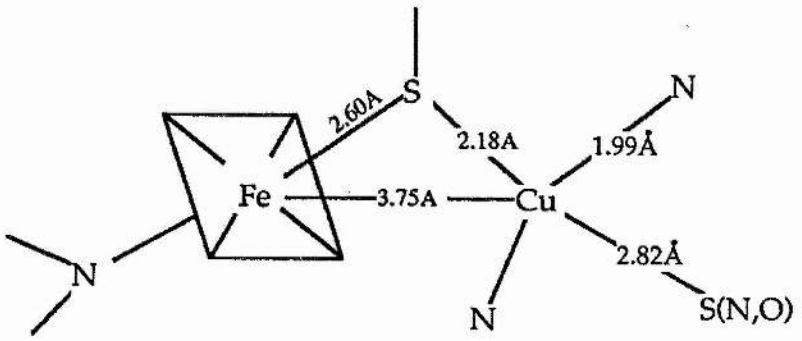

Pulsed *aa* $_3$

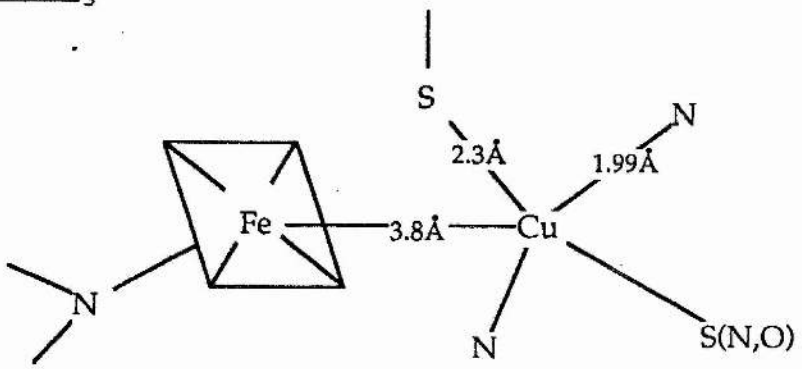

Fe_{a3} Cu_A

et al., 1986). The coordination character for the individual sites can then be inferred by comparing the data from derivatives of cytochrome *c* oxidase where the enzyme is in different valence states and/or in the presence of exogenous ligands. Using this approach Scott *et al.* suggest that there is no evidence for a Type I "blue" copper site in cytochrome *c* oxidase as proposed by Powers *et al.*, (1979). In their model, Scott *et al.* place three first shell ligands (N,O), with an average distance of 1.99Å from the Cu_B centre, with a longer interaction at 3.00Å proposed to be due to the iron site of the bi-metallic reaction centre. They suggest that the Cu_A centre is more covalently bound and has two shorter N (or O) ligands (1.99Å) and two longer Cu ---> S bonds (2.28Å). Cu EXAFS from Cu_A depleted cytochrome *c* oxidase shows 1^{st} shell peaks indicative of three Cu ---> N(O) coordinations at approximately 1.98Å and evidence for a longer sulphur interaction at 2.3Å (Li *et al.*, 1987). This might be the same interaction assigned to the sulphur bridge observed by Powers *et al.*, (1979), although this was not suggested by these authors. The significance of the sulphur-containing bridge remains unclear, especially in the context of it being found in the "resting" state of the enzyme, a species known to be kinetically incompetent (see Chapter 1). There have been XAS studies on the pulsed cytochrome *c* oxidase (Chance *et al.*, 1983) but these have been questioned since the identification of more than one form of "non-resting" oxidase; a pulsed form (characterised by an optical absorbance at 420nm) and a "pulsed peroxide"

form (428nm). Both derivatives of the oxidase appear to have quite distinct Fe a_3 enviroments, as distinguished by EXAFS (see Figure 5.11; Kumar *et al.*, 1988). Recently, evidence has been presented to show that the putative bridging sulphur ligand may be a Cl^- ion which can be eliminated (Scott *et al.*, 1988b; Blair *et al.*, 1986a).

It is clear from the above discussion that the interpretation of XAS data is by no means simple when presented with systems with multiple equivalent absorber sites. The extensive homology existing between the cytochrome *c* oxidase system and cytochrome *o* enzymes can be exploited to advantage in resolving some of these problems as the latter contains only one copper; that at the binuclear reaction centre. Figure 5.12 shows (a) the Cu EXAFS from purified cytochrome *o* (oxidised) and (b) the Fourier Transform and best fit curve of this data. There is no evidence to suggest a sulphur bridge, as indicated in the cytochrome *c* oxidase preparations, but there does appear to be a sulphur ligand (possibly the conserved methionine-353, Helix VIII on Subunit I). The best fit to the data was found for a single copper centre coordinated to two N (His) ligands at a distance of 1.83Å, one sulphur at 2.22Å with a longer iron interaction at 2.92Å.

Figure 5.12

EXAFS and Fourier Transforms of Cu EXAFS data from cytochrome o

Raw Cu K-edge EXAFS is shown (A) of purified cytochrome *o* (approx. 0.5mM) at 77K. Spectra are from the oxidised enzyme isolated in the absence of Cl^- ions. The data is a sum of 6 scans after normalisation. (B) shows the Fourier Transform of EXAFS data in (A) fitted with a single copper atom absorber and using wave curve theory. The abscissa in (A) represents the irradiating (X-ray) photon energy and the ordinate is of the fluorescence yield. The abscissa in panel (B) represents the wave vector, *k*, in $Å^{-1}$. Panel (B); solid line, experimental; broken line, theory.

A

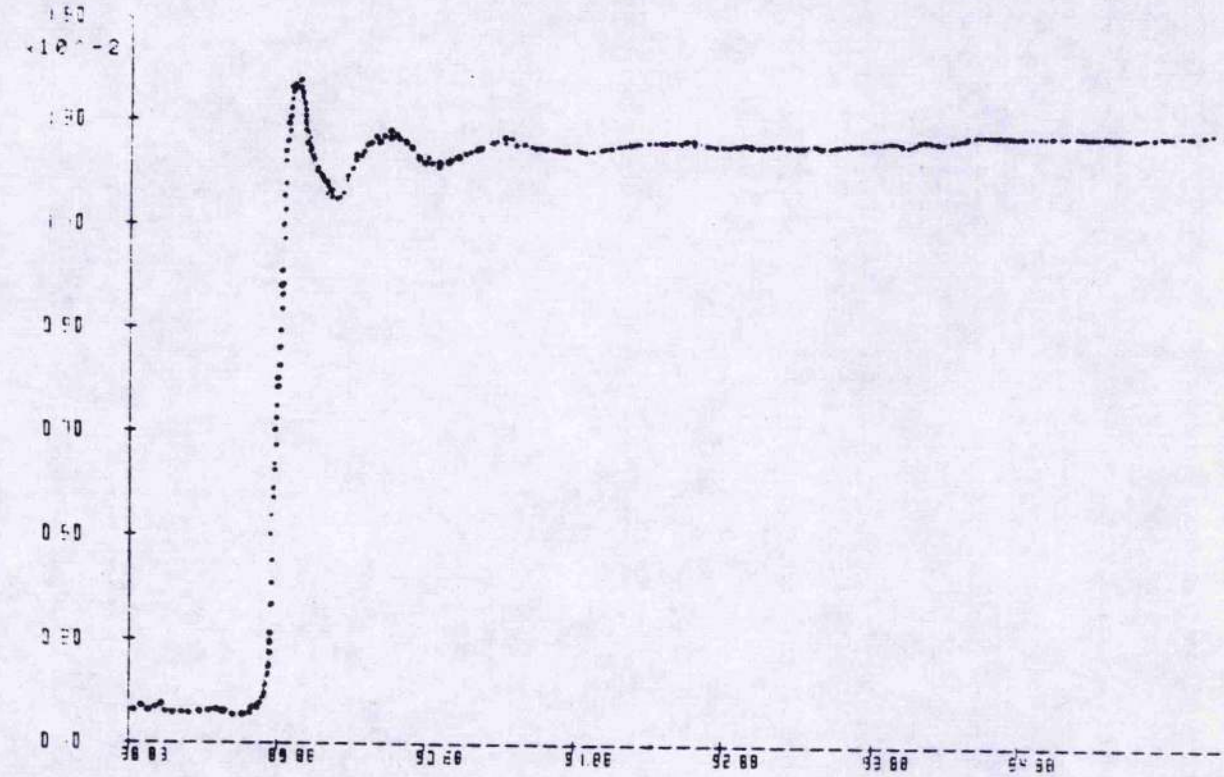

Mono pos	Time	Reference	Signal	Monitor	Flu Total	%
19595.00	80643.	594839[illegible]18.	118037.	113750.	762206.	[illegible]

Det 1	Det 2	Det 3	Det 4	Det 5	Det 6	Det 7	Det
49759.	72942.	77327.	61265.	67737.	83560.	78050.	58836.

B

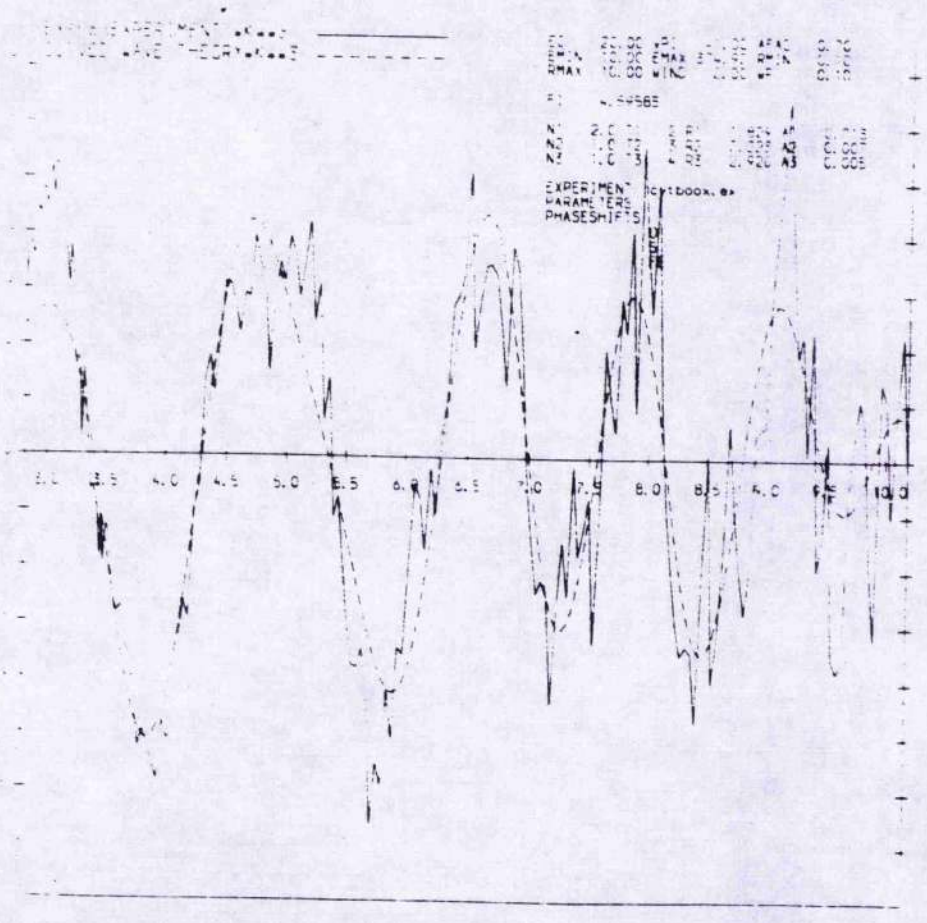

5.3 Conclusions

It has been shown that dysprosium increases the saturation parameter, $P1_{/2}$, of both centres in cytochrome *o*. The magnitude of this effect suggests the low-spin centre is approximately 16Å and the high-spin centre is 20.6Å from the site of closest approach. The sidedness of the centres was established in sphaeroplasts where the extrinsic probe had access to the periplasmic aspect of the membrane only. In these experiments the effect of Dys(III)EDTA on the low-spin centre was identical whilst little or no enhanced relaxation was observed in the haem *o*-NO (haem *o*) centre. Taken together these results suggest a model in which the low-spin haem *b* of cytochrome *o* lies 16Å within the protein surface towards the periplasmic side and the high-spin haem *o* lies 20.6Å from the cytoplasmic side of the protein. These findings compare with 6.5Å estimated between protein surface and haem *a* in cytochrome *c* oxidase (Ohnishi *et al.*, 1984), the difference is almost certainly a function of electron donor species employed by each enzyme.

The haem-copper interaction in cytochrome o is an antiferromagnetic coupling between the two metal centres which form the oxygen binding and reduction site, the haem-haem interaction is an effect on the mid-point potential and optical spectrum of one haem by the reduction/oxidation of the other (discussed in Chapter 4). The former requires close proximity of the two metal centres, the latter does not and is probably due to a

conformational effect.

However, there is an additional weak spin-spin interaction between both haem centres which was monitored by the enhanced saturation behaviour of the haem *o*-NO species when the low-spin centre is paramagnetic. The strength of this weaker interaction indicates that the inter-haem distance is approximately 12-16Å.

X-ray spectroscopic studies on purified cytochrome o have been facilitated by the presence of only one copper centre. At this time there seems to be some similarities between the XAS data from cytochrome aa_3 presented by some groups and the data reported herein. The presence of a sulphur ligand to Cu_o can be tentatively assigned to methionine-353, a conserved ligand (Chapter 1; Figure 1.2). The obvious difference between the two oxidases is the failure to identify a sulphur bridge in cytochrome *o*. However, the cytochrome *o* used in the XAS experiments described herein, was isolated in the absence of Cl^- ions. These experiments, therefore, need to be carried on cytochrome *o* isolated in the presence of Cl^- to determine whether or not a chloride ion is responsible for the data of cytochrome *c* oxidase.

It is important to note that EXAFS data reported provides additional evidence that there is only one copper centre in cytochrome *o*. A model is presented for the possible structure of cytochrome *o* based on the structural evidence presented herein and elsewhere (Figure 5.13).

Future XAS studies should be expanded to incorporate

Figure 5.13

Structure of cytochrome o: Subunit I and active site

Shown are models of the structure of cytochrome *o* based on (a) dysprosium experiments (EPR) and (b) Cu EXAFS data presented herein. Models are not to scale.

a

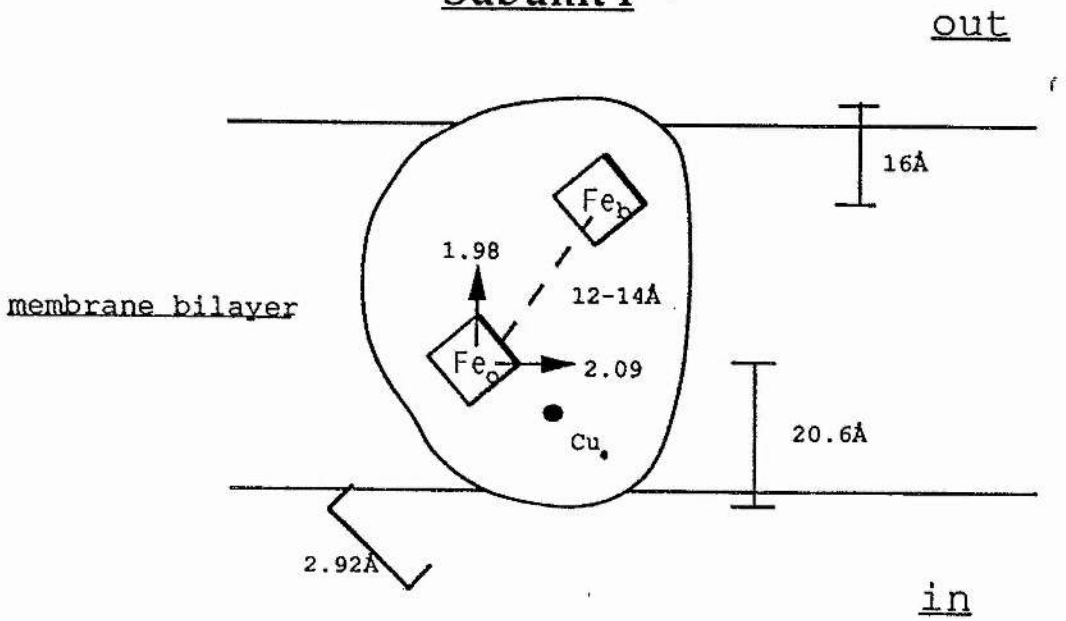
Subunit I
out
16Å
Fe_b
1.98
12-14Å
membrane bilayer
Fe_o
2.09
Cu_o
20.6Å
2.92Å
in

b

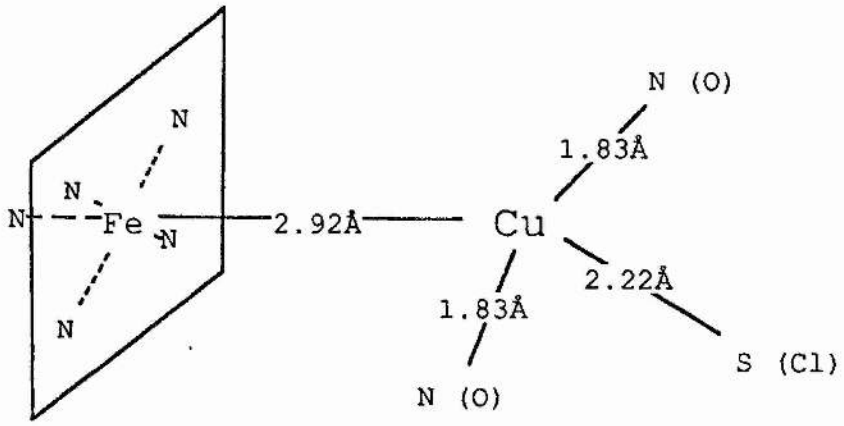
N (O)
1.83Å
N
N
N
Fe
N
N
2.92Å
Cu
2.22Å
1.83Å
S (Cl)
N (O)

Haem *o*

Cu_o

iron XAS. The analysis of iron EXAFS will be hampered by the presence of two haem centres within the native enzyme. Site directed mutagenesis applied to putative ligands to either haem centre will help resolve this problem. The Fe-Cu relationship may be further characterised using copper depleted derivatives of the enzyme through genotypic and phenotypic manipulation (see Chapter 3). Furthermore, application of XAS to multilaminar arrays of membranes will hopefully provide additional orientational information complementary to that already obtained from EPR studies (see Section 5.2.5 and *c.f.* George *et al.*, 1987).

Chapter 6

General Conclusions

6.1 *Characterisation of spectral properties of cytochrome o*

This chapter will only summarise the conclusions already drawn in Chapters 3, 4 and 5. The use of a purified preparation of cytochrome *o*, in some experiments, minimised the effects from other haem components which are not constituents of this enzyme. The catalytic activity and biophysical properties examined were essentially identical to the data obtained from membrane preparations from amplified and non-amplified strains. Cytochrome *o* possesses three known redox active metal centres. These are the low-spin haem *b* centre, the five coordinate high-spin haem *o* centre and copper. The redox chemistry of the haem components of this oxidase were examined in the purified enzyme at low temperatures using EPR spectroscopy (Chapter 3) and at room temperature (Chapter 4; optical). The low temperature potentiometric data verify the conclusions made by others (Salerno *et al.*, 1989, 1990), that a haem-haem cooperative interaction and copper-haem interaction are present in cytochrome *o*. From the data presented in this thesis, the mid-point potentials of haem *b* were (pH 7.5) +140mV and +240mV. The mid-point potentials of haem *o* were +150mV and +250mV. The haem-copper interaction manifests as a loss of the g = 6 (haem *o*) signal above +290mV and is due to an antiferromagnetic spin-coupling between the two centres. The mid-point potential of copper is estimated to be approximately +350mV.

The haem-haem interaction was also shown to adequately

explain the room temperature optical potentiometric data from the alpha band of purified cytochrome *o* (Chapter 4) and a cooperative model was presented.

The controversy surrounding the assignment of both optical bands in the α region of the reduced spectrum of the quinol oxidase, has been resolved herein. Based on the redox data from the carbon monoxide-inhibited oxidase (Section 4.2.5), there was no evidence to suggest haem *o* absorbed significantly in this region and haem *b* is proposed to be the origin of both the absorbance maxima at 558nm and 564nm. Titrations performed at various pH's showed the mid-point potential of haem *b*, and it's cooperative interaction with haem *o*, to be dependent on pH (Figure 4.5b). This indicates the involvement of a protonisable group associated with the haem *b* centre which may be involved in the proton pumping activity of this enzyme (Puustinen *et al.*, 1989, 1991).

A new absorbance in the reduced spectrum of cytochrome *o* has been identified (Chapter 4). This feature has an extremely weak extinction and has a wavelength maxima at 758nm at room temperature. This feature has been observed in the membrane bound and purified enzymes and is not an artifact of purification. The 758nm band corresponds to an absorbance identified in haemoglobin and myoglobin (band III). The effect of carbon monoxide and the redox behaviour of the 758nm band strongly suggest ferrous haem *o* is responsible for this feature. The broad optical absorbance of Cu_A in this region has hampered attempts to find a

similar transition in cytochrome *c* oxidase. However, a feature has recently been observed in the carbon monoxide-inhibited enzyme spectrum *minus* the flash photolysed spectrum of the carbon monoxide-inhibited enzyme (essentially a reduced-*plus*-carbon monoxide *minus* reduced difference spectrum) (W.J. Ingledew, personal communication).

The discovery of a new optical absorbance in cytochrome *c* oxidase is of great significance, particularly in view of the spectral overlap of haem *a* and a_3 absorbances, underlining the importance of cytochrome *o* as a appropriate model for cytochrome *c* oxidase.

6.2 *Conformations of cytochrome o?*

Chapter 1 summarised the similarities between the cytochrome *c* oxidase (aa_3) complex found in mitochondria and bacteria and cytochrome *o* from *E. coli*. Structural identity has been established by others (see Section 1.4.1) and biophysical (see above) and functional similarities e.g. the catalysis of the four electron reduction of molecular oxygen to water (Minghetti & Gennis, 1988), are well documented. However, our knowledge of these similarities has been further extended by the data presented in this thesis. Cytochrome *c* oxidase exists in a number of states which have distinguishable optical and magnetic resonance spectra, possess different reactivities to ligands and disparate internal electron transfer rates (see Chapter 1). These

states may be due to structural reorganisations within the enzyme or to ligand binding at the reaction site and are highly dependent on a number of factors including enzyme turnover, pH, preparative procedure of isolation and the presence of ligands (e.g. formate). Cytochrome *o*, as prepared for study in this thesis, does not appear to be so variable. The reaction between cytochrome *o* and cyanide was investigated in Chapter 3. Redox cycling did not affect the reactivity of the oxidase with this ligand. However, treatment with formate did induce a change in the cyanide binding rate broadly paralleling the behaviour of cytochrome *c* oxidase under similar conditions (although, there was still some biphasicity observed in the quinol oxidase). The effect of formate is most easily explained by assuming that the reaction between cyanide and cytochrome *o* is rate limited by the rate of dissociation of formate from the bi-nuclear reaction site. Unfortunately, the biphasic nature of the reaction between cyanide and cytochrome *o* cannot be explained at this time. It is clear, however, that it is not due to a ligand bound intermediate at the reaction site of cytochrome *o*, a proposal that adequately explains the effect of formate on ligand binding reactivities in cytochrome *c* oxidase.

X-ray absorption spectroscopy has identified structural differences in the bi-metallic site of fast and slow preparations of cytochrome *c* oxidase (Kumar *et al.*, 1988). Significantly, cytochrome *o* appears to more closely resemble the structure of the fast enzyme (*c.f.* Figure 5.11 & 5.13).

6.3 *Is there a copper analogue in cytochrome o to Cu_A of cytochrome c oxidase?*

One very significant difference between cytochrome aa_3 and cytochrome *o* is the complement of copper. The evidence presented in this thesis and elsewhere conclusively prove there to be only a single copper centre within the quinol oxidase. This evidence is summarised below. Lemieux *et al.* (1991) failed to find a potential copper binding site in *cyo*A, the gene with close sequence identity with subunit II (COII) of cytochrome aa_3 (*P. denitrificans*) which binds the Cu_A centre. The physical evidence against a second copper centre in cytochrome *o* includes; a distinct lack of a broad optical transition (*c.f.* the Cu_A cupric absorbance at 830nm) (Chapter 4); the inabilty to identify copper in anything more than substoicheiometric amounts by EPR spectroscopy (Salerno et al., 1990; Puustinen et al., 1991) and the good fit of the XAS data from purified cytochrome *o* with a single copper absorber (Chapter 5).

6.4 *Location and spatial organisation of the prosthetic groups of cytochrome o*

Cytochrome *o* from *E. coli* strain RG145 contains three prosthetic groups, a six coordinate low-spin haem *b*, a five coordinate high-spin haem *o* and a copper centre. The organisation of these redox centres was investigated in Chapter 5. The extrinsic paramagnetic probe Dys(III)-EDTA

was used to perturb the relaxation rates of the paramagnetic forms of haem *b* and haem *o*, the latter as the nitrosyl ferrous haem *o* adduct (haem *o*-NO). Haem *b* was found to be located on the periplasmic aspect of the cytoplasmic membrane, as demonstrated by the similar magnitude of saturation relief in membranes and sphaeroplasts. Haem *b* is located much deeper within the lipid membrane bilayer than haem *a* of cytochrome *c* oxidase, presumably because haem *b* accepts electrons from quinol whereas haem *a* accepts electrons (possibly mediated by Cu_A) from cytochrome *c* on the membrane surface. Haem *o* was found to be located closer to the cytoplasmic aspect of the membrane. A cytoplasmic (inner) location for the catalytic reaction cente is favoured for energetic reasons, proton consumption in dioxygen reduction will augment the $\Delta\mu H^+$ across the respiring membrane.

An interaction (spin-spin) was shown between both haem centres, as demonstrated by the relief of the saturation parameter, $P1_{/2}$, of the slow relaxing ferrous haem *o* nitrosyl adduct by the faster relaxing paramagnetic haem *b* centre. The inter-haem distance could be limited to approximately 14Å by this finding.

Further orientational information was obtained by the use of EXAFS on concentrated enzyme preparations. As mentioned previously, cytochrome *o* possesses only one copper centre and is therefore more amenable to study by this

technique than cytochrome *c* oxidase. In addition, cytochrome *o* is a bacterial enzyme and will be suitable for manipulation, either genotypic or phenotypic, which offers a number of alternative enzyme preparations with which to study the structure function relationship of this enzyme.

6.5 *Molecular oxygen reduction by cytochrome o: a model*

The terminal oxidases of the respiratory chains of mitochondria and *E. coli* catalyse the four electron reduction of molecular oxygen to water. This is achieved without the release of potentially damaging reduction products of oxygen such as superoxide (one electron reduced state) or peroxide (two electron). Bond cleavage and stabilisation of these intermediates is facilitated by a binuclear (bi-metallic) reaction centre, haem a_3 and Cu_B in cytochrome *c* oxidase, haem *o* and Cu_o in cytochrome *o*. The reduction of dioxygen is thermodynamically more favourable when two centres are involved (Malmstrom 1982). The unpaired electron over the bound oxygen adduct (Fe^{2+}-O_2) results in the formation of a bent configuration of the molecule (as with NO) resulting in bridging of the oxygen molecule between both centres of the reaction centre.

Understanding the chemistry of dioxygen reduction in these enzymes lies at the heart of understanding the mechanism by which the redox free energy of electrons is ultimately coupled to ATP synthesis and hence life. A model for this mechanism has already been described in Chapter 1

for cytochrome aa_3-type oxidases. In it, essentially sequential electron transfer steps lead to the full reduction of dioxygen to water.

The data presented in Chapter 4 suggests single sequential electron reduction events do not occur in cytochrome *o*, the mechanism of reduction might therefore be expected to be different in this quinol oxidase. Figure 6.1 depicts a working model for dioxygen reduction by cytochrome *o* which can be used to test a concerted two electron reduction mechanism. Starting with the fully reduced reaction centre (step 1), molecular oxygen initially binds to ferrous haem *o* to form the non-reduced oxygen adduct similar to Compound A of cytochrome *c* oxidase (step 2). This species has been identified by triple trapping data (Poole et al., 1979a; see Chapter 1). Elelctron redistribution at the bi-metallic centre forms a μ-peroxy bridging structure (step 3). Quinol donates two electrons together to form the half reduced oxygen product, the hydroxyferric and hydroxycupric species (step 4). This step occurs without the formation of a ferryl intermediate of the reaction centre which is observed in the cytochrome *c* oxidase cycle. Four protons, presumably originating from the cytoplasmic side of the membrane, are consumed in the reaction between steps 3 and 5 resulting in fully reduced oxygen (water) and generating the fully oxidised reaction centre. Quinol donates two more electrons to complete the catalytic cycle (step 1). Further experimentation is required to test this model.

Figure 6.1

A model for reduction of dioxygen by cytochrome o

A model is proposed for the reaction between molecular oxygen and the reaction centre of cytochrome *o* (haem *o* and Cu_o). For clarity, the ubiquinol binding site and the low-spin haem *b* centre have been omitted. The model is based on the available information discussed in Chapter 1 and presented in Chapter 3. Refer to the text for description of cycle. Only those protons directly involved in the reduction of oxygen are shown, additional protons are pumped by this enzyme during this cycle but these are not shown.

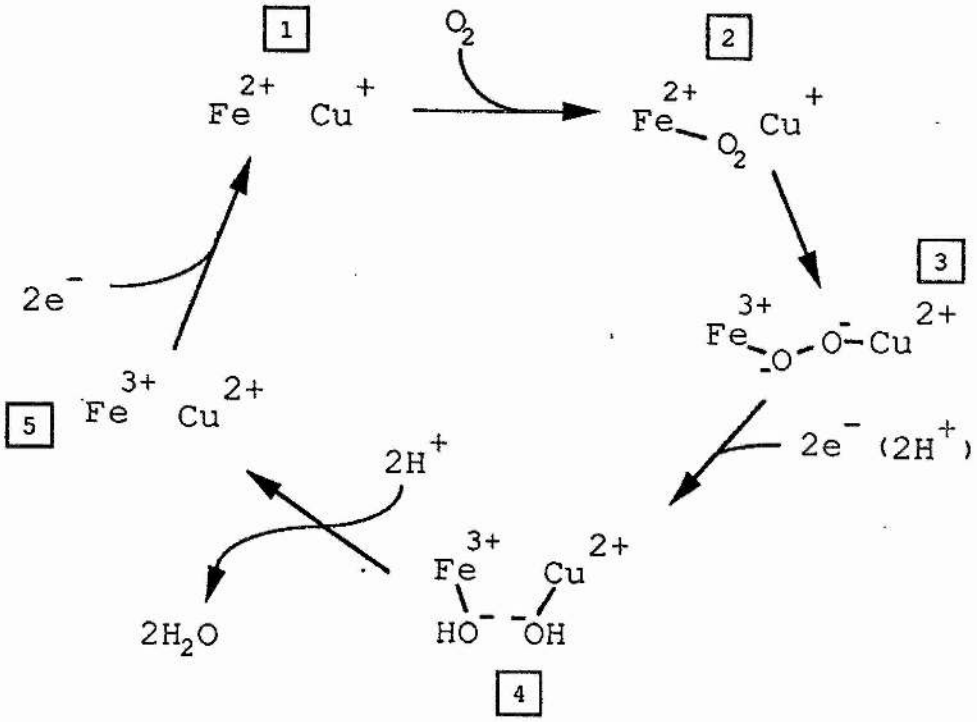
1
O_2
2
Fe^{2+} Cu^{+}
Fe^{2+} O_2 Cu^{+}
3
Fe^{3+} O^{-} O^{-} Cu^{2+}
$2e^{-}$ $(2H^{+})$
4
Fe^{3+} Cu^{2+}
HO^{-} ^{-}OH
$2H^{+}$
$2H_2O$
$2e^{-}$
5
Fe^{3+} Cu^{2+}

Bibliography

Alben,J.O., Moh,P.P., Fiamingo,F.G. Altschuld (1981) Proc. Natl. Acad. Sci. USA **78**:234-237.

Alberding,N., Austin,R.H., Chan,S.S., Eisenstein,L., Frauenfelder,H., Gunsalus,I.C. & Nordlund,T.M. (1976) J. Chem. Phys. **65**:4701-4711.

Anraku,Y. & Gennis,R.B. (1987) TIBS **12**:262-266.

Anraku,Y. (1988) Ann. Rev. Biochem. **57**:101-32

Ansari,A., Berendzen,J., Bowne,S.F., Frauenfelder,H., Iben,I.E.T., Sauke,T.B., Shyamsunder,E. & Young,R.D. (1985) Proc. Natl. Acad. Sci. USA **82**:5000-5004.

Antonini, E., Brunori,M., Colosimo,A., Greenwood, C. & Wilson, M. (1981) Proc. Acad. Natl. Sci. USA **78**:7115-7118.

Au,D.C.-T. & Gennis,R.B. (1987) J. Bacteriol. **169**:3237-3242.

Au,D.C.-T., Lorence,R.M. & Gennis,R.B. (1985) J. Bacteriol. **161**:123-127.

Azzi,A. (1980) Biochim. Biophys. Acta **594**:231-252.

Azzi,A. & Muller,M. (1990) Arch. Biochem. Biophys. **280**:242-251.

Baker,G.M., Noguchi,M. & Palmer,G. (1987) J. Biol. Chem. **262**:595-604.

Barber,M.J., Salerno,J.C. & Siegel,L.M. (1982) Biochemistry **21**:1648-1656.

Barlow,C. & Erecinska,M. (1979) FEBS Letts. **94**:9-12.

Beinert,H, Hansen,R.E. & Hartzell,C.R. (1976) Biochim. Biophys. Acta **423**:339-355.

Berry,E.A. & Trumpower,B.L. (1987) Anal. Biochem. **161**:1-15.

Blair,D.F., Ellis,W.R., Wang,H., Gray,H.B. & Chan,S.I. (1986a) J. Biol. Chem. **261**:11524-11537.

Blair,D.F., Gelles,J. & Chan,S.I. (1986b) Biophys. J. **50**:713-733.

Blasie,J.K., Erecinska,M., Samuels,S. & Leigh,J.S. (1978) Biochim. Biophys. Acta **501**:33-52.

Blokzijl-Homan,M.F.J & van Gelder,B.F. (1971) Biochim. Biophys. Acta **234**:493-498.

Blum, H., Harmon, H.J., Leigh, J.S., Salerno,J.C. & Chance,B. (1978a) Biochem. Biophys. Acta **502**:1-10.

Blum,H. & Ohnishi,T. (1980) Biochim. Biophys. Acta **621**:9-18.

Blum,H., Bowyer,J.R., Cusanovich,M.A., Waring,A.J. & Ohnishi,T. (1983) Biochim. Biophys. Acta **748**:418-428.

Blum,H., Cusanovich,M.A., Sweeney,W.V. & Ohnishi,T. (1981) J. Biol. Chem. **256**:2199-2206.

Blum,H., Leigh,J.S. & Ohnishi,T. (1980) Biochim. Biophys. Acta **626**:31-40.

Blum,H., Leigh,J.S., Salerno,J.C. & Ohnishi,T. (1978b) Arch. Bioch. Biophys. **187**:153-157.

Boelens,R. & Wever,R. (1979) Biochim. Biophys. Acta **547**:296-310.

Bolgiano,B., Salmon,I., Ingledew,W.J. & Poole,R.K. (1991) Biochem. J. **274**:723-730.

Brandt,U., Schagger,H. & von Jagow,G. (1989) Eur. J. Biochem. **182**:705-711.

Brudvig,G.W., Stevens,T.H. & Chan, S.I. (1980) Biochemistry **19**:5275-5285.

Brudvig,G.W., Stevens,T.H., Morse,R.H. & Chan,S.I. (1981) Biochemistry**20**:3912-3921.

Brunori,M., Colosimo,A., Rainoni,G., Wilson,M. & Antonini,E. (1979) J. Biol. Chem. **254**:10769-10775.

Calhoun,M.W., Newton,G. & Gennis,R.B. (1991) J. Bacteriol. **173**:1569-1570.

Calhoun,M.W., Lemieux,L.J., Thomas,J.W., Hill,J.J., Alben,J.O. & Gennis,R.B. (1992) Biophys. J. **61**:A193

Campbell,B.F., Chance,M.R. Friedman,J.M. (1987) Science **238**:373-376.

Capaldi,R.A. (1990) Archives Biochem. Biophys. **280**:252-262.

Capaldi,R.A., Takamiya,S., Zhang,Y-Z., Gonzalez-Halphen,D. & Yanamura,W. (1987) Current Topics in Bioenergetics **15**:91-112.

Carter,K. & Gennis,R.B. (1985) J. Biol. Chem. **260**:10986-10990.

Case,G.D. & Leigh,J.S. (1979) Biochem. J. **160**:769-783.

Caster,L.N. & Chance, B. 1959 J. Biol. Chem. **234**:1587-1592.

Caster,L.N. & Chance,B. (1955) J. Biol. Chem. **217**:453-465.

Chan,S.I. & Li,M. (1990) Biochemistry **29**:1-12.

Chan,S.I. (1988) Annals New York Acad. Sci. **550**:207-222.

Chan,S.I., Witt,S.N. & Blair,D.F. (1988) Chem. Scr. **28A**:51-56.

Chance,B. (1978) Methods Enzymol. **54**:102-111.

Chance,B., Kumar,C., Powers,L. & Ching,Y. (1983) Biophys. J. **44**:353-363.

Chance,B., Saronio,C. & Leigh,J.S. (1975) J. Biol. Chem. **250**:9226-9237.

Chavez,M.D., Courtney,S.H., Chance,M.R., Kiula,D., Nocek,J., Hoffman,B.M., Friedman,J.M. & Ondrias,M.R. (1990) Biochemistry **29**:4844-4852.

Chepuri,V. & Gennis,R.B (1990) J. Biol. Chem. **265**:12978-12986.

Chepuri,V., Lemieux,L., Hill,J. Albens,J.O. & Gennis,R.B. (1990b) Biochim. Biophys. Acta **124**:124-127.

Chepuri,V., Lemieux,L. Au,D.C.-T & Gennis (1990a) J. Biol. Chem. **265**:11185-11192.

Cooper, E.C., Moody,A.J., Rich,P.R., Wrigglesworth,J.M. & Ioannidis,N. (1991) Biochem. Soc. Trans. **19**:259. (Reading 638th Meeting Communications)

Cotter,P.A., Chepuri,V., Gennis,R.B. & Gunsalus,R.P. (1990) J. Bacteriol. **172**:6333-6338.

Daniel,R.M. (1970) Biochim. Biophys. Acta **216**:328-341.

Dutton,P.L. (1978) Methods Enzymology **54**:411-435.

Eaton,W.A., Hanson,L.K., Stephens,P.J., Sutherland,J.C. & Dunn,J.B.R. (1978) J. Am. Chem Soc. **100**:4991-5003.

Edwards,S.L., Kraut,J. & Poulos,T.L. (1988) Biochemistry **27**:8074-8081.

Einarsdottir,O. & Caughey,W.S. (1984) Biochem. Biophys. Res. Commun. **124**:836-842.

Einarsdottir,O. & Caughey,W.S. (1985) Biochem. Biophys. Res. Commun. **129**:840-847.

Erecinska,M., Wilson,D.C. & Blaisie,J.K. (1977) FEBS Letts. **76**:235-239.

Erecinska,M., Wilson,D.F. & Blaisie,J.K. (1978) Biochim. Biophys. Acta **501**:53-62.

Fiamingo,F.G. & Alben,J.O. (1985) Biochemistry **24**:7964-7970.

Frey,B., Janel,G., Michelson,U. & Kersten,H. (1989) J. Bacteriol. **171**:1524-1530.

Frond,S.J. & Anthony,C. (1984) J. Gen. Microbiol. **130**:2201-2212.

Gelles,J. & Chan,S.I. (1985) Biochemistry **24**:3963-3972.

Gelles,J., Blair,D.F. & Chan,S.I. (1986) Biochim. Biophys. Acta **853**:205-236.

George, G.N., Cramer, S.P., Frey, T.G. & Prince, R.C. (1987) *In* Advances in Membrane Biochemistry & Bioenergetics. Plenum Press. New York. pp 429-438.

Georgiou,C., Cokic,P., Carter,K., Webster,D.A. & Gennis,R.B. (1988a) Biochim. Biophys. Acta **933**:179-183.

Georgiou,C.D., Dueweke,T.J. & Gennis,R.B. (1988b) J. Bacteriol. **170**:961-966.

Georgiou,C.D., Fang,H. & Gennis,R.B. (1987) J. Bacteriol. **169**:2107-2112.

Gibson,Q.H., Greenwood,C., Wharton,D.C. & Palmer,G. (1965)

J. Biol. Chem. **240**:888-894.

Giorgio,A.J., Cartwright,G.E. & Wintrobe,M.M. (1963) J. Bacteriol. **86**:1037-1040.

Hackenbrock,C.R., Chazotte,B. & Gupte,S.S. (1986) J. Bioenergetics Biomemb. **18**:331-368.

Haddock,B.A., Downie,J.A. & Garland,P.B. (1976) Biochem. J. **154**:285-294.

Han,S., Ching,Y.-C & Rousseau,D.L. (1990b) Biochemistry**29**:1380-1384.

Han,S., Ching,Y.-C. & Rousseau,D.L. (1990a) Nature **348**:89-90.

Hasnain,S.S (ed.) (1990) *In* X-ray Absorption Fine Structure, Ellis Horwood.

Hata,A., Kirino,Y., Matsuura,K., Itoh,S., Hiyama,T., Konishi,K., Kita,K. & Anraku,Y. (1985) Biochim. Biophys. Acta **810**:62-72.

Henry,Y. & Banerjee,R. (1973) J. Mol. Biol. **73**:469-482.

Hill,B.C., Greenwood,C. & Nicholls,P. (1986) Biochim. Biophys. Acta **853**:91-113.

Hill.B.C. (1991) J. Biol. Chem. **266**:2219-2226.

Holm,L., Saraste,M. & Wikstrom,M. (1987) EMBO J. **6**:2819-2823.

Hori,H., Ikeda-Saito,M. & Yonetani,T. (1981) J. Biol. Chem. **256**:7849-7855.

Hori,H., Ikeda-Saito,M., Lang,G. & Yonetani,T. (1990) J. Biol. Chem. **265**:15028-15033.

Hudig,H & Drews,G. (1984) Biochim. Biophys. Acta **765**:171-177.

Hyde,J.S. & Rao,K.V.S. (1978) J. Mag. Res. **29**:509-516.

Iizuka,T., Yamamoto,H., Kotani,M. & Yonetani,T. (1974) Biochim. Biophys. Acta **371**:126-139.

Ingledew,W.J. & Poole,R.K. (1984) Microbiol. Rev. **49**:222-271

Ingledew,W.J. & Bacon,M. (1991) Biochem. Soc. Trans. **19**:613-616.

Ingledew,W.J., Rothery,R.A., Gennis,R.B. & Salerno,J.C. (1992) Biochem. J. **282**:255-259.

Iuchi,S. & Lin,E.C.C (1988) Proc. Natl. Acad. Sci. USA **85**:1888-1892.

Kita,K., Konishi,K. & Anraku,Y. (1984b) J. Biol. Chem. **259**:3375-3381.

Kita,K., Konishi, K. & Anraku,Y. (1984a) J. Biol. Chem. **259**:3368-3374.

Kita,K., Kasahara,M. & Anraku,Y. (1982) J. Biol. Chem. **257**:7933-7935.

Knowles,P.F., Marsh,D. & Rattle,H.W.E. (1976) *In* Magnetic Resonance of Biomolecules, John Wiley & Son, London.

Kohara,Y., Akiyama,K. & Isono,K. (1987) Cell **50**:495-508.

Kon,H. & Kataoka,N. (1969) Biochemistry**8**:4757-4762.

Kranz,R.G. & Gennis,R.B. (1985) J. Bacteriol. **161**:709-713.

Kranz,R.G. & Gennis,R.B. (1983) J. Biol. Chem. **258**:10614-10621.

Kumar,C., Naqui,A., Powers,L., Ching,Y.-C. & Chance,B. (1988) J. Biol. Chem. **263**:7159-7163.

Leigh,J.S., Wilson,D.F., Owen,C.S. & King,T.E. (1974) Arch.

Biochem. Biophys. **160**:476-486.

Lemberg & Barrett, (1972) *In* The Cytochromes, pp.8 and 59, Academic Press, N.Y.*

Lemieux,L.J., Calhoun,M.W., Thomas,J.W., Ingledew,W.J. & Gennis,R.B. (1991) J. Biol. Chem. in press

Li,P.M., Gelles,J., Chan,S.I., Sullivan,R.J. Scott,R.A. (1987) Biochemistry **26**:2091-2095.

Li,P.M., Malmstrom,B.G. & Chan,S.I. (1989) FEBS Letts. **248**:210-211.

LoBrutto,R., Wei,Y-H., Mascarenhas,R., Scholes,C.P. & King.T.E. (1983) J. Biol. Chem. **258**:7437-7448.

Lowry,O.H., Rosenbrough,N.J., Farr,A.L. & Randall,R.J. (1951) J. Biol. Chem. **193**:265-275.

Lukat,G.S., Jabro,M.N., Rodgers,K.R. & Goff,H.M. (1988) Biochim. Biophys. Acta **954**:265-270.

Malmstrom,B.G. (1979) Biochim. Biophys. Acta **549**:281-303.

Malmstrom,B.G. (1982) Ann. Rev. Biochem. **51**:21-59.

Malmstrom,B.G. (1990) Arch. Biochem. Biophys. **280**:233-241.

Mascarenhas,R., Wei,Y-H., Scholes,C.P. & King,T.E. (1983) J. Biol. Chem. **258**:5348-5351.

Matsushita,K., Patel,L. & Kaback,H.R. (1984) Biochemistry**23**:4703-4714.

Matsushita,K., Patel,L., Gennis,R.B. & Kaback,H.R. (1983) Proc. Natl. Acad. Sci. **80**:4889-4893.

Matsushita,K., Shinagawa,E., Adachi,O. & Ameyama,M. (1982) FEBS Letts. **139**:255-258.

Matsushita,K., Shinagawa,E., Adachi,O. & Ameyama,M. (1987) Biochim. Biophys. Acta **894**:304-312.

Miller,M.J. & Gennis,R.B. (1983) J. Biol. Chem. **258** 9159-9165.

Minagawa,J., Nakamura,H., Yamato,I., Mogi,T. & Anraku,Y. (1990) J. Biol. Chem. **265**:11198-11203.

Minghetti,K.C. & Gennis,R.B. (1988) Biochem. Biophys. Res. Commun. **155**:243-248.

Mitchell,M., Mitchell,P. & Rich,P.R. (1991) FEBS Letts. **280**:321-324.

Moodie,A.D. (1990) PhD thesis; University of St. Andrews,

UK.

Moody,A.J. & Rich,P.R. (1991) Biochem. Soc. Trans. **19**:262.

Morgan,J.E., Li,P.M., Jang,D.J., Ed-Sayed,M.A. & Chan,S.I. (1989) Biochemistry**28**:6975-6983.

Morse,R.H. & Chan,S.I. (1980) J. Biol. Chem. **255**:7876-7882.

Nakamura,H., Yamata,I., Anraku,Y., Lemieux,L. & Gennis,R.B. (1990) J. Biol. Chem. **265**:11193-11197.

Naqui,A., Powers,L., Lundeen,M., Constantinescu,A. & Chance,B. (1988) J. Biol. Chem. **263**:12342-12345.

Ohnishi,T., Blum,H., Harmon,H.J. & Hompo,T. (1980) *In* Interaction Between Iron & Proteins in Oxygen & Electron Transport (Ho,C.,ed.) (Elsevier/North Holland, NY.)

Ohnishi,T., Harmon,H.J. & Waring,A.J. (1984) Biochem. Soc. Trans. **13**:607-611

Ohnishi,T., LoBrotto,R., Salerno,J.C., Bruckner,R.C. & Frey,T.G. (1982) J. Biol. Chem. **257**:14821-14825.

Ohnishi,T., Schagger,H., Mienhardt,S.W., LoBrutto,R., Link,T.A. & von Jagow,G. (1989) J. Biol. Chem. **264**:735-744.

Orii,Y. (1988) Annals New York Acad. Sci. **550**:105-117.

Pan,L.P., Li,Z., Larsen,R. & Chan,S.I. (1991) J. Biol. Chem. **266**:1367-1370.

Petrouleas,V. & Diner,B.A. (1990) Biochim. Biophys. Acta **1015**:131-140.

Poole,R.K. & Ingledew,W.J. (1987) *In* Escherichia coli and Salmonella typhemurium and molecular biology. (Neirdardt, F.C. ed.) pp.170-200. American Soc. of Microbiology

Poole,R.K. (1983) Biochim. Biophys. Acta **726**:205-243

Poole,R.K. (1988) *In* Bacterial Energy Transduction. (Anthony,C., ed.), pp 231-291. Academic Press.

Poole,R.K. Waring,A.J. & Chance,B. (1979a) Biochem. J. **184**:379-389.

Poole,R.K., Sivaram,A. & Chance,B. (1982) FEBS Letts. **141**:237-241.

Poole,R.K., Waring,A.J. & Chance,B. (1979b) FEBS Letts. **101**:56-58.

Poole,R.K., Williams,H.D., Downie,J.A. & Gibson,F. (1989) J. Gen. Microbiol. **135**:1865-1874.

Powers,L., Blumberg,W.E., Chance,B., Barlow,C.H., Leigh,J.S., Smith,J., Yonetani,T., Vik,S. & Peisach,J. (1979) Biochim. Biophys. Acta **546**:520-538.

Powers,L., Chance,B., Ching,Y. & Angiolillo,P. (1981) Biophys. J. **34**:465-498.

Puustinen,A. & Wikstrom,M. (1991) Proc. Natl. Acad. Sci. USA **88**:6122-6126.

Puustinen,A., Finel,M., Haltia,T., Gennis,R.B. & Wikstrom,M. (1991) Biochemistry **30**:3936-3942.

Puustinen,A., Finel,M., Virkki,M. & Wikstrom,M. (1989) FEBS Letts **249**:163-167.

Raitio, M., Jalli, T. & Saraste, M. (1987) EMBO J. **6**:2825-2833.

Rice,C.W. & Hempfling,W.P. (1978) J. Bacteriol. **134**:115-124.

Rich,P.R., West,I.C. & Mitchell,P. (1988) FEBS Letts. **233**:25-30.

Rothery,R.A. (1989) PhD thesis; University of St. Andrews, UK.

Salerno,J.C. & Ingledew,W.J. (1991) Eur. J. Biochem. **198**:789-792.

Salerno,J.C., Blum,H. & Ohnishi,T. (1979a) Biochim. Biophys. Acta **547**:270-281.

Salerno,J.C., Bolgiano,B. & Ingledew,W.J. (1989) FEBS Letts. **247**:101-105.

Salerno,J.C., Bolgiano,B., Poole,R.K. Gennis,R.B. & Ingledew,W.J. (1990) J. Biol. Chem. **265**:4364-4368.

Salerno,J.C., Lim,J., King,T.E., Blum,H. & Ohnishi,T. (1979b) J. Biol. Chem. **254**:4828-4835.

Saraste,M., Raitio,M., Jalli,T., Chepuri,V., Lemieux,L. & Gennis,R.B. (1988) Annals of New York Acad. Sci. **550**:314-324.

Sassaroli,M. & Rousseau,D.L. (1987) Biochemistry **26**:3092-3098.

Schagger,H., Borchart,U., Uquila,H., Link,T. & von Jagow,G. (1985) FEBS Letts. **190**:89-94.

Schagger,H. & von Jaggow,G. (1987) Anal. Biochem. **166**:368-379.

Scott,R.A., Cramer,S.P., Shaw,R.W., Bienert,H. & Gray,H.B. (1981) Proc. Natl. Acad. Sci. USA **78**:664-667.

Scott,R.A., Li,P.M. Chan,S.I. (1988b) Annals New York Acad. Sci. **550**:53-58.

Scott,R.A., Schwartz,J.R. & Cramer,S.P. (1986) Biochemistry **25**:5546-5555.

Scott,R.A., Sullivan,R.J., DeWolf,W.E., Dolle,R.E. & Kruse,L.I. (1988a) Biochemistry **27**:5411-5417.

Scott,R.I & Poole,R.K. (1982) J. Gen. Microbiol. **128**:1685-1696.

Sedgwick,E.G. & Bragg,P.D. (1988) FEBS Letts. **229**:127-130.

Sone,N. Kutoh,E & Sato,K. (1990) J. Biochem. **107**:597-602.

Steffens,G.C.M., Biewald,E. & Buse,G. (1987) Eur. J. Biochem. **164**:295-300.

Steffens,G.J. & Buse,G. (1979) *In* Cytochrome oxidase King,T., Orii,Y. Chance,B. & Okunuki,K. eds. Elsevier/North-Holland, Amsterdam. pp 79-90.

Stern,E.A. (1976) Sci. American **234**:96-103.

Stevens,T.H. & Chan,S.I. (1981) J. Biol. Chem. **256**:1069-1071.

Stevens,T.H., Bocian,D.F. & Chan,S.I. (1979) FEBS Letts. **97**:314-316.

Stevens,T.H., Brudvig,G.W., Bocian,D.F. & Chan,S.I. (1979) Proc. Natl. Acad. Sci. USA **76**:3320-3324.

Thornstrom,P.-E., Brzezinski,P. Fredriksson,P.-O. & Malmstrom,B. (1988) Biochem **27**:5441-5447.

Trumpower,B.L. (1990) Microbiol. Rev. **54**:101-129.

Tyree,B. & Webster,D.A. (1978a) J. Biol. Chem. **253**:6988-6991.

Tyree,B. & Webster,D.A. (1978b) J. Biol. Chem. **253**:7635-7637.

Uno,T., Nishimura,Y., Tsubio,M., Kita,K. & Anraku,Y. (1985) J. Biol. Chem. **260**:6755-6760.

van Buuren,K.J.H, Nicholls,P. & van Gelder,B.F. (1972b) Biochim. Biophys. Acta **256**:258-276.

van Buuren,K.J.H., Zuuredonk,P.F., van Gelder,B.F. & Muijsers,A.O. (1972a) Biochim. Biophys. Acta **256**:243-257.

van Gelder,B.F. & Beinert,H. (1969) Biochim. Biophys. Acta **189**:1-24.

van Wielink,J.E., Oltmann,L.F., Leeuwerik,F.J., De Hollander,J.A. & Stouthamer,A.H. (1982) Biochim. Biophys. Acta **681**:177-190.

Wakabayashi,S., Masubara,H. & Webster,D.A. (1986) Nature **322**:481-483.

Wallace,B.J. & Young,I.G. (1977) Biochim. Biophys. Acta **461**:84-100.

Warburg,O. (1924) Biochem. Z. 152:479-494.

Webster,D.A. & Hacket,D.P. (1966) J. Biol. Chem. **241**:33-3315.

Wieghardt,K. (1984) Advances in Inorganic & Bioinorganic Mechanisms **3**:213-274.

Wikstrom,M. (1989) Nature **338**:776-778.

Wikstrom,M & Krab,K. (1979) Biochim. Biophys. Acta **549**:177-222.

Wikstrom,M. (1977) Nature **266**:271-273.

Wikstrom,M., Krab,K. & Saraste,M. (1981a) *In* Cytochrome *c* oxidase - A Synthesis. Academic Press; Ney York

Wikstrom,M. (1981) Proc. Natl. Acad. Sci. USA **78**:4051-4054.

Wikstrom,M. (1988) Chem. Scr. **28A**:71-74.

Wikstrom,M. Krab,K. & Saraste,M. (1981b) Ann. Rev. Biochem. **50**:623-655.

Williams,H.D. & Poole,R.K. (1988) Curr. Micro. **16**:277-280.

Williams,H.D., Hubbard,A.M., Nugent,H.A. & Poole,R.K. (1991) Biochem. J. **276**:555-557.

Wilson,D.F., Gordon Lindsay,J. & Brocklehurst,E.S. (1972) Biochim. Biophys. Acta **256**:277-286.

Wilson,M.T., Peterson,J., Antonini,E., Brunori,M., Colosimo,A. & Wyman,J. (1981) Proc. Natl. Acad. Sci. USA **78**:7115-7118.

Withers,H.K. & Bragg,P.D. (1987) Biochim. Biophys. Acta **892**:10-22.

Withers,H.K. & Bragg,P.D. (1990) Biochem. Cell Biol. **68**:83-90.

Witt,S.N. & Chan,S.I. (1987) J. Biol. Chem. **262**:1446-1448.

Wood,P.M. (1984) Biochim. Biophys. Acta **768**:293-317.

Xie,X. & Simon,J.D. (1991) Biochemistry **30**:3682-3692.

Yang,T. & Jurtshuk,P (1978) Biochim. Biophys. Acta **502**:543-548.

Yang,T. (1982) Eur. J. Biochem. **121**:335-341.

Yang,T. O'Keefe,D. & Chance,B. (1979) Biochem. J. **181**:763-766.

Yang,T. (1986) Biochim. Biophys. Acta **848**:342-351.

Yewey,G.L. & Caughey,W.S. (1988) Annals New York Acad. Sci. **550**:22-32.

Yonetani,T., Yamamoto,H, Erman,J.E., Leigh,J.S. & Reed,G.H. (1972) J. Biol. Chem. **247**:2447-2455.